

Phytanyl substituted asymmetric gemini surfactant-based transfection vectors for gene therapy

by

Haitang Wang

A thesis
presented to the University of Waterloo
in fulfillment of the
thesis requirement for the degree of
Doctor of Philosophy
in
Chemistry

Waterloo, Ontario, Canada, 2013

© Haitang Wang 2013

AUTHOR'S DECLARATION

I hereby declare that I am the sole author of this thesis. This is a true copy of the thesis, including any required final revisions, as accepted by my examiners.

I understand that my thesis may be made electronically available to the public.

Abstract

To achieve successful gene therapy, safe and efficient gene delivery vectors are needed. As an alternative to viral vectors, non-viral vectors, incorporating compounds such as cationic polymers and lipids have been widely studied. Much effort has been made to enhance transgene delivery efficiency, such as development of more effective cationic lipids or polymers, optimization of transfection formulations, and investigation on structural-activity of delivery vectors. Gemini surfactant, consisting of two surfactant monomers linked by a spacer group, is a thrust research area for gene therapy as non-viral vectors due to their high stability, longer storage on shelves, easiness to produce.

A series of phytanyl substituted asymmetric gemini surfactants, phy-3-m ($m = 12, 16, \text{ and } 18$) and phy-7NH-m ($m = 12, 16, \text{ and } 18$), were rationally designed and synthesized. Due to the bulky nature and increased hydrophobicity of phytanyl branch, phy-3-m surfactants showed much lower values of critical micelle concentration (CMC) compared to their corresponding symmetric m-3-m. Particle size and transmission electron microscopy (TEM) imaging indicate that this type of gemini surfactants tends to form stacked bilayers rather than spherical or rod-like micelles which are typically observed in gemini surfactants with shorter spacers. Phy-3-m surfactants have higher degree of micelle ionization, indicating that the counter ions of the gemini surfactants can be easily replaced by other anionic ions, such as DNA, which is an advantage of phy-3-m used as transgene vectors.

To evaluate transfection ability, transfection assays were carried out in OVCAR-3 cells. Transfection complexes formed by a plasmid pVGteIRL, coding enhanced green fluorescence protein (EGFP) gene, phy-3-m, and a neutral lipid, 1,2-Dioleoyl-*sn*-glycerophosphatidylethanolamine (DOPE), at the charge ratios (+/-) of 2:1, 5:1, 10:1, and 20:1, were incubated with OVCAR-3 cells. Treated cells at all charge ratios except 20:1 showed EGFP signals under fluorescence microscopy. Meanwhile, EGFP expression and cell toxicity was quantified using fluorescence-activated cell sorting (FACS). For each gemini surfactant complex, the transfection efficiency and cytotoxicity go through a maximum, occurring at different values of the charge ratio. Considering both transfection efficiency and cytotoxicity, the optimal charge ratio to formulate the complexes containing phy-3-m was found to be 5:1 for *in vitro* transfection. Compared to a positive control, 16-3-16, phy-3-m showed higher transfection ability and lower cytotoxicity to OVCAR-3 cells.

Initial characterization of transfection complexes was investigated by measuring particle size and zeta potential. At all charge ratios, transfection complexes were positively charged, and greater than +30 mV at 5:1 and 10:1, indicating that the complexes would be stable in solution at the ratio above 2:1. Transfection complexes were larger at lower charge ratio, but particle size dropped with increasing charge ratio (+/-). Comparing particle size and zeta potential with transfection efficiency, no correlation between size/zeta potential and transfection ability was observed. The larger particles may enter cells through caveolin-mediated pathway or phagocytosis, and smaller ones through a clathrin-mediated endocytosis.

In addition, phase structures of the complexes were investigated using small angle X-ray scattering (SAXS). The complexes containing phy-3-m gemini surfactants were found to be able to adopt multiple phase structures, such as L_{α} , H_{II} , and other highly ordered unidentified phase structures. By contrast, L_{α} structure was dominant in the transfection complexes formed by 16-3-16. The ability of phy-3-m system to adopt multiple phases appears correlated with their higher transfection efficiency in OVCAR-3 cells.

Acknowledgements

First and foremost, I would like to thank my supervisor, Dr. Shawn Wettig for his professional support and guidance. I appreciate his patience and encouragement over the years. He is one of greatest mentors I ever met!

I would like to thank the committee members, Drs Roderick Slavcev, Shirley Tang, and Adrian Schwan, for their advice and helpful discussion on my research. Special thanks go to Dr. Roderick Slavcev for providing the plasmid for this study.

I thank Dr. Michael Chong (Chemistry, University of Waterloo) for his assistance with the synthesis of phytanyl bromide; Dr. Eric Prouzet (Chemistry, University of Waterloo) for the use of the SAXS instrument; Dr. Marianna Foldvari (School of Pharmacy, University of Waterloo) for providing the TEM images; Dr. Jamie Joseph (School of Pharmacy, University of Waterloo) for his technical assistance with the use of fluorescence microscopy; Janet Venne (Chemistry, University of Waterloo), Mishi Savulescu (Biology, University of Waterloo) for the assistance of NMR and FACS analysis, respectively.

I thank all Wettig's group members and special thanks go to Tanya Sheinin, Javed Akbar, Tranum Kaur, Naser Tavakoli and Samantha Shortal for their help and support.

Finally, I would like to thank my family and friends for their support.

Dedication

I dedicate this work to my husband, Xi Chen.

Table of Contents

AUTHOR'S DECLARATION	ii
Abstract.....	iii
Acknowledgements.....	vi
Dedication.....	vii
Table of Contents.....	viii
List of Figures	xi
List of Tables	xiii
List of Schemes	xiv
List of Abbreviations.....	xv
Chapter 1 Introduction	1
1.1 Gene therapy.....	1
1.2 Gene delivery vectors	4
1.2.1 Naked DNA	4
1.2.2 Viral vectors.....	6
1.2.3 Non-viral vectors	8
1.3 Barriers involved in lipid-based gene delivery system	25
1.3.1 Cellular binding.....	25
1.3.2 Cellular uptake	27
1.3.3 Endosome escape.....	28
1.3.4 Nuclear entry	30
1.3.5 Summary	31
1.4 Gemini surfactants.....	32
1.4.1 Molecular structure and properties of gemini surfactants	34
1.4.2 Interaction between cationic gemini surfactants and DNA.....	41
1.4.3 Gemini surfactants and gene transfection	46
Chapter 2 Hypothesis and Objectives.....	56
2.1 Basis for rational design of novel gemini surfactants.....	56
2.2 Hypothesis.....	58

2.3 Objectives	60
Chapter 3 Synthesis and characterization of phytanyl substituted gemini surfactants for gene delivery	62
3.1 Introduction	62
3.2 Methods and Materials	63
3.2.1 Synthesis of phytanyl bromide.....	63
3.2.2 Synthesis of phy-3-m (m = 12, 16, and 18)	64
3.2.3 Synthesis of the protected spacer (N-2-(tert-butyloxycarbonyl) amino-N,N-bis(3-(dimethylamino)propyl)-acetamide)	65
3.2.4 Synthesis of phy-7NH-m (m = 12, 16, and 18)	66
3.2.5 Characterization of the phytanyl substituted gemini surfactants.....	67
3.2.6 <i>In vitro</i> transfection	70
3.3 Results and Discussion	72
3.3.1 Krafft temperature (T_k).....	72
3.3.2 Surface tension and head group area	75
3.3.3 Conductivity measurement.....	80
3.3.4 Aggregate shape and particle size of the phytanyl substituted surfactants	84
3.3.5 Preliminary investigation on transfection activity of the phytanyl substituted gemini surfactants	88
3.4 Conclusions	90
Chapter 4 Transfection and structural properties of phytanyl substituted gemini surfactant-based vectors for gene delivery	91
4.1 Introduction.....	91
4.2 Methods and Materials	92
4.2.1 The preparation of the plasmid.....	92
4.2.2 OVCAR-3 Cell preparation	93
4.2.3 Transfection assay	93
4.2.4 Fluorescence microscopy.....	94

4.2.5 Fluorescence activated cell sorting (FACS).....	94
4.2.6 Characterization of the transfection complexes.....	95
4.2.7 Small angle X-ray scattering (SAXS).....	96
4.2.8 Statistical analysis	98
4.3 Results and Discussion	98
4.3.1 Evaluation of transfection efficiency <i>in vitro</i>	98
4.3.2 Characterization of transfection complexes (size and zeta potential).....	107
4.3.3 Structures investigation using SAXS	111
4.4 Conclusions	118
Chapter 5 Conclusions and future perspectives	120
References	125
Appendices	138

List of Figures

Figure 1.1 Summary of various steps involved in an ideal delivery vector.....	3
Figure 1.2 Chemical structures of the cationic lipids with 0, 1, 2, or 3 double bonds. ⁷⁹	19
Figure 1.3 Schematic pictures of the Lamellar (left) and inverted hexagonal (right) phase structures of lipoplexes. ⁹⁶	22
Figure 1.4 The molecular structure of SAINT-2	27
Figure 1.5 Scheme for gemini surfactant structure (left) and structure of the m-s-m gemini surfactant (right).	32
Figure 1.6 Schematic pictures of lyotropic mesophases in surfactant-water mixtures.	36
Figure 1.7 The CMC values as a function of the number of carbon atoms in the spacer of 12-s-12 ($2 \leq s \leq 16$). Adapted from Zana et al. ¹⁵⁷	40
Figure 1.8 Effect of 12-s-12 ($s = 3, 4, 6, 8, 10, 12,$ and 16) on the transfection of PAM 212 cells with pGTmCMV.IFN-GFP plasmid. Adapted from Badea et al. ¹⁸⁷ ...	52
Figure 1.9 Chemical structures of 12-s-12 with nitrogen-substituted spacers. ¹⁹³	54
Figure 3.1 Conductance vs. temperature behavior of surfactant solutions: 16-8-16 (●) and 12-16-12 (Δ). The Krafft temperatures (T_K) were indicated by the arrows. ²⁰¹	69
Figure 3.2 Determination of the Krafft temperature of the phy-3-m ($m = 16$ and 18).	73
Figure 3.3 Surface tension vs. Log concentration for the phy-3-12 at 25 °C , phy-3- 16 at 50 °C, and phy-3-18 at 65 °C.....	76
Figure 3.4 Variation of the logarithm cmc as a function of alkyl tail length for the gemini surfactants: m-3-m (□, data from reference ⁴⁴) phy-3-m (O,); <i>m</i> -6-6 (Δ, data from reference ²⁰⁷).	78
Figure 3.5 Specific conductivity vs. concentration for phy-3-12 at 25 °C, phy-3-16 at 50 °C, and phy-3-18 at 65 °C.....	81

Figure 3.6 Variations of degree of micelle ionization (α) with alkyl tail length of $C_mH_{2m+1}(CH_3)_3N^+Br^-$ at 25°C (data from reference ²¹⁶).....	83
Figure 3.7 Transmission electronic micrographs of phy-3-12 (upper) and 12-3-12 (lower), bar represents 50 nm.....	87
Figure 3.8 <i>In vitro</i> transfection of OVCAR-3 cells with plasmid-gemini surfactant-DOPE complexes.....	89
Figure 4.1 A classical cell for measuring zeta potential. ²²¹	96
Figure 4.2 EGFP images for non-treated cells (a), cells treated with plasmid only (b), cells treated with Lipofectamine TM 2000 (c), and cells treated with complexes comprised of phy3-16, plasmid, and DOPE at charge ratios of 2:1 (d), 5:1 (e), 10:1 (f), and 20:1 (g). The bright spots represent live cells expressing EGFP.	99
Figure 4.3 FACS dot plots for OVCAR-3 cells: untreated (a), cells treated with plasmid only (b), Lipofectamine TM 2000 (c), and phy-3-16 at charge ratios of 2:1 (d), 5:1 (e), 10:1 (f), and 20:1 (g)	101
Figure 4.4 EGFP expression in OVCAR-3 cells was quantified by FACS. (A) The cells were transfected by the complexes composed of the gemini surfactant, pVGtelRL, and DOPE at charge ratio of 2:1, 5:1, 10:1, and 20:1, respectively.	104
Figure 4.5 Cell viability for OVCAR-3 cells (expressed as percentage of viable cells) varied with charge ratios for the transfection complexes containing phy-3-12 (■), phy-3-16 (●), phy-3-18 (▲), or 16-3-16 (○).	106
Figure 4.6 Two main endocytotic pathways for lipoplexes: clathrin-mediated and caveolin-mediated endocytosis. ¹¹⁹	108
Figure 4.7 SAXS profiles of the lipid mixture of DOPE and 16-3-16 (A), and the complexes formed phy-3-12 (B), phy-3-16 (C), phy-3-18 (D), or 16-3-16 (E), plasmid, and DOPE, at the charge ratios of 2:1, 5:1, and 10:1.	113

List of Tables

Table 1.1 The structure of common studied cationic polymers used for gene delivery.	9
Table 1.2 Common cationic lipids used for gene delivery. ⁴⁵	15
Table 1.3 Common helper lipids used for gene delivery.	23
Table 1.4 Packing parameter and expected aggregate shape. ¹⁴⁹	35
Table 1.5 Molecular structures of peptide-based and sugar-based gemini surfactants	48
Table 2.1 Gemini surfactants used in the project.	61
Table 3.1 The Krafft temperature (T_K) and Krafft point (T_P) of the gemini surfactants	74
Table 3.2 Critical micelle concentration (CMC) and head group area (a_0) obtained by surface tension measurements.	79
Table 3.3 Critical micelle concentration (CMC) and degree of micelle ionization (α) obtained from conductivity measurements.	84
Table 3.4 Calculated packing parameter (P) and measured particle sizes (diameter, d) for the phy-3-m and m-3-m (m=12, 16, and 18).	85
Table 4.1 Size and zeta potential measurements of the transfection complexes at different charge ratios of gemini surfactants to DNA.	109
Table 4.2 Structural parameters and possible phase structures of the complexes composed of gemini surfactant, plasmid, and DOPE, at different charge ratios. ...	115

List of Schemes

Scheme 3.1 Synthesis of phytanyl bromide.	64
Scheme 3.2 Synthesis of phy-3-m (m = 12, 16, and 18).	65
Scheme 3.3 Synthesis of phy-7NH-m (m=12, 16, and 18).	67

List of Abbreviations

12-3-12	1,3-propanediyl-bis(dimethyldodecylammonium) dibromide
16-3-16	1,3-propanediyl-bis(dimethylhexadecylammonium) dibromide
18-3-18	1,3-propanediyl-bis(dimethyl-octadecylammonium) dibromide
α	degree of micelle ionization
a_0	head group area
BOC	tert-butoxycarbonyl
CHO	Chinese hamster ovary
CMC	Critical Micelle Concentration
COS	CV-1 in Origin, and carrying the SV40
Dc-chol	3 β -[N-(N',N-dimethylethylenediamine)-carbamoyl] cholesterol
DMEM	Dulbecco's Modified Eagle's Medium
DNA	deoxyribonucleic acid
DOGS	dioctadecyl amini glycil spermine
DOPC	1,2-dioleoyl- <i>sn</i> -glycero-3-phosphocholine
DOPE	1,2-Dioleoyl- <i>sn</i> -glycerophosphatidylethanolamine
DOSAP	2,3-dioleyloxy-N-[2-(sperminecarboxamido)ethyl]-N,N-dimethyl-1-propanaminium
DOTAP	1,2-dioleoyl-3-trimethylammonium propane
DOTMA	N-[1-(2,3-dioleyoxy)propyl]-N,N,N-trimethylammonium chloride
DSC	differential scanning calorimetry
EGFP	enhanced green fluorescent protein
EM	electron microscopy
EO	oxyethylene

FACS	fluorescence activated cell sorting
FBS	fetal bovine serum
GFP	green fluorescence protein
H _I	the hexagonal phase
H _{II}	the inverted hexagonal structure
HSPGs	heparan sulfate proteoglycans
IFN- γ	Interferon-gamma
ITC	isothermal titration calorimetry
L _{α}	lamellar structure
mM	millimolar concentration
OVCAR-3	ovarian carcinoma
P	packing parameter
PAMAM	polyamidoamine
PBS	phosphate buffered saline
PEG	polyethylene glycol
PEI	polyethylenimine
Phy-3-12	N ¹ -dodecyl,N ¹ ,N ¹ ,N ³ ,N ³ -tetramethyl-N ³ -(3,7,11,15-tetramethylhexadecyl) propane-1,3-diammonium dibromide
Phy-3-16	N ¹ -hexadecyl,N ¹ ,N ¹ ,N ³ ,N ³ -tetramethyl-N ³ -(3,7,11,15-tetramethylhexadecyl) propane-1,3-diammonium dibromide
Phy-3-18	N ¹ -(3,7,11,15-tetramethylhexadecyl),N ¹ ,N ¹ ,N ³ ,N ³ -tetramethyl-N ³ -octadecyl propane-1,3-diammonium dibromide
PI	propidium iodide
PLL	poly (L-lysine)
q	scattering vector

RPMI	Roswell Park Memorial Institute
SAXS	small angle X-ray scattering
Γ	surface excess concentration
TEM	Transmission Electron Microscopy
T_K	Krafft temperature
T_P	Krafft point
γ	surface tension values

Chapter 1 Introduction

1.1 Gene therapy

Gene therapy is usually defined as the treatment of human disease by transferring genetic material into target cells or tissues. With advancements in life science, biotechnology, and the significant achievements in the Human Genome Project, a number of disease-related genes have been identified. Gene therapies involve the replacement of errant genes within the affected cells, or the delivery of genes to enhance native proteins in the human body, alter the expression of existing genes, or produce cytotoxic proteins or enzymes to kill tumor cells.

To date, gene therapy has been experiencing a number of major developments. Researchers have been trying to improve gene therapy efficiency and reduce cytotoxicity in normal tissue through numerous approaches. The first clinical trial of gene therapy was performed on two children in the United States in 1990.¹ Using a retroviral vector, the adenosine deaminase (ADA) gene was transferred into the T cells of two children with severe ADA deficiency. Gene treatment was ended after 2 years. This trial showed the great potential efficacy of using gene-corrected autologous cells for treating children with ADA deficiency. The safety problems that were observed in later trials had not appeared in such a short term study with few patients.

The use of cationic lipids as a deliver vector in a clinical trial was initiated in 1993.² Nabel and colleagues tried to introduce a gene encoding a protein (HLA-B7) into

HLA-B7-negative patients with advanced melanoma by injecting DNA-liposome complexes. The plasmid DNA was detected in the treated tumor nodules after the injection; the recombinant protein (HLA-B7) was observed in the tumor tissue; and no antibodies to DNA were detected in the patients. This study demonstrated the feasibility, safety, and potential of gene transfer by using liposomes in humans. In 2003, a research team successfully inserted genes into the brain using modified liposomes which shows the potential to treat Parkinson's disease.³ At the same time, the first gene therapy product was approved by the Chinese Drug Regulatory Agency, under the trade name Gendicine, consisting of an adenovirus-based delivery system that can insert the p53 (tumor suppressor protein) gene into tumor cells.⁴ Clinical trials using Gendicine showed complete tumor regression.⁵ Advexin™ is another gene therapy product based on the p53 expression.⁶ In 2006, Oncorine™, developed by Shanghai Sunway Biotech, has entered the market.⁶ In 2012, a gene therapy treatment was approved by European Medicines Agency, under the trade name Glybera, which is the adeno-associated virus based vector for the treatment of the human lipoprotein lipase deficiency.⁷ To date, a number of genes and delivery vectors have been developed and evaluated. Approximately 1340 gene therapy clinical trials had been completed by 2007 and over 800 clinical trials in gene therapy have been aimed at cancer treatment.⁵ Unfortunately, the number of successful treatments observed in clinical trials has been few.

For the potential of gene therapy to be realized, there are numerous factors to be considered. The therapeutic gene introduced into target cells must be active and the

cells must be stable and long-lived. In addition, gene therapy requires the delivery of a gene to target cells with high efficiency. Gene delivery vectors must be stable (in particular within the blood stream), must be able to cross membrane barriers including blood vessels and other tissues, and should specifically bind to the target cells. Therefore, the optimization of the delivery system has become a key step in the development of a safe and efficient human gene therapy. An ideal gene delivery system, described by Figure 1.1, should 1) transport the DNA across the plasma membrane and into the nucleus of target cells; 2) protect the therapeutic gene from degrading by serum and nucleases; 3) release the therapeutic gene easily in the

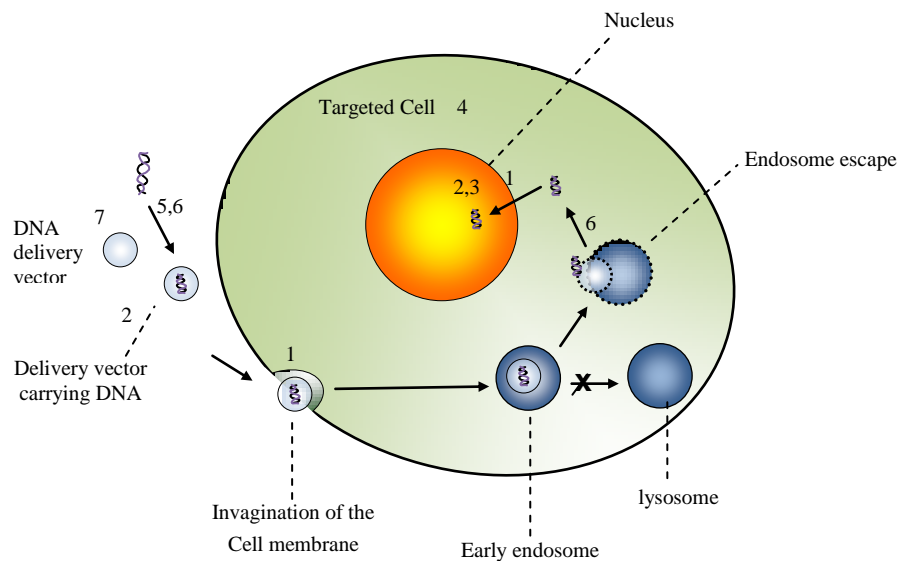


Figure 1.1 Summary of various steps involved in an ideal delivery vector. These steps are: 1) transport the DNA across the plasma membrane and into the nucleus of target cells; 2) protect the therapeutic gene from degrading by serum and nucleases; 3) release the therapeutic gene easily in the nucleus; 4) target specific cells of interest; 5) be easily formulated and cost-effective to synthesize; 6) efficiently compact any size of DNA and unpack the DNA inside the cells; and 7) have low immunogenicity and cytotoxicity.

nucleus; 4) target specific cells of interest; 5) be easily formulated and cost-effective to synthesize; 6) efficiently compact any size of DNA and unpack the DNA inside the cells; and 7) have low immunogenicity and cytotoxicity.

1.2 Gene delivery vectors

Gene delivery vectors can be divided into three major categories: naked DNA or plasmid delivered by physical transfer techniques, such as the gene gun, needle injection, and electroporation; viral vectors, such as adenovirus, retrovirus, assisted-adenovirus, among others; and nonviral vectors, including those formed from cationic polymers and cationic lipids. Each gene delivery system will be described in more detail below.

1.2.1 Naked DNA

Naked DNA or plasmid DNA can be directly injected into a target tissue or cell without the need of any additional delivery vector. Direct injection has been used in muscle,⁸ liver,^{9, 10} skin,¹¹ or lung tissues.¹² The method is simple (although time-consuming) and less toxic to cells; however, gene delivery with naked DNA leads to a very low gene expression because the negatively charged DNA is generally repelled from the negatively charged cell membrane. There is also difficulty in passing through nuclear pores **if** entry into the cells is achieved. In addition, the large DNA molecules are easily bound by blood serum albumin and other negatively charged proteins, leading to the removal by phagocytic cells and the

reticuloendothelial system,¹³ or the naked DNA is degraded by nucleases which reduce the chance of DNA entering the nucleus.¹⁴

Naked DNA has also been introduced into cells by employing mechanical and electrical strategies, such as the gene gun and electroporation. In the gene gun method, DNA is deposited on the surface of gold particles, then accelerated by compressed gas into cells or tissues.¹⁴ Disadvantages of this method include: the gold particles can only penetrate a few millimeters deep into tissue; the nano-sized particles are limited in terms of the size of DNA that can be carried; and there are inconsistencies in the coating of the gold particles by DNA. Advantages of the gene gun method are that it is simple to operate and effective in delivering genes.

Electroporation, commonly used *ex vivo*, has been extensively used in many types of tissues, such as skin¹⁵ and muscles.¹⁶ Compared to direct injection of naked DNA, the reported gene expression obtained from such a strategy has been observed to be 2 to 3 orders of magnitude higher.¹⁷ It has also been reported that large plasmids (i.e. 100 kilobase pairs) can be effectively delivered into muscle cells.¹⁸ However, several drawbacks exist with respect to the *in vivo* application of electroporation. It is only effective on a limited range of tissue between two electrodes, and is also invasive. Before electroporation, a procedure is required to insert two electrodes into the target internal organs. The high voltage applied to the tissue can result in the damage of the tissue because of the thermal heating.¹⁹ Although transfection efficiencies are significant using the gene gun or electroporation, they are difficult to

standardize in human clinical trials and are considered laborious and impractical.²⁰ Therefore, these types of techniques will likely be unsuccessful in the long term.

1.2.2 Viral vectors

In viral delivery vectors, the therapeutic gene is assembled in the viral genome and the virus then uses its own infection mechanisms to enter target cells and release the transgene in the cytoplasm. The gene is then transported to the nucleus of the host cells through cytoskeletal transport, transcription factors, and importins, and is eventually expressed.²¹ Viruses such as adenovirus, retrovirus, and adeno-associated virus, are most commonly being used to transfer DNA, although there are others. Viral vectors are capable of delivering transgenes to numerous cell lines with high transfection efficiency; currently, viral vectors are used in more than 70% of human clinical gene therapy trials,⁵ such as commercially available gene therapy products, GendicineTM, AdvexinTM, and OncorineTM, and a recently approved product, GlyberaTM.

Compared to other delivery vectors, the most significant advantage of viral vectors is their very high transfection efficiency. To date, more than 50 human and many nonhuman subgenuses of the adenovirus have been used to mediate gene delivery to a wide range of tissues, such as eye, liver, urinary tract,²²⁻²⁴ etc. Adeno-associated viruses have become ideal candidates for gene delivery because these vectors can mediate long-term gene expression in many dividing and non-dividing cells *in vivo*.^{25 26} Retroviruses are a family of enveloped viruses with a singled

stranded RNA genome.²⁷ To date, around 45%-95% of primary human endothelial and smooth muscle cell types, some of which are extremely difficult to transfect, have been transfected by retroviral vectors.²⁸

Despite such a large advantage in terms of increased transfection efficiencies, several significant limitations in use of viral vectors exist. The primary concern is that of safety, and the potential of a strong immune response caused by the viral capsid proteins.²⁹⁻³¹ Jessi Gelsinger was unfortunately the first person to die in a clinical trial for gene therapy in 1999. He joined a clinical trial run by the University of Pennsylvania and was treated with an adenoviral vector carrying a gene to correct ornithine transcarbamylase (OTC) deficiency in order to test the safety of the vector and the gene therapy protocol. He died four days later as a result of a massive immune response triggered by the use of the viral vector, resulting in multiple organ failure and brain death.³² The decision to include Jessi in the trial was strongly criticized since the disease had been well controlled.

In addition to an immune response, insertion mutation can occur, and possibly results in genetic disorders if the transgene is not inserted in the DNA sequence accurately. Retroviral gene therapy used to treat X-linked severe combined immunodeficiency (X-SCID) has been the most successful application of gene therapy so far.³³ An unfortunate outcome of this trial was that several children have developed leukemia as a result of insertion mutation by the retroviral vector.³⁴ Other factors also limit the use of viral vectors for gene therapy, such as a limit in the size of the therapeutic gene to carry because the viral envelope has a finite capacity,³⁵

and the significant costs associated with the scale-up and production of viral vectors.³⁶ Given these concerns, alternatives to viral vectors are in high demand, driving research into the development of highly efficient non-viral vectors.

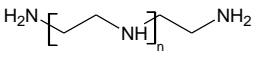
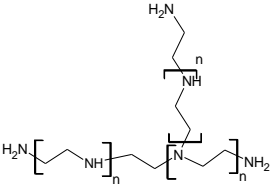
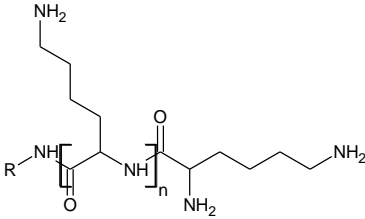
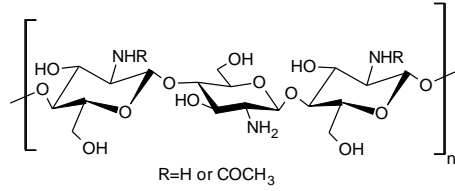
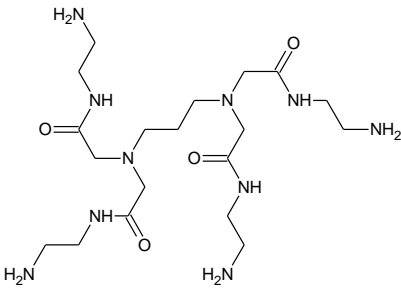
1.2.3 Non-viral vectors

As stated above, non-viral vectors are generally comprised of cationic polymers or cationic lipids, and may include additional polymers or lipids to improve their overall efficiency. These vectors rely on the electrostatic interaction between the cationic lipid or polymer and the anionic DNA to efficiently compact and deliver the DNA into cells. Non-viral vectors, generally, have much lower immunogenicity and cytotoxicity than viral vectors; there is no limitation on the size of DNA that can be delivered; and they can be manufactured and stored easily using standard good manufacturing practice (GMP) methods.^{37, 38}

1.2.3.1 Cationic polymers

Currently, the most widely studied polymers for gene delivery include polyethylenimine (PEI), poly (L-lysine) (PLL), chitosan, and polyamidoamine (PAMAM) dendrimers (Table 1.1). The complex formed by cationic polymers and DNA is called a polyplex. Cationic polymers bind DNA with certain functional groups, such as primary, secondary, and tertiary amines. Due to the abundance of amine groups within the structure of the polymers, a very popular mechanism for polyplexes escaping endosomes, called the proton-sponge hypothesis, has been proposed.³⁹⁻⁴¹ The proton-sponge mechanism is described as following.

Table 1.1 The structure of common studied cationic polymers used for gene delivery.

Generic name	Chemical name	Chemical structure
PEI	Polyethylenimine	linear 
		branched 
PLL	Poly(L-lysine)	
Chitosan		 R=H or COCH ₃
PAMAM	Polyamidoamine dendrimer	
		Generation-0, PAMAM

At physiological pH, amines of proton-sponge polymers, such as PEI and chitosan, are not fully charged, but they are protonated in endosomes because of acidic conditions that exist in endosomes. Endosomes are acidified through an ATPase enzyme that actively transports protons from the cytosol into the endosomes. Due to the protonation of the polymers, larger quantities of protons are pumped into endosomes to reach the endosomal pH. The accumulation of protons in the endosomes must be balanced by chloride ions and the increased chloride ion concentration raises the osmotic pressure, causing osmotic swelling and rupture of the endosome membranes, thus releasing the polyplexes into the cytosol. The hypothesis has been quantitatively verified through comparing the transfection activity before and after the removal of protonable amines.^{39, 40, 42}

PEI is one of the most popular cationic polymers capable of gene transfection. Transfection efficiency is reported to increase with increased molecular weight.⁴³ The most active PEI reported has a molecular weight of 25 kDa, but also shows high cell toxicity. Compared to PEI, PLL exhibits lower transfection efficiency mostly because of the lack of rapid release of the complexes from the endosomes. All primary amino groups of PLL are already protonated at physiological pH, thus no proton sponge mechanism occurs in endosomes.⁴⁴

Chitosan, a naturally occurring polymer, is a linear polysaccharide and produced by the deacetylation of chitin.⁴⁵ Due to its biodegradability, biocompatibility, and low toxicity, chitosan has become an attractive component for non-viral vectors. It has been shown that the molecular weight of chitosan can strongly affect gene

transfection efficiency.⁴⁶ Chitosan with high molecular weight can form more stable complexes with DNA due to a chain entanglement effect which is defined as an effect that polymer molecules with long chains can become entangled with one another.⁴⁷ In addition, transfection efficiency increases with the molecular weight of chitosan because the high molecular weight polymers can entrap DNA more efficiently than low molecular weight polymer does. Chitosan with lower molecular weight was reported to be less efficient at retaining the DNA upon dilution, which results in it being less capable of protecting the condensed DNA from the degradation by DNase and other serum component.⁴⁸

Another novel class of macromolecular polymers called “dense star” polymers are the polyamidoamine dendrimers. Dendrimers are highly symmetric, spherically shaped compounds, and are dominated by specific functional groups on the surface, such as amino acid residues which can complex with DNA. Bielinska et al. showed that transfection efficiency was influenced by both the dendrimer-DNA charge ratio and the dendrimer generation.⁴⁹ At a charge ratio less than 1, the DNA-polymer complexes are soluble but do not compact; at charge ratios between 1 and 100, insoluble complexes are formed; and at higher charge ratios (greater than 100), resolubilization occurs.⁵⁰ The higher generation structures were more efficient in condensing DNA because the dendrimers of higher generation contain larger fractions of tightly bound DNA regions.⁵¹

1.2.3.1.1 Strategies for improving cationic polymer mediated gene delivery

To improve cationic polymer mediated gene transfection, various strategies have been investigated, such as PEGylation, copolymer synthesis, and other chemical modifications. PEGylation is the most common modification, which conjugates polyethylene glycol (PEG) to cationic polymers. This modification can increase both the stability of polyplexes and circulation time by reducing the interaction of the polyplexes with serum proteins and other blood components.⁴⁵ It has been shown that a high density of relatively short PEG grafted onto PEI achieved an extremely significant DNA transfection.^{52, 53} Similarly, Kim et al. showed that the attachment of PEG to PAMAM significantly improved gene transfection efficiency and lowered the cytotoxicity.⁵⁴ Although PEGylation is helpful in increasing the stability of polyplexes, the conjugation of PEG to polymers may decrease the surface charges that can lead to reduced interaction with the cell membrane, lowering the cellular uptake of the polyplexes.⁵⁵

In addition to using PEGylated polymers, improvements have been observed using other copolymer synthesis. The conjugation of chitosan and polylysine showed increased transfection efficiency and reduced toxicity compared to chitosan and polylysine individually.⁵⁶ It was shown that the copolymer can bind and condense plasmid DNA much better than the individual polymers, which contributed to the enhanced transfection efficiency. Another study reported a copolymer of PAMAM-PLL which showed a better ability to bind and condense DNA with the PLL moiety, and an increased buffering capacity to facilitate endosomal release offered by the PAMAM segment.⁵⁷

Another strategy used to improve cationic polymer mediated transfection is to modify the chemical structure of the cationic polymer. To increase charge density, the quaternized modification of chitosan, such as trimethylated chitosan, was examined, resulting in improved transfection efficiency but with increased cytotoxicity.^{58, 59} To improve transfection efficiency, the amine functionality of PEI has been modified. By linking cholesterol to the secondary amine groups of PEI, Wang et al.⁶⁰ found that the modified PEI with low molecular weight showed increased transfection efficiency and reduced toxicity. The authors believe that the conjugation through the secondary amines gives the modified PEI special advantage because the free primary amino groups have a significant role in DNA condensation. Also, the conjugation leaves enough space for the steric interactions of the PEI's primary amines with the DNA. It has been reported that a modified PAMAM having a more flexible structure was developed which also showed improved transfection efficiency. This result was attributed to a more efficient endosomal release resulting from the flexible structure.⁴⁵ Some of the modified PAMAM polymers have become commercial products, such as Superfect and Polyfect (Qiagen), used as standards in gene transfection assay for comparison.⁶¹

1.2.3.2 Cationic lipids

A cationic lipid consists of a cationic head group, usually two hydrophobic moieties, and the linker between two portions. Since the first cationic lipid, N-[1-(2,3-dioleoyloxy)propyl]-N,N,N-trimethylammonium chloride (DOTMA), was reported to transfect cells *in vitro* in 1987,⁶² a number of cationic lipids have been designed and

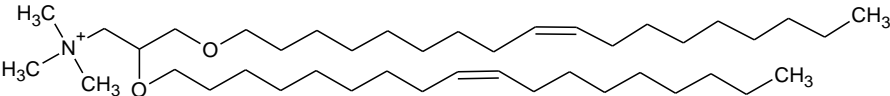
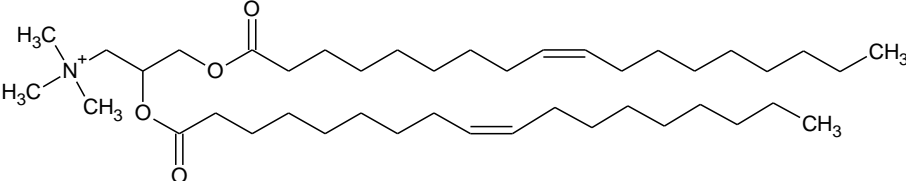
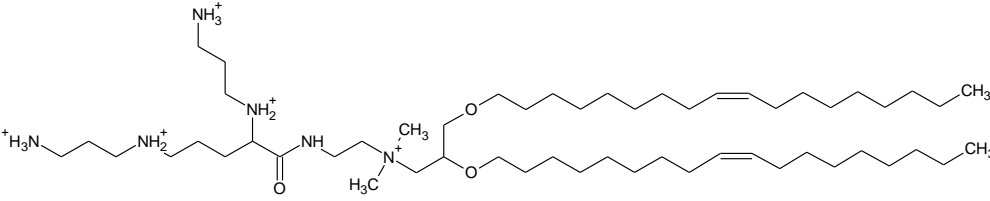
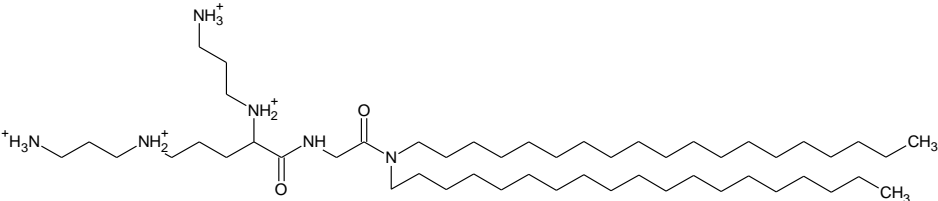
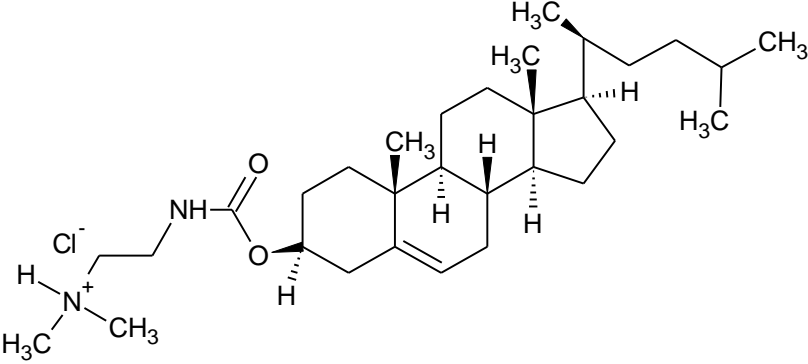
developed for gene therapeutics. The commonly used cationic lipids include 1,2-dioleoyl-3-trimethylammonium propane (DOTAP), DOTMA, 2,3-dioleoyloxy-N-[2-(sperminecarboxamido)ethyl]-N,N-dimethyl-1-propanaminium (DOSPA), dioctadecyl amido-glycylspermine (DOGS), and 3β -[N-(N', N'-dimethylaminoethane)-carbamoyl] cholesterol (DC-chol). Their chemical structures are shown in Table 1.2. These lipids differ in the number of charges in their hydrophilic head group and/or in the structure or length of their hydrophobic tail groups. The chemical structure of cationic lipids plays an important role in transfection efficiency. The effect of variations in these groups with respect to transfection efficiency is discussed in more detail below.

1.2.3.2.1 Effect of head-group structure

The density and nature of the head group has been shown to influence gene transfection efficiency.^{45, 63} In general, lipids with multivalent head groups and long, unsaturated hydrocarbon tails show more efficient transfection than those with monovalent head group and the same length and type of hydrocarbon tails. The multivalent lipids increase DNA binding and thus significantly enhance lipid-mediated gene delivery.^{45, 64} The commercial product, Lipofectamine™ 2000 (Invitrogen), consisting of DOSPA with five quaternary ammonium groups in the head portion, is an example of a vector incorporating such lipids.⁶⁵

While DNA binding increases with an increased number of cationic groups within the head group, it has also been shown that the spacing between the ammonium groups of a multivalent head group strongly influences transfection efficiency.

Table 1.2 Common cationic lipids used for gene delivery.⁴⁵

Generic name	Chemical structure
DOTMA	
DOTAP	
DOSPA	
DOGS	
DC-Chol (HCl salt)	

For cationic lipids with a tetraammonium head group, a decrease in the spacing between ammonium groups from four to two methylene groups resulted in reduced transfection activity. The results showed that at a neutral pH, the positive charges of the cationic lipids with a spacing of four and two methylene groups were 2.4 and 1.8, respectively. The authors believe that the significantly different positive charge distribution caused by the different methylene spacing may result in the significant difference of the transfection efficiency observed in the study.⁶⁶

In addition to the effect on positive charge distribution, the spacing between head groups influences the lipid structures, resulting in different transfection activity. To design cone-shaped vectors as a means of inducing the formation of inverted hexagonal structures, Gaucheron et al. synthesized tetraalkylated cationic lipids.⁶⁷ Two derivatives of the cationic lipid N,N-dioleoyl-N,N-dimethylammonium chloride (DODAC), have been synthesized: N,N,N',N'-tetraoelyl-N,N'-dimethyl-1,3-propanediammonium chloride (TODMAC3) and N,N,N',N'-tetraoelyl-N,N'-dimethyl-1,6-hexanediammonium chloride (TODMAC6), which has three and six methylene groups between the ammonium head groups, respectively. It was found that when mixing with anionic lipids, TODMAC6 was more prone to forming nonbilayer structures than TODMAC3. Also, TODMAC6 showed greater transfection capacity than TODMAC3.⁶⁷ This observation is also found in the gemini surfactants with one N-CH₃ substitution in the spacer: 12-5N-12 and 12-7N-12. SAXS profiles obtained from the complexes containing 12-5N-12 showed a lamellar structure, while an additional unidentified phase was observed in the complexes containing 12-7N-12.

This may explain why 12-7N-12 demonstrated a higher luciferase expression in COS7 cells than 12-5N-12 did. It is believed that lipoplexes with nonlamellar phase structures are more amenable to membrane fusion with endosomal lipid components. This facilitates the DNA release from lipoplexes and thus leading to a higher transfection efficiency.

In addition, the modification of the head group of monovalent phospholipids by replacing the ammonium group with different monovalent cationic moieties has been investigated. Gene transfection has shown that phospholipids with arsonium (As) and phosphonium (P) ions achieve significantly lower cytotoxicities than the ammonium (N) analogues.⁶⁸ The reduced toxicity was attributed to the increased atomic radii of As and P compared to N. The replacement of the ammonium group with As or P may result in the formation of the larger cationic complexes with reduced charge densities.⁴⁵ Another report has shown that surfactants with a cationic pyridinium head group showed 3 to 6-fold higher transfection efficiency *in vivo* than that of Lipofectin, a commercially available cationic lipid which is the mixture of DOTMA and DOPE.⁶⁹ It has been proposed that the higher transfection efficiency would be related to the formation of vesicular aggregates of this type of cationic lipid.⁴⁵

1.2.3.2.2 Effect of tail-group structure

The manipulation of the hydrophobic portion, such as the length or the saturation of tails, also affects the transfection efficiency. The effect of length of the hydrocarbon tails on gene transfection is conflicting. Several studies have shown that gene

transfer increases with reduced chain length;^{70, 71} while a decrease in the carbon length from 18 to 12 resulting in the reduced transfection efficiency was observed in a polyamine lipid⁷² and polylysine based surfactants;⁷³ it has also been reported that there is no correlation observed between lipid chain length and transfection efficiency for lipospermine derivatives.⁶³

Regardless, modification(s) or various alternatives of the alkyl chain(s) have been examined to improve gene transfection. For example, cholesterol and other steroidal groups have been investigated as replacements for the aliphatic tails of lipids because of favorable properties such as their rigidity, biodegradability, and fusogenic capacity^{37, 74}. Cholesterol was first incorporated to form 3 β -[N-(N',N'-dimethylethylenediamine)-carbamoyl] cholesterol (DC-Chol) lipid by Huang et al.,⁷⁵ and subsequently other cholesterol based cationic lipids have been designed and investigated, such as bis(guanidinium)-tren-cholesterol (BGTC) and 3 β -[6'-kanamycin-carbamoyl] cholesterol (KanaChol).^{76, 77} BGTC has been reported to deliver DNA into cells through a different pathway of endosomal escape from other cationic lipids, such as dioleoyl succinyl paramomycin (DOSP).⁷⁸ DNA was dissociated partially or completely from the BGTC before endosomal escape, while for DOSP, DNA release from the lipoplexes may concomitantly escape from the endosomes. These different pathways of endosomal escape could contribute to their difference in transfection efficiency.

The incorporation of unsaturated bond(s) to the hydrophobic portion of the lipids can improve gene transfer by promoting endosomal escape and disassociation of

DNA from the lipoplexes. A series of cationic lipids with 0, 1, 2, or 3 double bonds were synthesized (their structures are listed in Figure 1.2) and the correlation between lipid saturation, phase transition temperature, and transfection efficiency *in vitro* was investigated.⁷⁹ The results have shown that the temperature of phase transitions from the lamellar to inverted hexagonal structures increases with an increase in saturation; and the highest gene expression efficiency was achieved with particles containing lipids with two double bonds; particles containing lipids with 3 unsaturated bonds showed the second highest efficiency; ³¹P-NMR analysis determined that lipids with two double bonds had the lowest phase transition temperature, being the most fusogenic lipid.⁷⁹

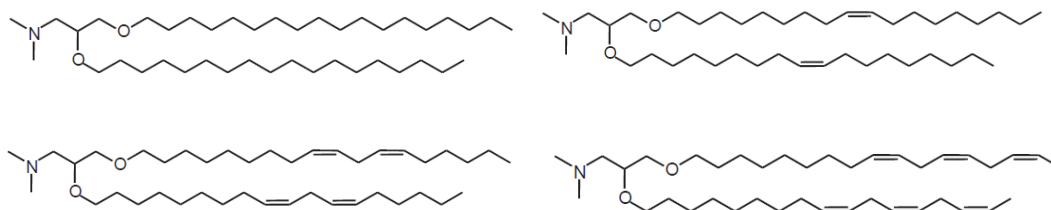


Figure 1.2 Chemical structures of the cationic lipids with 0, 1, 2, or 3 double bonds.⁷⁹

Lipids in which the two alkyl chains are of different length have also been examined. It has been reported that the combination of C₁₂/stearyl or C₁₂/oleoyl may result in vectors with increased fusogenicity, which facilitates endosomal escape.^{71,}

⁸⁰ Asymmetric lipids showed *in vitro* activities superior to the best symmetric analogues;⁸⁰ however, the degree of asymmetry influences gene transfection activity. A small degree of asymmetry (e.g. C₁₂:C₈ and C₁₄:C₈) showed the best *in vitro* activity, while highly asymmetric compounds (C₁₈:C₈) performed poorly.⁸⁰ The

lipid with a high degree of asymmetry ($C_{18}:C_8$) was hypothesized to form micelles instead of bilayer structures. This could lead to its inefficient transfection.³⁷ A conflicting result was obtained for a series of dialkyl lipids containing either C_{12} , C_{14} , C_{16} , C_{18} or C_{oleyl} chains; the best transfection activity was observed for the asymmetric lipids with one tail C_{12} and the other C_{18} or C_{oleyl} .⁷¹ The above results indicate that high transfection efficiency may require both the appropriate degree of asymmetry (increased fusogenicity of lipids) and also the formation of the lipid bilayer structures.

1.2.3.2.3 Lipoplex composition and structure

Typically, lipoplexes are prepared by mixing cationic liposomes and DNA in a buffer solution. The formation of the lipoplex is mainly driven by electrostatic interaction between the positive charged cationic lipid head groups and the negative charged phosphate backbones of DNA.⁸¹ This step is simple but very important in determining the characteristics and transfection efficiency of lipoplexes. Thus, any protocol for lipoplex formation should consider the charge ratio of lipoplex to DNA, incubation conditions (temperature and time), and mixing order.

It is believed that use of an excess of cationic lipids result in a higher transfection efficiency.^{62, 82} This result has been attributed to more efficient interaction between lipoplexes with a net positive charge and the negatively charged cell membrane.⁸³ Lipoplex size has also been shown to be a function of lipid-DNA charge ratios.⁸³⁻⁸⁵ At high charge ratios, lipoplex particles are generally homogeneous and small, while at charge ratios close to neutrality, lipoplexes tend to form larger and less stable

aggregates. Precipitation of lipoplexes has been reported at neutral or a slight excess of positive charge.⁸³⁻⁸⁵

Charge ratio also impacts the extent to which DNA can be condensed and protected against degradation by cellular nucleases. It was reported that the accessibility of ethidium bromide to DNA dropped with increasing of the charge ratios, implying better compaction and protection at higher charge ratios.⁸⁶

Unfortunately, given that the cationic charge carriers in lipids are generally quaternary ammonium groups, lipoplexes prepared at high charge ratios generally also exhibit higher cytotoxicity because of the high number of free quaternary ammonium groups.⁸¹

The structure of lipoplexes has been shown to correlate to gene transfection efficiency. Lipoplex structures have been examined by biophysical and thermal techniques, such as electron microscopy (EM), small angle X-ray scattering (SAXS), differential scanning calorimetry (DSC),⁸⁷⁻⁸⁹ and isothermal titration calorimetry (ITC)^{88, 90} among others. Freeze-fracture EM images have revealed lipoplexes with both spherical structures (representing liposomes) and filamentous structures (representing the DNA surrounded by a lipid bilayer).^{84, 91, 92} SAXS has been applied to investigate lipoplex structures, such as the inverted hexagonal (H_{II}) structure, lamellar (L_{α}) structure, and other highly ordered structures.^{93, 94} Lamellar structures consist of DNA molecules that are sandwiched between lipid bilayers in an alternating fashion. The inverted hexagonal morphology is one where DNA “rods”

are coated with the lipid monolayers which are then arranged on a hexagonal lattice.⁹⁵ Their structures are illustrated in Figure 1.3.

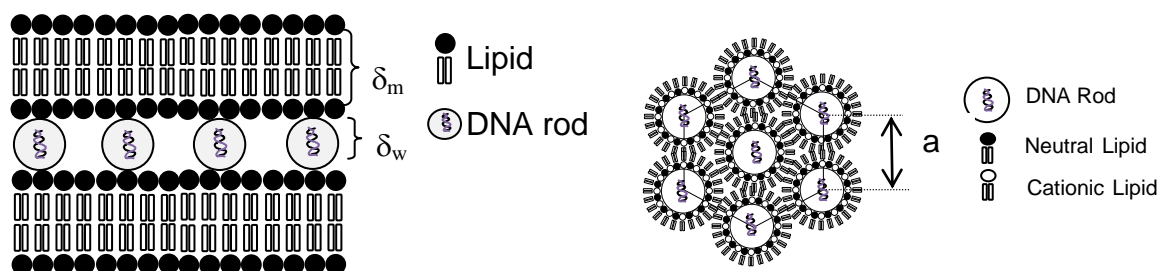


Figure 1.3 Schematic pictures of the Lamellar (left) and inverted hexagonal (right) phase structures of lipoplexes.⁹⁶ The bilayer spacing is δ_m , the spacing for intercalated monolayer of DNA is δ_w , and interlayer spacing for lamellar complexes is $d = \delta_m + \delta_w$. For an inverted hexagonal phase of lipoplexes, a unit cell spacing (a) is the distance between the centers of two neighbouring rods.

Lipoplex structure depends on the structure of a cationic lipid, the charge ratio of lipids to DNA (introduced above), the structure of any helper lipids (the common used helper lipids are listed in Table 1.3), and their mole ratio with respect to the cationic lipid(s). At physiological conditions, most phospholipids adopt a lamellar structure.⁹⁷ Generally, lipids with the L_α crystal structure prefer to form L_α structures within lipoplexes, with the DNA molecules organized between lipid bilayers.^{98, 99} Phospholipids such as DOPE (1,2-dioleoyl-*sn*-glycerophosphatidylethanolamine), with relatively small head groups and longer or unsaturated alkyl chains have a tendency to form the H_{II} phase. DOPE is a helper lipid which is generally used to incorporate with a cationic lipid for gene transfection. DOPE was reported to undergo a phase transition from L_α to H_{II} structures at neutral pH and temperature

above 10-15 °C.¹⁰⁰ Although cationic lipids such as DOTAP and DOTAM, prefer to form L_{α} structures, the incorporation of DOPE with this type of lipids influences the packing geometry and results in a rearrangement of the liposomes. Thus, when mixed with DOPE, phase transitions were observed for DOTMA¹⁰¹ or DOTAP liposomes.¹⁰²

Table 1.3 Common helper lipids used for gene delivery.

Generic name	Chemical structure
DOPE	
DOPC	
Cholesterol	

Additionally, the amount of a neutral lipid can affect lipoplex morphology. Different weight ratios of a cationic lipid to a neutral lipid in liposomes can produce different lipoplex structures. The phase transition from L_{α} to H_{II} can be manipulated in terms of the adjustment of the neutral lipid amount in the total lipids. Koltover et al. investigated lipoplex structures at various concentration of DOPE with a fixed ratio of DOTAP to DNA.⁹⁶ At a weight fraction $DOPE/(DOPE+DOTAP)$ of 0.41, SAXS profiles showed a lamellar morphology; at 0.65, a mixed structure of L_{α} and H_{II} phases was observed; at 0.75, SAXS results showed the H_{II} phase structure only; and at 0.87, the coexistence of the H_{II} lipoplexes and inverted H_{II} pure DOPE was obtained. The phase transition caused by changing the weight ratio of DOPE is believed to be attributed to the interplay between the electrostatic and membrane elastic interactions.¹⁰³ The membrane elastic energy favors a curved interface.^{103, 104} DOTAP, with the head group area roughly equal to the hydrophobic tail area, tends to form lamellar L_{α} structures. While DOPE with larger volume of two chains and smaller head group area, forms an inverted H_{II} phase. The actual curvature of the lipid mixture depends on the fraction of DOPE in the mixture and the natural curvature of DOPE itself. With an increase in the fraction of DOPE in the mixture, the actual curvature is more negative, indicating the membrane elastic energy is dominant. This results in a transition of the lipid mixture from the lamellar to the hexagonal phase. Thus, the manipulation of weight fraction of neutral lipid in the lipid mixture can change the final structure of the lipoplexes formed.

1.3 Barriers involved in lipid-based gene delivery system

Gene delivery vectors face numerous barriers in transporting transgenes from a test tube to a target cell nucleus. The physicochemical properties of the cationic and neutral lipids that comprise the lipoplexes, and properties of lipoplexes themselves influence the ability of lipoplexes to overcome these barriers. Some of the important barriers include stability in the blood serum, targeting to specific cells, the cellular internalization pathway, endosomal escape, and nuclear entry; these will be discussed in detail in the following sections.

1.3.1 Cellular binding

As early steps in the gene transfection process, the mechanism(s) by which lipoplexes bind to the cell surface and their subsequent internalization have been examined widely. The binding process is believed to be driven by electrostatic interactions between positively charged lipoplexes and the negatively charged cell surface.^{83, 105} There is limited data on the importance of specific cell surface receptors and possible roles of cell surface components with respect to the binding of lipoplexes to the cellular membrane, although heparan sulfate proteoglycans (HSPGs) have been implicated in the binding of lipoplexes.^{106, 107} HSPGs are a class of membrane-anchored proteins and function as specific growth factor receptors. They have been shown to mediate the cellular entry of pathogens.^{108, 109}

HSPG mediated binding in transfection was demonstrated by using proteoglycan-deficient Chinese hamster ovary (CHO) mutant cells.¹¹⁰ These mutant cells showed much lower transfection efficiency when using poly-L-lysine and cationic lipids

vectors as compared to the normal cells. Furthermore, the results showed the inhibition of intracellular DNA uptake and DNA binding to the cell membrane. These results were confirmed using HeLa cells treated with specific enzymes that degrade proteoglycans.¹¹⁰ However, the distribution of HSPGs varies in cells, which may explain why some cell types are more accessible to transfection complexes.

An ideal gene delivery vector can target and kill cancer cells while affecting as few healthy cells as possible. To improve cellular binding and the effectiveness of gene delivery, a variety of targeting ligands has been studied. Transferrin, epidermal growth factor (EGF), and folic acid, have been widely examined as cancer-targeting delivery systems. The cationic polymer, PEI, conjugated to transferrin or EGF through a linker of polyethylene glycol (PEG) showed luciferase production 10-100 times higher in tumor models than in other organs.¹¹¹ The folate receptor is abundantly expressed on the surface of cancer cells, which makes folic acid an excellent target ligand for a number of types of cancer, such as the ovary, lung, breast kidney, brain, colon, etc.^{112, 113} Liposomes conjugated to folate target ligand through a PEG spacer have been used to deliver therapeutic agents to cancer cells.¹¹⁴⁻¹¹⁶ Some researchers have also studied folate-linked microemulsions as carriers for chemotherapeutic agents in cancer cells.^{117, 118} *In vitro* and *in vivo* studies showed that folate modification with a PEG linker on emulsions is an effective way to target emulsions to cancer cells.¹¹⁸

1.3.2 Cellular uptake

Once bound to the cell surface, internalization of the lipoplexes must take place. It has been revealed using electron and fluorescence microscopy that lipoplexes can be found in intracellular vesicles, indicating that lipoplexes enter cells by endocytosis.⁹² To date, the widely accepted internalization pathway for lipoplexes is through endocytosis, including phagocytosis, macropinocytosis, clathrin-mediated and non-clathrin-mediated (cellular entry via caveolae) endocytosis;¹¹⁹ however, which endocytotic pathway is involved may be specific to a particular cell type. Using lipoplexes composed of the cationic lipid SAINT-2 (Figure 1.4) and DOPE, Zuhorn et al. have shown a cholesterol-dependant endocytosis pathway in African green monkey kidney cell line (COS-7), Human hepatocellular liver carcinoma cell line (HepG2), and CHO cells.¹²⁰ Simoes and colleagues concluded that a non-clathrin-coated-pit pathway (clathrin-independent endocytosis) was involved in the internalization of the DOTAP-DOPE/DNA lipoplexes in Hela cells.¹²¹ The examination of gene transfection using different lipoplexes and cell lines concluded that for primary cells, binding and endocytosis are important rate-limiting steps for the transfection efficiency,¹²²⁻¹²⁴ while for established cell lines, such as COS cells, Hela cells, endocytosis is not a rate-limiting step.^{125, 126}

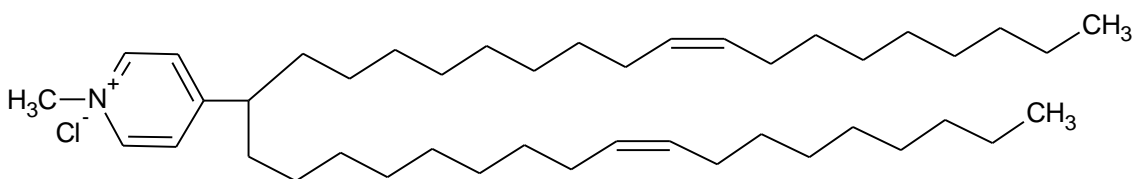


Figure 1.4 The molecular structure of SAINT-2

Lipoplex size seems related to cellular entry pathway. Lipoplexes with a size of 150-800 nm were reported to be internalized by clathrin-mediated endocytosis;^{120, 127} however, Grosse et al. have reported that particles larger than 200 nm may be internalized via macropinocytosis, rather than via a clathrin-mediated pathway.¹²⁸ Although particle size is an important parameter in gene transfection, a direct correlation between particle size and the entry pathway of lipoplexes has not been universally demonstrated or accepted.

1.3.3 Endosome escape

Following endocytosis, lipoplexes are internalized to form early endosomes. Generally, endosomes undergo a rapid maturation and late endosomes end up by fusing with lysosomes. This is not expected to be efficient for transfection since the lipoplexes tend to be degraded in lysosomes. Thus, it is essential that lipoplexes carrying DNA escape the early endosomes for efficient transfection. Unlike viral vectors, non-viral vectors lack the protein machinery to destabilize the endosomal membrane. Therefore, the effect of various structural morphologies of lipoplexes to facilitate endosome escape is critical.

As introduced above, the inclusion of helper lipids such as DOPE or cholesterol has been found to promote the gene transfection efficiency of lipoplexes.¹²⁹⁻¹³² This result is mainly attributed to the neutral lipids' ability to facilitate a phase transition in the lipoplex structure to non-bilayer structures, such as the H_{II} phase. Using SAXS and optical microscopy, the H_{II} morphology was observed in lipoplexes containing DOPE. DOPE has a negative natural curvature because of its larger volume of the

hydrophobic chains and smaller head group area. When incorporating DOPE into a cationic lipid DOTAP, the phase transition from L_{α} to H_{II} occurs. The phase transition is known to catalyze the fusion of the lipoplexes with endosomal membranes, thus promoting the release of transgenes from endosomes.^{96, 101} Although inclusion of DOPE into lipoplexes can induce such a phase transition, it may also be triggered in endosomes by mixing with cellular lipids such as phosphatidylserine (PS).¹³⁰ It has been suggested that ion pairing of negatively charged cellular lipids, such as PS, with cationic lipids in lipoplexes mediate the formation of H_{II} lipoplexes, enhancing endosomal escape.¹³³ In addition, PS itself also undergoes a L_{α} - H_{II} phase transition under acidic conditions below pH4.¹³⁴

In addition to the presence of a helper lipid, the membrane charge density (σ_m) also influences the destabilization of endosomal membrane. The membrane charge density is defined as the average charge per membrane area.¹³⁵ Cationic liposomes typically consist of a mixture of cationic and neutral lipids, thus the membrane charge density may be manipulated by changing the molar fraction of neutral lipid or changing the head group charges of cationic lipid. The bilayers of lamellar lipoplexes are more stable when the complexes enter cells through endocytosis. Lin et al. think that the lamellar lipoplexes escaping from endosomes depend on their membrane charge density. Only those with a large enough membrane charge density may escape from endosomes through activated fusion with endosomal membrane lipids.¹³⁶ Safinya and colleagues have shown that endosomal escape is the rate and efficiency limiting step for gene transfection with lamellar lipoplexes of low to

intermediate membrane charge density.¹³⁵ Lamellar lipoplexes with an optimal membrane surface charge at $(17.4 \pm 0.2) \times 10^{-3} \text{ e}/\text{\AA}$ achieved a comparable transfection efficiencies to that obtained from H_{II} lipoplexes.¹³⁵ At the optimal membrane charge density regime $10^{-2} < \sigma_m < 2 \times 10^{-2} \text{ e}/\text{\AA}$, Caracciolo et al. studied the effect of multicomponent lipoplexes on transfection efficiency.¹³⁷ Compared to binary lipoplexes, multicomponent systems consisting of several lipid components showed the superior transfection efficiency. This result may be mainly related to their higher fusogenicity and compatibility with endosomal membrane lipids.¹³⁷ Remarkably different from lamellar lipoplexes, the transfection efficiencies of hexagonal lipoplexes are independent of membrane charge density.^{136, 137} The difference in curvature between the outer endosomal monolayer (positive curvature) and the lipids coating DNA inside the complexes (negative curvature) is assumed to drive a rapid fusion of hexagonal lipoplexes with endosomal membrane, resulting in the release of DNA from the complexes.¹³⁶

1.3.4 Nuclear entry

In order to achieve in successful gene transfection, transgenes must enter the nucleus and undergo transcription. Transgenes cannot passively diffuse through the nuclear membrane; this membrane, also called the nuclear envelope, is a major barrier to effective gene transfer. The nuclear envelope is a lipid double layer, and nuclear pores perforate it to form channels for the bidirectional shuttling of molecules between the nucleus and the cytoplasm.¹³⁸ Generally, these channels have a limiting diameter of around 25 to 30 nm.¹³⁹ It allows the passage of small molecules, but

large molecules require active transport through specific nuclear import proteins located in nuclear pores.

To date, there are two mechanisms proposed to explain how a transgene enters into the nucleus.⁸¹ The first one is passive entry into the nucleus of dividing cells. During cell mitosis, the nuclear envelope breaks down which facilitates transgene access to the nucleus. It has been shown that transfection efficiency is higher at or near cell mitosis than that obtained at quiescent cell phases.^{140, 141} The other mechanism for transgene entry into the nucleus of quiescent cells is an active transport of transgenes through the nuclear pores. It is well known that proteins bearing nuclear localization signals (NLSs) can bind to the nuclear envelope and be imported into the nucleus.¹³⁸ The first NLS was identified from a SV40 T-antigen in 1984.¹⁴² It has been evidenced that nuclear entry of plasmid DNA is dependent on whether the plasmid contains a SV40 sequence.¹⁴³

1.3.5 Summary

Although cationic lipids have been studied for gene application since 1987, only 7.6% of human gene delivery clinical trials have employed cationic lipid-based vectors.⁵ The biggest limitation is low transfection efficiency observed for cationic lipids. This limitation continues to drive research into alternatives to cationic lipids in the formulation of non-viral transfection vectors. One such alternative is a novel family of cationic surfactants, known as gemini surfactants. Compared to cationic lipids used in gene therapy, gemini surfactants can be synthesized from very inexpensive starting materials and on a laboratory scale, are easily prepared, are

able to dissolve in aqueous solution at room temperature, and are stable enough to be stored for months under room conditions. Thus, this new class of non-viral vector is cost effective, efficient, and very competitive for gene delivery. They will be discussed in detail below.

1.4 Gemini surfactants

Gemini surfactants are a class of surfactants made up of two surfactant monomers that are linked by a spacer group, as illustrated in Figure 1.5. The spacer group may be short (i.e., two methylene groups) or long (up to 20 or more methylene groups), hydrophobic or hydrophilic, and may contain other functional groups (i.e., pH sensitive amine groups). Similar to cationic lipids, gemini surfactants are amphiphilic molecules; however, compared to cationic lipids, gemini surfactants possess a higher charge per mass and have superior surface properties.¹⁴⁴

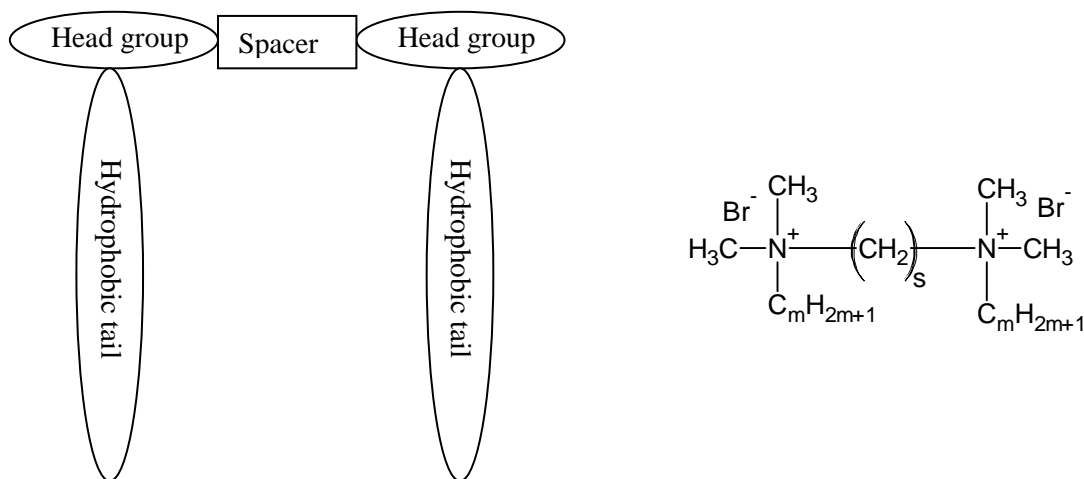


Figure 1.5 Scheme for gemini surfactant structure (left) and structure of the m-s-m gemini surfactant (right).

Compared to typical monomer surfactants, gemini surfactants demonstrate very unique properties and aggregation morphology. They can form aggregates at very low concentrations, and also demonstrate polymorphism (spherical micelles, cylindrical or bilayers, or inverted micelles).¹⁴⁵ Critical micelle concentration (CMC, the concentration of surfactants above which micelles form.) values of gemini surfactants are one to two orders of magnitude lower than for the corresponding monomer surfactants,¹⁴⁶ and they are much more efficient in lowering surface tension of water. They also show other enhanced features, such as low viscosity, better solubilizing properties, and stronger antimicrobial properties.¹⁴⁶

Because of their unique properties gemini surfactants have been well characterized by studying their solution properties, polymorphism behavior, and applications. Many of the synthesized cationic gemini surfactants are made of two alkyldimethyl-ammonium bromide moieties linked by a spacer with hydrophobic polymethylene groups, abbreviated m-s-m (see Figure 1.5); m is the number of carbon atoms in the alkyl tails and s represents the number of carbon atoms in the hydrophobic polymethylene spacer.⁴⁴ Another widely studied class of dimeric surfactants are the sugar-based gemini surfactants; their head groups are made of reduced sugars, such as glucose and mannose, connected to tertiary amines or amides; and their spacer is usually polymethylene groups with different length.¹⁴⁷ The physico-chemical properties and micellar structures can be manipulated by varying the length of alkyl chains or spacer, degree of unsaturation of alkyl tails, and

symmetry or asymmetry of alkyl tails to rationally design better candidates for gene delivery.

1.4.1 Molecular structure and properties of gemini surfactants

The shape of aggregates formed by a gemini surfactant is influenced by its molecular structure. A popular theory used to predict the shape of micellar aggregates is that of the packing parameter (P) defined as:¹⁴⁸

$$P = V/la_0$$

where V is the volume of the alkyl tails, l is the length of alkyl chains, and a_0 is the surface area occupied by the head group. The expected micellar aggregate shapes at different P values are listed in Table 1.4. For example, spherical micelles are expected when P is less than 0.33, which is generally seen for single-chained surfactants with relatively large head groups; vesicles or flexible bilayer structures are formed when P is in the range of 0.5-1, which can be observed for double-chained surfactants with large head groups and flexible chains.

Although the packing parameter can be used to predict the curvature of surfactant aggregates, the description of mesophases of surfactants in aqueous solution must also consider the arrangement of surfactant aggregates. In and Zana reviewed lyotropic mesophases in gemini surfactants-water mixtures.¹⁴⁵ The lyotropic mesophases, illustrated in Figure 1.6, include the hexagonal phase (H_I) which is made of spherical micelles packed on a hexagonal lattice, the inverted hexagonal phase (H_{II}) which are made of inverted micelles arranged on a hexagonal lattice,

Table 1.4 Packing parameter and expected aggregate shape.¹⁴⁹

P	Aggregate structure	General surfactant type
<0.33	Spherical micelles	Single-chain surfactants with relatively large head groups
0.33-0.5	Cylindrical or rod-shaped micelles	Surfactants with relatively small head group
0.5-1.0	Vesicles or flexible bilayer structure	Double-chain surfactants with large head groups and flexible chains
1.0	Planar bilayer structures	Double-chain surfactants with small head groups or rigid chains
>1.0	Inverted micelles	Double-chain surfactants with small head groups, very bulky chains

the lamellar phase (L_{α}) consisting of infinite bilayers separated by layers of water, and the cubic phase which is made either of spherical micelles arranged on a cubic lattice or of infinite layers of surfactants folded into a cubic bicontinuous structure. To lower the free energy of the mixture and optimize the distance between micelles, aggregate organization in water is spontaneous and driven by inter-micellar repulsion.¹⁵⁰ From an energy minimization point of view, the most frequently observed mesophase is lamellar; with hexagonal and cubic phases being rarely found.¹⁵¹

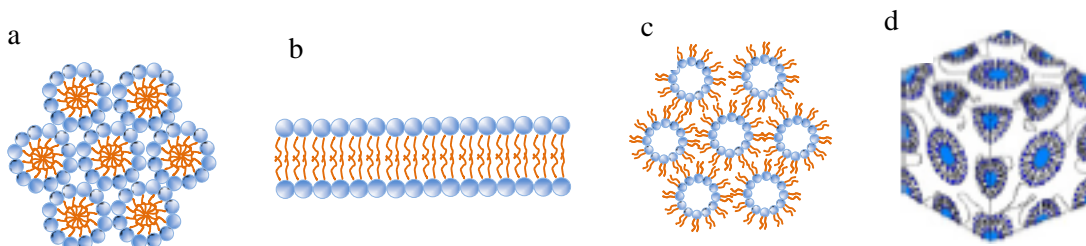


Figure 1.6 Schematic pictures of lyotropic mesophases in surfactant-water mixtures. The normal hexagonal (H_I), the lamellar (L_α), and the inverted hexagonal phases (H_{II}) are illustrated by a, b, and c, respectively. The cubic phases are described by d.¹⁵²

Micelle shapes can be manipulated by changing the molecular structure of surfactants, such as the length of the spacer and the alkyl tails, the degree of asymmetry of the alkyl tails, and the type of head groups. For m-s-m type of surfactants, the literature shows that the effect of alkyl tail length on the aggregate shape is similar to that obtained with conventional surfactant monomers. An increase in the length of the alkyl tails results in a less curved micelle shape. Take a series of m-3-m ($m = 10, 12, \text{ and } 16$) surfactants as an example. Spherical micelles were observed for $m = 10$; spherical micelles were formed at low concentrations for $m = 12$ and rod-shaped micelles at higher concentrations; and disklike micelles were observed for $m = 16$.¹⁴⁶ Correspondingly, the effect of alkyl tail length on the mesophases of gemini surfactant-water mixtures has been examined. The phase behavior of m-6-m ($m = 8, 10, \text{ and } 12$) mixing with water has also been reported.¹⁵³ With the increase of weight fraction of surfactant in their mixture with water, micelle phases as one-phase solution (A), a gel phase (B), a coagel phase (C), and mixture of a gel and a coagel phase (D), were obtained for 8-6-8; micelle phases at different

concentrations of 10-6-10 were A, B, and C; but for 12-6-12, in addition to A, B, C, and D, the presence of hydrated surfactant crystals with the surfactant solution was observed. These results indicate that micelle characteristics change with the variation of alkyl tail length.

The effect of the spacer group on aggregate shape has also been investigated. Threadlike micelles were observed for the 12-2-12 surfactant at a concentration of 2 wt% and the 12-3-12 surfactant at a concentration of 7 wt%;¹⁵⁴ spherical micelle aggregates were formed for the 12-s-12 ($4 < s \leq 12$) surfactants; at $s \geq 14$, vesicles were observed.¹⁵⁴ In contrast, the 16-s-16 surfactants show a more complex behavior. A mixture of vesicles, bilayer fragments, and disk-like micelles were revealed for 16-3-16 by Cryo-TEM; disk-like micelles for 16-4-16 were observed; and spherical micelles were shown for 16-8-16.¹⁵⁴ Additionally, spherical micelles were observed in the 16-12-16 using small angle neutron scattering (SANS).¹⁵⁵ The aggregate morphology has not been investigated for 16-s-16 surfactants with s greater than 12.

In terms of packing parameter, the 12-2-12 has a P above 0.33 and elongated micelles should be formed, in agreement with experimental results.¹⁴⁶ Head group area increases rapidly for m-s-m surfactants with $s \leq 8$ at the micelle surface, while the volume and length of the alkyl tails change little. Thus, P decreases with increasing s ($s \leq 8$), corresponding to a change from elongated micelles to spherical micelles, also as has been observed experimentally.¹⁵⁶ Because of increasing hydrophobicity, the longer spacers ($s > 10$) fold into hydrophobic micelle core,

leading to an increase of volume of alkyl tails and decrease of head group area. This results in a rapid increase of packing parameter and the formation of less curved aggregates, such as vesicles. This is also revealed by Cryo-TEM images.¹⁵⁶

The aggregate properties of sugar-based gemini surfactants have been determined by Engberts and colleagues.¹⁴⁷ The head group area is considered as a decisive parameter that influences the packing parameter. The head group having tertiary amines is pH-sensitive, for which the packing parameter decreases with a decrease in pH. At lower pH, more gemini surfactants become protonated and the head group area becomes larger due to increased electrostatic repulsion between the head groups. Thus, the aggregate shape changes to a more curved structure, from vesicles to spherical micelles.¹⁴⁷ This protonation-driven vesicle-to-micelle transition was observed only for those sugar-based gemini surfactants containing an amine linkage.¹⁴⁷ If the head group contains an amide group instead of amine, protonation of the head group does not occur, and no change in aggregate structure with pH is observed.

In addition to aggregate structure, another property influenced by the molecular structure of gemini surfactants is their CMC values. The effect of variations to the alkyl tails on the CMC of a gemini surfactant is similar to that observed for traditional, monomeric surfactants. The CMC values decrease with an increase in the alkyl tail length because of the corresponding increase in hydrophobicity. The linear relationship of log CMC as a function of the alkyl tail length is observed for most surfactants, including conventional surfactants (one head with one tail), bolaform

surfactants (one head with two tails), and gemini surfactants (two heads with two tails).¹⁵⁷

CMC values can be manipulated by introducing asymmetric hydrocarbon tails as well. The most investigated asymmetric gemini surfactants are m-s-n type with two alkyl tails of different carbon numbers. The CMC values of 12-2-12, 14-2-10, and 16-2-8 (which have the same spacer within the molecular structure) were reported to be 0.96, 0.95, and 0.75 mM, respectively.¹⁵⁸ Although the overall length ($m + n = 24$) of the tails and the spacer were kept constant, the dissymmetry of those surfactants influenced their CMC values. Bai et al. investigated a type of gemini surfactants, m-6-n, with $m + n = 24$ and $m = 12, 13, 14, 16,$ and 18 .¹⁵⁹ The CMC values decreased linearly with an increase in the m/n ratios. From a thermodynamic point of view, the increase of assymetry showed a more negative micellization enthalpy, indicating a larger effective hydrophobicity caused by the addition of a CH_2 group to the long alkyl tail than that of adding a CH_2 group to the short tail.¹⁵⁹ Thus, the increase of dissymmetry actually results in the increased hydrophobicity of surfactants.

Compared to conventional surfactants, the nature and structure of a spacer group are critical factors that give rise to the unique properties of the gemini surfactant. CMC values are influenced by the length of spacer group. For the 12-s-12 gemini surfactants, in the plot of log CMC as a function of spacer length (Figure 1.7), the CMC values reached a maximum when s is 5 or 6, then nonlinearly decreased with the increase of the spacer length in the range of $5 < s < 10$, and linearly decreased for $s \geq 10$.¹⁵⁷ It is believed that the conformational change of spacer and the resulting

effect on head group hydration and alkyl tail orientation resulted in the maximum of CMC at $s = 5$ or 6 .¹⁶⁰ At higher s , the spacer is long enough to be part of the micelle hydrophobic core, leading to the decreased CMC.

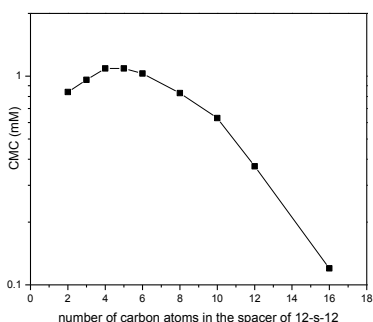


Figure 1.7 The CMC values as a function of the number of carbon atoms in the spacer of 12-s-12 ($2 \leq s \leq 16$). Adapted from Zana et al..¹⁵⁷

The effect of substitution within the spacer group on the CMC is complex, and depends upon the nature of the substituents. For hydrophilic oxyethylene (EO) substituted spacers, an increase in the number of EO groups within the spacer (also corresponding to an increase in spacer length) results in an increase in the CMC of 12-2(EO)_x-12 ($x=1, 2, \text{ and } 3$), which is contrary to the observation from the 12-s-12 gemini surfactants. This is possibly because of the increased solubility of 12-2(EO)_x-12 surfactants and the decreased hydrophobicity between tails due to the steric effect caused by EO groups.^{161, 162} Compared to 12-4-12, the hydroxyl substituted (12-4(OH)_n-12) surfactants showed the decreased CMC values with increasing the number of hydroxyl group in the spacer. This is because the -OH group(s) form hydrogen bonds with water molecules, thus facilitating the location of the spacer toward the aqueous phase to form micelles.¹⁶³⁻¹⁶⁵ The addition of an amine

functional group to the spacer of the gemini surfactants has been recently reported by Wettig et al.¹⁶⁶ Compared to 12-2(EO)_x-12 (x=1, 2, and 3), the gemini surfactants having N-CH₃ in the spacer, 12-5N-12, 12-8N-12, and 12-7N-12, are more hydrophobic. However, these compounds with N-CH₃ substituent showed higher CMC values. This increase is likely attributed to the increased steric repulsion and correlated packing at the micelle-water interface. Changes in chemical structure of the spacer have also been studied to determine the influence on aggregation properties of the gemini surfactants. For example, three gemini surfactants, 12-2(EO)-12, 12-6-12, and 12-xylyl-12, having the same head groups, C₁₂ tails, and approximately the same length of spacer, have been reported that the spacer nature influenced their aggregation properties.¹⁶⁷ As expected, 12-2(EO)-12 showed the lowest CMC due to the formation of hydrogen bonds with water. 12-xylyl-12 having a hydrophobic and rigid ring within the spacer showed the largest CMC value, indicating that it is difficult to incorporate such a spacer into the hydrophilic region of micelles.

1.4.2 Interaction between cationic gemini surfactants and DNA

The interaction of gemini surfactants with DNA triggers a new research area in which gemini surfactants have been widely studied as gene delivery vectors for gene therapy.¹⁶⁸ Because of their low cost, efficient binding with and compaction of DNA,¹⁶⁹ the use of cationic gemini surfactants as gene delivery vectors has become an attractive research area for the past two decades. Because of the large variation of aggregate structures that can be accessed through simple modifications of the

molecular structure of the gemini surfactants, it should be possible to more easily optimize DNA delivery efficiencies by taking advantage of changes in uptake mechanism and endosomal escape without substantially impacting on the factors such as formulation and toxicity.

1.4.2.1 Effect of length and nature of alkyl tails

With an increase in alkyl tail length, hydrophobic interactions between surfactant molecules increases, resulting in more efficient compaction with DNA molecules.¹⁷⁰ Dias et al. examined the interaction between DNA and cationic surfactants with different tail length, cetyl trimethyl ammonium bromide ($C_{19}H_{42}BrN$, CTAB), tetradecyl trimethyl ammonium bromide ($C_{17}H_{38}BrN$, TTAB), and dodecyl trimethyl ammonium bromide ($C_{15}H_{34}BrN$, DTAB).¹⁷¹ CTAB was shown to bind DNA more strongly due to its longer alkyl tail. This study indicates the importance of the hydrophobicity of the surfactant molecules to DNA binding process. Furthermore, the authors performed SAXS studies to evaluate the structure of the DNA with CTAB, TTAB, and DTAB, respectively.¹⁷⁰ Both CTAB and TTAB showed inverted hexagonal diffraction peaks with different lattice spacing of 54.4 and 53.1 Å, respectively. It is known that CTAB and TTAB prefer to form rod-shaped micelles with an increase in ionic strength in water, and the addition of DNA is believed to have a similar effect.¹⁷⁰ Compared to CTAB and TTAB, DTAB has a smaller packing parameter because of the shorter hydrophobic chain length. This results in more curved spherical micelles formed.¹⁷⁰

Similar results have been observed with gemini surfactants. The effect of alkyl tail length on cationic gemini surfactants-DNA structure has been investigated using m-4-m (m = 12, 13, 14, and 16) gemini surfactants and calf thymus DNA.¹⁷² The SAXS profiles revealed that for m = 12, 13, and 14, the gemini surfactants-DNA complexes were packed in a hexagonal lattice at 25 °C, but more gemini surfactant was required for those with the shorter alkyl tail length; while for 16-4-16, two scattering peaks corresponding neither to the lamellar nor the hexagonal phase were observed for the 16-4-16-DNA complexes at 25 °C. These results indicate that the length of alkyl tails of gemini surfactants has an effect on structures of surfactant-DNA complexes.

Additionally, it has been reported that the condensation of DNA can be improved by increasing asymmetric extent of gemini surfactants. For m-s-n type of gemini surfactants with different length of saturated hydrocarbon tails, the hydrophobic interaction among asymmetric gemini surfactant molecules is believed to be stronger with increasing the assymetry degree. However, the addition of DNA disrupts the hydrophobic interaction among the surfactant molecules due to the electrostatic attractive interaction between the head groups of gemini surfactants and DNA backbones. With an increased degree of dissymmetry, the interaction of the m-6-n (m + n = 24, and m = 12,14, 16, and 18) surfactants with DNA was examined by ITC.¹⁷³ The results show that the dissymmetry degree (m/n) dramatically influences the interaction of the m-6-n with DNA. The critical aggregation concentration (CAC, specifically representing the concentration at which micelle aggregates begin to form

along the DNA molecule.¹⁶⁸) and saturation concentration (C_2 , defined as the concentration at which any added surfactant does not interact with the DNA molecules.¹⁶⁸) decreased with increased dissymmetry. The enthalpy change (ΔH) and Gibbs free energy change (ΔG) for the aggregation process were more negative with increased m/n , representing that the hydrophobic interaction between the hydrophobic tails of the surfactants increases and the aggregation process is more spontaneous. The Gibbs free energy change (ΔG) for the interaction between the gemini surfactants and DNA was negative, but increased with the increased m/n , indicating that the interaction of the m - n surfactants with DNA is weaker.

In addition to the effect caused by changing alkyl tail length, molecular structure of alkyl tails also influences the interaction of gemini surfactants with DNA. Two gemini surfactants containing pyrenyl groups in one of the alkyl chains of the surfactants (pyr-3-12 and pyr-6-12) were synthesized by Wang et al.¹⁷⁴ and the binding interaction between pyrenyl-substituted gemini surfactants and salmon sperm DNA was examined by Wettig et al..¹⁷⁵ Compared to the 12-s-12 surfactants with DNA, the enthalpy profiles obtained from ITC measurements for the pyr-s-12 ($s = 3$ and 6) showed a significant difference. The enthalpy profiles obtained from 12-s-12 ($s = 3$ and 6) with DNA have shown that the binding process occurs in three steps: an initial step of interactions between DNA and gemini surfactant micelles, the formation of large aggregates, and finally precipitation of a neutral complex occurring at the addition of DNA. Similar to the 12-s-12 ($s = 3$ and 6), the initial binding of the pyr-s-12 ($s = 3$ and 6) resulted in the formation of “beads on a string complex”;¹⁷⁴

different from the 12-s-12, the complexes formed by pyr-s-12 ($s = 3$ and 6) in the presence of DNA do not precipitate in the formation of flocs because the pyrenyl groups can be intercalated between DNA base pairs.

1.4.2.2 Effect of spacer length

The compaction of bacteriophage T4 DNA by the 12-s-12 ($2 \leq s \leq 10$) gemini surfactants has been reported by Karlsson and colleagues.¹⁷⁶ It was found that the 12-s-12 surfactants with shorter spacers ($s \leq 3$) showed more efficient compaction of the DNA, while those surfactants with intermediate length ($s = 5-10$) were less efficient. The results of a circular dichroism (CD) study show that cationic gemini surfactants induce a structural transition of DNA from a native B-form (right-handed secondary DNA conformation¹⁷⁷) to a tertiary ψ phase (left-handed DNA conformation¹⁷⁷).¹⁷⁸ The study regarding spacer length of the 12-s-12 on DNA phase structure found that the 12-s-12 surfactants with shorter ($s < 4$) or longer ($s > 10$) spacers were more efficient in inducing the tightly packed ψ phase.¹⁷⁹ A recent study also shows that the spacer length has a great effect on the properties of the complex structures. At $s \leq 6$, CD signal indicates that 18-s-18 surfactants induce a structural change of DNA from the double-stranded helix to a tertiary ψ phase.¹⁸⁰

In addition to changes in DNA phase, molecular areas of gemini surfactant-DNA complex monolayers have been reported to change with spacer length. The molecular areas of the 12-s-12-DNA complex monolayers reached a maximum at $s = 6$, and then decreased as the number of methylene groups increases.¹⁸¹

Furthermore, atomic force microscopy (AFM) images revealed the effect of the

spacer length on the 12-s-12-DNA complex morphologies. The width of the fiber-like structures and the distance between these structures were related to the spacer length of the gemini surfactants.¹⁸¹

1.4.2.3 Summary

As introduced above, molecular structure of gemini surfactants plays an important role in the interaction with DNA, which then gives rise to different structural properties of gemini surfactant-DNA complexes. This is very important for gemini surfactants used as a novel class of gene delivery vectors. Structural changes of resultant gemini surfactant-DNA complexes can be achieved by manipulating the length or nature of alkyl tails and spacer of gemini surfactants. Therefore, a rational design based on such information can produce more efficient gemini surfactants for gene delivery.

1.4.3 Gemini surfactants and gene transfection

To date, gemini surfactants widely studied for gene delivery include sugar-based gemini surfactants, peptide-based gemini surfactants, and m-s-m surfactants.¹⁶⁸ In this section, the first two types will be briefly introduced and the third one will be discussed in greater detail because the gemini surfactants involved in this thesis project are closely related to the m-s-m surfactants.

1.4.3.1 Peptide-based gemini surfactants

Peptide-based gemini surfactants contain head groups derived from positively charged amino acids and/or amine-linked carbohydrates (Table 1.5). This type of

gemini surfactant has been synthesized and studied widely by the European Network on Gemini Surfactants (ENGEMS) group. In general, higher transfection efficiency has been observed in the peptide-based surfactants, depending on the length of the alkyl tails, the peptide sequence used, and the manner in which the peptide sequences interacted with the backbone of the compounds.¹⁸² There are general observations summarized by Wettig et al.: the length of peptide localization sequence for spermine-based gemini compounds did not show any difference; for cystine dimer-based gemini compounds, the use of lysine as the α -amino acid to the spacer (a disulfide bond) showed a higher transfection efficiency than that of histidine or arginine; the greatest transfection activity was achieved using cystine dimer-based compounds having triamino acid peptide residues and linkages where lysine residues were coupled with the side-chain ϵ -amino acid groups; for the peptide-based compounds, oleyl chains usually showed a higher efficiency than did saturated alkyl chains.¹⁶⁸

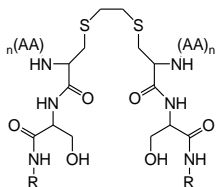
1.4.3.2 Sugar based gemini surfactants

Sugar-based gemini surfactants consist of glucose or mannose head groups which connect to a spacer through an amide or amine linker group (Table 1.5). The transfection activity of this type of gemini surfactants was examined in Chinese hamster ovary (CHO)-K1 cells. The results showed that

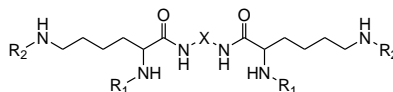
- the mannose head group was more efficient than the glucose;

Table 1.5 Molecular structures of peptide-based and sugar-based gemini surfactants

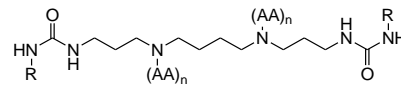
Peptide-based gemini surfactants



$R = C_mH_{2m+1}$, $m = 12, 14, 16, 18:1$ (oleyl),
AA = amino acid

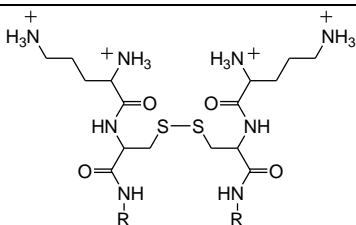


$R = C(O) C_mH_{2m+1}$,
 $9 < m < 23$

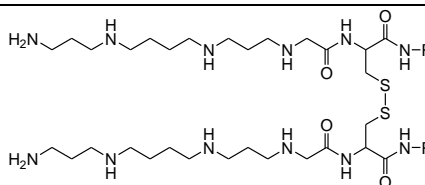


R = oleyl
AA = amino acid

Cystine-dimer gemini surfactants

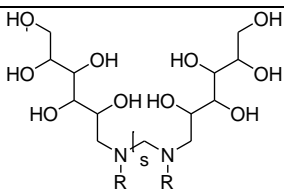


$R = C_mH_{2m+1}$, $m = 12, 14,$

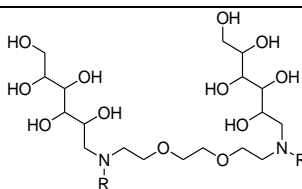


$R = C_{18}H_{37}$

Sugar-based gemini surfactants



$R = C_mH_{2m+1}$, $m = 12, 14, 16, 18:1$, $s = 4, 6$
sugar = mannose, glucose



R = oleyl, oleoyl
sugar = mannose, glucose

- spacer with EO-substitutions were more efficient and less toxic than those without EO substitution;¹⁸²
- introduction of double bonds in the alkyl chains enhanced the transfection efficiency;¹⁸³
- and the presence of an amine-based linker improved transfection efficiency compared to an amide-based linker.¹⁸⁴

Using SAXS and Cryo-TEM, the structure of the complexes formed by DNA with glucose-based gemini surfactants with 9-octadecenyl chains has been investigated in the pH range of 3.0-8.8.¹⁸⁴ Three morphologies of complexes were observed at different pHs: lamellar phase, condensed lamellar phase, and inverted hexagonal phase. The complexes showed a phase transition from the lamellar to the inverted hexagonal at an endosomal pH, which is hypothesized to be a dominant reason for its pronounced transfection activity. Bell et al. proposed key features for the rational design of efficient glucose-based gemini surfactants for gene delivery such as

- a spacer with six methylene groups,
- the presence of a head group containing tertiary amine groups that can experience a protonation at the physiological pH range and induce the formation of H_{II} in endosomes,
- unsaturated alkyl chains.

Wasungu et al. reported that the improved gene transfection was mediated by pH-sensitive sugar-based gemini surfactants in CHO cells and *in vivo*.¹⁸⁵ The surfactants can efficiently transfect CHO cells *in vitro*. This may be correlated with the observation that the complexes formed by this type of surfactants and DNA at physiological pH exhibited a lamellar phase, but exhibited a H_{II} morphology in endosomes. Two compounds among these surfactants were further investigated in male nude mice and they demonstrated *in vivo* transfection using a bioluminescence assay.

1.4.3.3 *M-s-m gemini surfactants and their derivatives for gene transfection*

Inspired by the mixture of dimethyldioctadecyl ammonium bromide and DOPE (trade marked as Lipofectin[®] and marketed by Life Technology), as a gene transfection vector, Rosenzweig and colleagues synthesized 16-s-16 (s=2, 3, and 6) and 18:1-s-18:1 (s=2, 3, and 6) surfactants and investigated their transfection activity in baby hamster kidney (BHK) cells using a β -galactosidase assay.¹⁸⁶ The results showed that the saturated derivatives with a six-methylene spacer, and the unsaturated derivatives with both three- and six-methylene spacers, were the most efficient agents for the gene transfection; the addition of DOPE to the 16-2-16 at different mole ratios decreased the transfection efficiency compared to the one without DOPE; The transfection efficiency was dramatically inhibited in the presence of 10% serum. The authors hypothesized that the different hydration behavior dominated by the saturated and the unsaturated derivatives resulted in the different transfection activity.

In order to improve gene transfection efficiency, a number of m-s-m type gemini surfactants have been synthesized and examined since Rosenzweig's work. The effect of alkyl tail length on transfection activity has been examined. Badea investigated the transfection activity of m-3-m (m=12 and 16) and 18:1-3-18:1 surfactants and found that the expression of IFN- γ in PAM 212 cells increased with alkyl tail length; the highest IFN- γ was observed for gemini surfactants with oleyl tails. Additionally, the incorporation of DOPE significantly improved the gene expression in PAM 212 cells.¹⁷⁹

Meanwhile, the influence of spacer nature and length on gene transfection has also been studied. The 12-s-12 ($3 \leq s \leq 16$) was examined in PAM 212 cells using the pGTmCMV.IFN-GFP plasmid.^{187, 188} The transfection efficiency was found to be related to the length of the spacer (the data is plotted in Figure 1.8); the 12-3-12 surfactant showed the highest transfection efficiency; and the minimum expression of IFN- γ was observed at $s = 8$. It is believed that the distance between head groups in the gemini surfactants with shorter spacer ($s \leq 4$) is close to the distance between two phosphate groups in DNA molecules, resulting in stronger complexation of the gemini surfactant and DNA.¹⁶⁸ The longer spacer ($s \geq 12$) was believed to bend into the hydrophobic core formed by the alkyl tails, which decreases the distance between the head groups, resulting in the increase of the transfection efficiency for long spacers. Although Dauty et al. think that a high CMC is preferable to surfactant-DNA complex formation and a low CMC value may improve the stability of the complexes,¹⁸⁹ no correlation was observed between the CMC values of 12-s-12 and

transfection efficiency.¹⁹⁰ Wettig and colleagues believe that the enhanced transfection observed for the 12-s-12 with longer spacers most likely results from a bilayer membrane disruption effect caused by the folding of the longer spacers into the alkyl tails of a membrane.¹⁶⁸

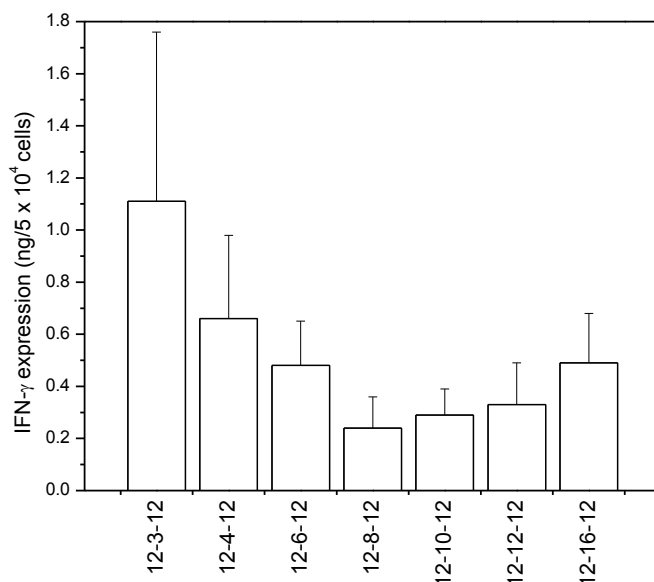


Figure 1.8 Effect of 12-s-12 (s = 3, 4, 6, 8, 10, 12, and 16) on the transfection of PAM 212 cells with pGTmCMV.IFN-GFP plasmid. Adapted from Badea et al..¹⁸⁷

Transfection activity of the m-s-m type of gemini surfactants containing ethylene oxide, hydroxyl groups, or methoxy groups in their spacers has been studied. The mono-, di-, and tri-ethylene oxide substituted derivatives of the 12-s-12 compounds have been examined by Wettig et al.¹⁶⁸ The results showed that the transfection did not significantly change with addition of one or more ethylene oxide repeat units. A single hydroxyl group incorporated to the spacer of 12-4-12 was observed to increase transfection efficiency four times higher than that obtained with 12-4-12; the

addition of two hydroxyl groups in the spacer did not show the same level of enhancement. The methoxy-substituted derivatives of 16-4-16 were examined in COS7, LA7 (rat mammary adenocarcinoma cell line), and human fibroblast cells.¹⁷⁸ The highest efficiency was observed for the 2R,3S-16-4(OCH₃)₂-16, followed by 16-4-16, and finally 2S,3S-16-4(OCH₃)₂-16. The authors proposed that the rearrangement of charged phosphate and nitrogen ions in the bilayer resulted in the enhanced transfection. In fact, the stereochemistry of the compounds may be important when it is involved in the targeting to the cell surface receptors.^{191, 192}

In addition to the modification in the spacer introduced above, Wettig et al. investigated the transfection of the 12-s-12 series gemini surfactants with modified spacers ((N-CH₃) and (N-H)- substitutes, seen in Figure 1.9) in COS7 cells using a pMASIA.Luc plasmid.¹⁹³ It was expected that the modified spacer would enhance the gene transfection. The results have shown that the N-CH₃ substituted gemini surfactants (12-5N-12, 12-7N-12, and 12-8N-12) do enhance the luciferase expression in COS7 cells; however, the N-H substituted 12-7NH-12 was the even more efficient. A structural analysis on the spacing between the nitrogen centers suggests that the trimethylene spacing between nitrogen centers in the 12-7N-12 and 12-7NH-12 surfactants is closer to the “optimal” spacing which facilitates DNA compaction. The lower transfection observed for the 12-5N-12 and 12-8N-12 compounds may be caused by a less than optimal two-methylene unit spacing between nitrogen centers. The highest luciferase expression achieved by the 12-7NH-12 is also believed to be correlated to pH-dependent morphology change under

lipid control the phase structure(s) of the lipoplexes and thereby the transfection efficiency.¹³¹ Wettig et al. compared the phase structures of complexes formed by DNA, m-s-m (m=12, 16, and 18:1; s=2, 3, and 4) compounds, and DOPE using SAXS.¹⁶⁸ It has been found that compounds having shorter spacers formed a mixture of lamellar and cubic structures. Compared to the unsubstituted compound, the amine-substituted 12-7NH-12 delivery system showed a lamellar morphology, as well as other hypothesized to be cubic phases; such compounds showed significantly higher transfection efficiencies.¹⁹³

1.4.3.4 Summary

As introduced above, it is very important that gemini surfactants can efficiently compact with DNA and adopt a flexible phase structure for effective cellular uptake and endosomal release. Many factors influence DNA compaction and the structure of surfactant-DNA complexes. One of the factors is the molecular structure of the gemini surfactants. Variations on molecular structures of gemini surfactants have been shown to influence their interaction with DNA and the resulting phase structures of surfactant–DNA complexes. Such studies regarding the molecular properties of gemini surfactants, interaction of surfactants and DNA, and structural activity of gemini surfactants in gene transfection provide a valuable background for rational design of new gemini surfactants as novel candidates for gene delivery.

Chapter 2 Hypothesis and Objectives

2.1 Basis for rational design of novel gemini surfactants

Rational design is a strategy to develop new molecules with specific functionality, based on the ability to predict how the new molecules will influence their activity through the modified structures. The rational design of novel gemini surfactants can be done based on observations reported in literature. Firstly, a pH-sensitive group has been introduced into gemini surfactants. Sugar-based gemini surfactants with the amine functional groups in the head groups have shown pH-dependent aggregation behavior.^{147, 195} Vesicles are formed near neutral pH which were observed to transform into cylindrical or wormlike micelles at pH<5.5. Aggregates stability was also related to aqueous pH with positively charged vesicles having good stability at pH < 7; but become unstable and sediment out from the solution when close to neutral pH. By counting GFP-positive cells from the total survival cells, the pH-sensitive sugar-based gemini surfactants achieved around 70% GFP expression in CHO cells. *In vivo* studies exhibited a prolonged stability in salt and serum.¹⁸⁵ Similarly, the incorporation of a pH-sensitive secondary amine substitute in the spacer group of the basic m-s-m gemini surfactants led to 9-fold increase of transfection efficiency compared to an unsubstituted gemini surfactant. Correspondingly, pH dependent behavior of the complexes was observed, such as a transition in size and zeta potential occurring at pH 5.5, and multiple phase structures formed from the mixture of 12-7NH-12, DNA, and DOPE, which are absent when the 12-7N-12 is used instead of 12-7NH-12.¹⁹³ Although the

mechanism of pH-sensitive gemini surfactants for improving transfection efficiency has not been fully investigated, it is certain that pH-sensitive substitutes incorporated into gemini surfactants can influence the aggregation behavior and structure of the complexes formed by the gemini surfactant and DNA with/without a neutral lipid, thus affecting gene transfection efficiency.

Secondly, surfactants with unsaturated hydrocarbon chains have shown unique aggregate morphologies and higher transfection efficiency. Gemini surfactants with oleyl tails showed highest IFN- γ expression in PAM 212 cells.¹⁹³ The glucose-based gemini surfactant with oleyl chains demonstrated more effective transfection efficiency than the saturated analogue. Unsaturated chains are believed to increase the structural flexibility of the complex formed by the gemini surfactants and DNA, which facilitates endosomal fusion and release of the transgene materials.¹⁸⁴ Additionally, surfactants with bulky hydrocarbon chains showed structural flexibility in terms of exhibiting cubic or inverted hexagonal phase structures. It has been reported that glycerate surfactants with oleyl, or hexahydrofarnesyl (3,7,11-trimethyl-dodecyl), or phytanyl (3,7,11,15-tetramethyl-hexadecyl) tails, exhibited cubic or inverted hexagonal phases at the interface with water.¹⁹⁶ Compared to conventional phospholipids, phytanyl-chained phospholipids showed unique characteristics, such as reduced permeability and higher salt tolerance.¹⁹⁷ These early studies provide a good background for the design of novel gemini surfactants with unsaturated and/or bulky alkyl tails (i.e., phytanyl substituted tails).

To rationally design and develop more efficient gemini surfactants, a few other general observations for the m-s-m type of compounds are made as follows.

- Compounds with longer alkyl chains (C₁₆ or C₁₈) show higher transfection efficiency.^{179, 194}
- Compounds containing a shorter spacer (≤ 4) achieve higher transfection activity.¹⁹³ The spacer has an effect on interactions between nitrogen groups of the gemini surfactants and the DNA phosphate groups; compared to dimethylene or longer spacing, the trimethylene spacing is believed to provide a closer match for the electrostatic interaction with phosphate groups of the DNA.
- Most literature shows the addition of a neutral lipid to gemini surfactant-DNA complexes enhances transfection efficiency; DOPE is the most widely used neutral lipid so far.^{188, 190, 193, 194}
- Gemini surfactants that prefer to form non-bilayer structures (such as the inverted hexagonal or cubic) are more effective than those forming lamellar morphologies.^{168, 193}

2.2 Hypothesis

Based on literature regarding non-viral vectors for gene therapy and research progress in our laboratory, the rational design of novel gemini surfactants should incorporate the following.

- 1) Asymmetric hydrocarbon tails of gemini surfactants expected to increase the phase flexibility of the complexes formed by the gemini surfactants, DNA, and a neutral lipid. This will result in the formation of flexible phase structures within the complexes, facilitating endosomal fusion.
- 2) A pH-sensitive group incorporated into the spacer group. The protonation of the pH-sensitive group under endosomal conditions should result in a change in the phase structure of the complexes, leading to enhanced membrane fusion and/or osmotic swelling and rupture of the endosomal membrane due to enhanced endosomal Cl^- accumulation caused by “proton-sponge mechanism”.
- 3) Three-methylene unit spacing between nitrogen centers. It has been proposed that the distance between ammonium head groups of the gemini surfactants with a spacer less than 4 is close to the distance between two phosphate groups in DNA molecules, which results in stronger complexation of the gemini surfactants and DNA.

Given the above, **it is hypothesized that asymmetric phytanyl-chained gemini surfactants having a shorter spacer and/or secondary amine within the spacer will improve gene transfection efficiency.** The enhancement may be attributed to their ability to adopt flexible phase structures and/or induce pH-sensitive phase transition(s) that facilitate endosomal escape.

2.3 Objectives

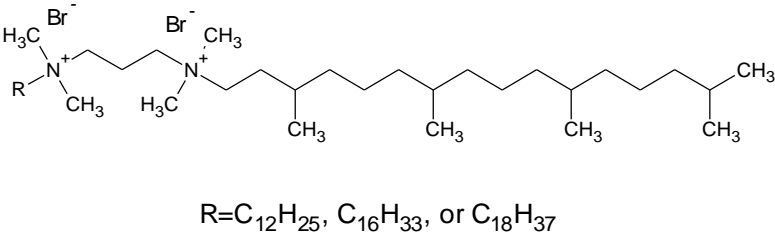
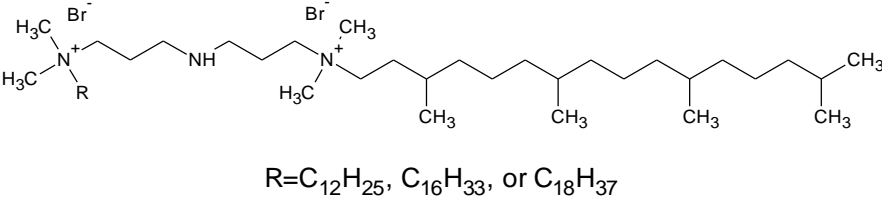
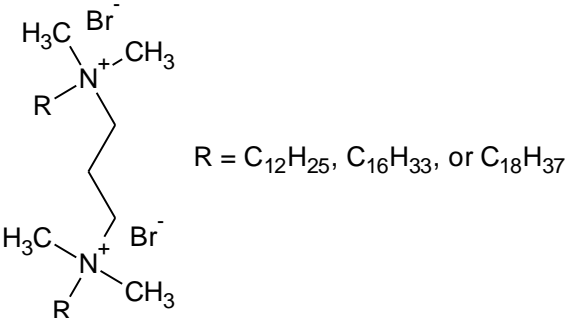
The overall objective of the project is to design, synthesize, and characterize asymmetric gemini surfactants-based transfection vectors for use in ovarian cancer gene therapy. Specific objectives are detailed below.

- 1) Synthesize and characterize the asymmetric phytanyl substituted gemini surfactants: phy-3-m and phy-7NH-m (m=12, 16, and 18). Molecular structures of the surfactants are shown in Table 2.1.
- 2) Determine *In vitro* transfection efficiencies for the phytanyl substituted gemini surfactants as vectors for ovarian cancer gene therapy.
- 3) Characterize the complexes formed by the phytanyl substituted gemini surfactants, DNA, and DOPE, by measuring particle size and zeta potential.
- 4) Investigation of the transfection complexes phase structures using SAXS.

The results and discussion regarding the first objective will be detailed in Chapter 3.

Chapter 4 outlines the results and discussion about the objectives 2, 3, and 4.

Table 2.1 Gemini surfactants used in the project.

Code name	Chemical structure
<p>Phy-3-m m=12, 16, and 18</p>	 <p>$R = C_{12}H_{25}, C_{16}H_{33}, \text{ or } C_{18}H_{37}$</p>
<p>Phy-7NH-m m=12, 16, and 18</p>	 <p>$R = C_{12}H_{25}, C_{16}H_{33}, \text{ or } C_{18}H_{37}$</p>
<p>m-3-m m=12, 16, and 18</p>	 <p>$R = C_{12}H_{25}, C_{16}H_{33}, \text{ or } C_{18}H_{37}$</p>

Chapter 3 Synthesis and characterization of phytanyl substituted gemini surfactants for gene delivery

3.1 Introduction

The focus of this project is to rationally design and develop novel gemini surfactants for use as improved gene delivery vectors. As introduced in Chapter 1, the nature and length of spacer group influences gene transfection efficiencies; however, little work has been carried out that investigates the effect of changes in the hydrophobic **volume** of the alkyl tails though studies on variations in the length of alkyl tail have been reported. The increased hydrophobic volume of the alkyl tails may give rise to a larger packing parameter (P), indicative of such surfactants adopting the inverted hexagonal and/or cubic phases. This could result in enhanced transgene activity.

In this work, a series of phytanyl-substituted gemini surfactants were designed and synthesized. The aggregation properties of these surfactants were studied using surface tension, specific conductance, particle size, and transmission electron microscopy techniques. The objective of this study was to investigate the effect of phytanyl groups as the alkyl tails on the micelle aggregation properties of the gemini surfactants compared to their corresponding symmetric gemini surfactants as a part of our efforts to design gemini surfactants that are more efficient transgene delivery vectors than the cationic lipids and surfactants currently in use for transgene delivery.

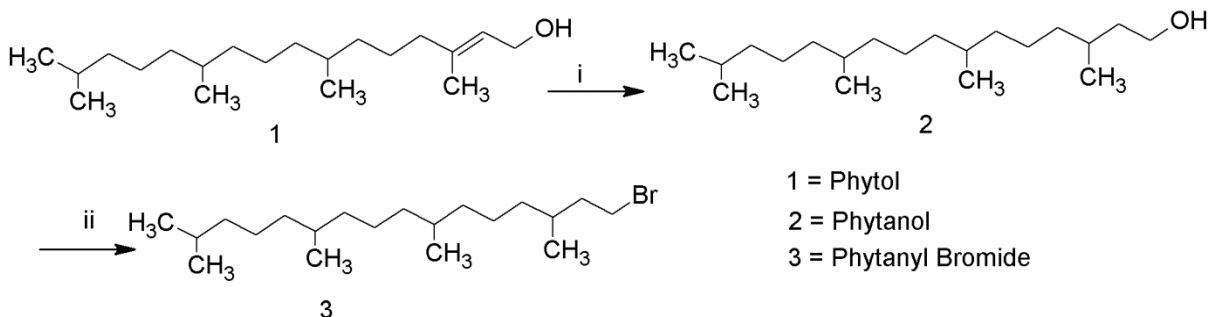
3.2 Methods and Materials

All gemini surfactants used in this project were synthesized in our laboratory. The symmetric m-3-m (m = 12, 16, and 18) was synthesized using the method from Wettig and Verrall.⁴⁴

3.2.1 Synthesis of phytanyl bromide

Phytanyl bromide is one of starting reagents for the synthesis of phy-3-m and phy-7NH-m (m=12, 16, and 18). The synthesis of phytanyl bromide was carried out according to the method of Bendavid et al.¹⁹⁸ Briefly, the first step is the hydrogenation of phytol over Raney nickel to produce phytanol; the second step is to expose phytanol to hydrogen bromide acid to give phytanyl bromide (Scheme 3.1). The method to produce phytanyl bromide is described as following. Phytol (Acros Organics, 10.0 g) in 50 mL of ethanol was reduced under hydrogen at atmospheric pressure over Raney nickel (2 g, Aldrich) for 3 days. The catalyst was removed by filtration through Celite and the filtrate concentrated under reduced pressure to give phytanol (95%). Next, concentrated sulfuric acid (Aldrich, 98%, 10 mL) was added slowly over 2 minutes to a solution of 48% hydrobromic acid (Fluka, 100mL). Phytanol (9.5 g, 0.032 mol) was added to the above mixture, and the mixture was refluxed for 6 h. After cooling to room temperature, the mixture was extracted with diethyl ether (2 x 60 mL), and the combined ether layers were washed with 10% NaHCO₃ in water (3 x 40 mL). The combined aqueous layers were extracted with diethyl ether (2 x 36 mL), and the combined ether layers were washed with saturated NaCl (3 x 40 mL). The ether layer was dried by adding anhydrous Na₂SO₄ (20 g)

and concentrated by rotary evaporation. The crude product was distilled under vacuum (130-140 °C/0.4 mmHg) to give pure phytanyl bromide (9.2 g, 0.026 mol, 80%). The purified product was characterized by ¹H NMR. The NMR data is given in Appendix A.

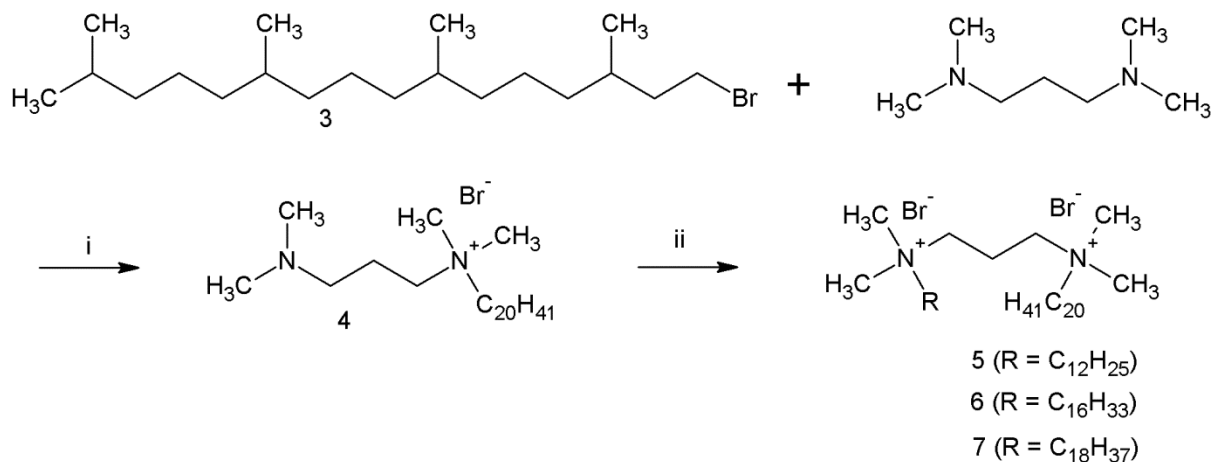


Scheme 3.1 Synthesis of phytanyl bromide. i. H₂, RaNi, EtOH, 3 days; ii. H₂SO₄ (98%), HBr (48%), reflux for 6 h.

3.2.2 Synthesis of phy-3-m (m = 12, 16, and 18)

The synthesis of phy-3-m was carried out according to the method from Wang et al., which was used to prepare pyrenyl-modified gemini surfactants.¹⁷⁴ Phytanyl bromide (1.09 g, 3.02 mmol) was added to N,N,N',N'-tetramethyl-1,3-propane-diamine (Aldrich, 0.489 g, 3.75 mmol) in 30 mL of anhydrous acetonitrile. The mixture was stirred at 50 °C for 3 days. The solvent was reduced under vacuum to approximately 1 mL. The mixture was transferred to another round bottom flask to which 1-bromododecane (Acros Organics), 1-bromohexadecane (Acros Organics), or 1-bromooctadecane (Acros Organics) was added with 10 mL of acetone and refluxed for 2 days. The crude product was recrystallized from anhydrous acetonitrile and produced a final product (phy-3-12, phy-3-16, and phy-3-18), respectively; (Scheme

3.2). The purified products were characterized by ^1H NMR and mass spectroscopy (MS). The NMR and MS data is given in Appendix A and B, respectively.



Scheme 3.2 Synthesis of phy-3-m ($m = 12, 16, \text{ and } 18$). i. CNCH_3 , 50°C , 3 days; ii. RBr (R = $\text{C}_{12}\text{H}_{25}$ or $\text{C}_{16}\text{H}_{33}$ or $\text{C}_{18}\text{H}_{37}$), CNCH_3 , reflux, 2 days.

3.2.3 Synthesis of the protected spacer (N-2-(tert-butyloxycarbonyl) amino-N,N-bis(3-(dimethylamino)propyl)-acetamide)

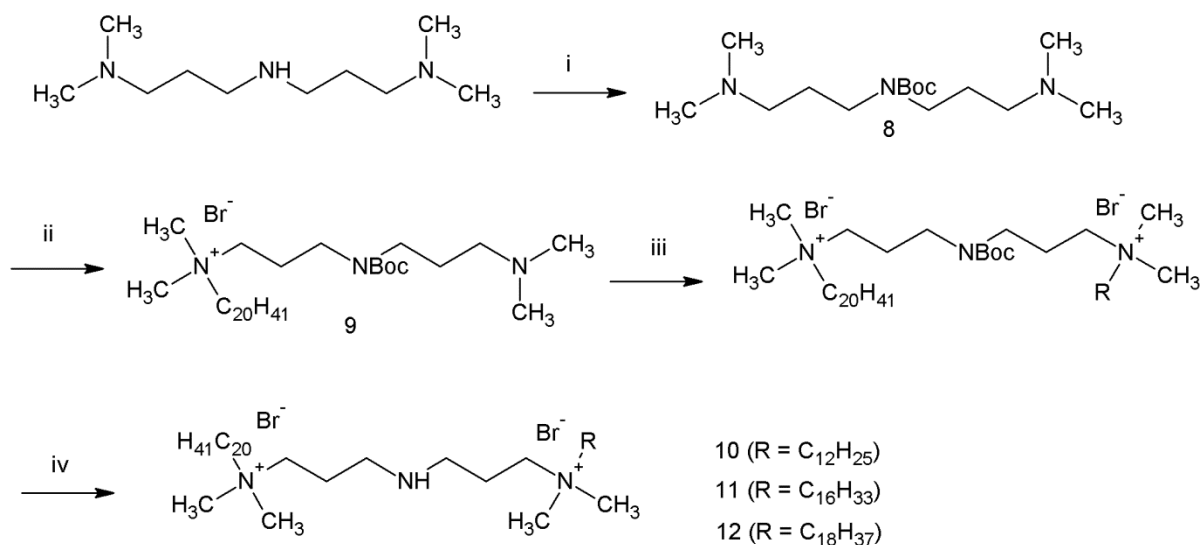
Prior to the synthesis of phy-7NH-m ($m = 12, 16, \text{ and } 18$), a starting reagent (chemical 8 in Scheme 3.3) having a NH group within the spacer needs a protection of $-\text{NH}$ group by replacing the hydrogen of the amine group with a tert-butyloxycarbonyl (BOC) group. The BOC group is one of most frequently used for protection of NH_2 or NH groups. There are several reagents used for the introduction of BOC group.¹⁹⁹ Di-tert-butyl dicarbonate (Boc_2O) is the best in most applications because of its high stability and low price. The N-protection of the amine can be carried out in acetonitrile using dimethylaminopyridine (DMAP) as base. The method

used in this study was that of Hara et al.²⁰⁰ In our experiment, 3,3'-iminobis(N,N-dimethylpropylamine) (chemical 8 in Scheme 3.3, Sigma-Aldrich, USA) was added to Boc₂O (Sigma-Aldrich, USA) in the presence of DMAP (Sigma-Aldrich, USA), at the molar ratio of 1:1:1.1, and stirred at room temperature for 2 h. The reaction was followed thin layer chromatography (TLC) with hexane (EMD chemicals, USA): ethyl acetate (Fisher Scientific, Canada) (50:50) as solvent until completion. The solvent was removed under reduced pressure. The crude product was purified by recrystallization (hexane:ethyl acetate, 50:50) to give a pure product. The purified product, named N-2-(tert-butyloxycarbonyl) amino-N,N-bis(3-(dimethylamino)propyl)acetamide, was characterized by ¹H NMR. The NMR data is given in Appendix A.

3.2.4 Synthesis of phy-7NH-m (m = 12, 16, and 18)

The same method as for the synthesis of phy-3-m was used to make phy-7NH-m. The BOC-protected 3,3'-iminobis(N,N-dimethylpropylamine) (1.08 g, 3.75 mmol, chemical 8 in Scheme 3.3) was added to phytanyl bromide (1.08 g, 3.00 mmol) in 30 mL of anhydrous acetonitrile. The mixture was stirred at 50 °C for 3 days. The solvent was reduced by rotary evaporator to approximately 1 mL. The mixture was transferred to another round bottom flask to which 1-bromododecane (Acros Organics), 1-bromohexadecane (Acros Organics), or 1-bromooctadecane (Acros Organics) was added with 10 mL of acetonitrile and refluxed for 24 h. The molar ratio of product 9 in scheme 3.3 to 1-bromododecane or 1-bromohexadecane or 1-bromooctadecane (Acros Organics) was 1:2.25 (Scheme 3.3). After 24 h, the mixture was cooled to room temperature and transferred to a 250 mL round bottom

flask. HCl (6N) was added to the mixture in the presence of 40 mL of dichloromethane. The molar ratio of BOC and HCl was 1:1. The mixture was refluxed for 2 h. The solvent was removed by rotary evaporation. The crude product was recrystallized and produced the final products phy-7NH-m (m=12, 16, and 18) (Scheme 3.3). The purified products were characterized by ^1H NMR. The NMR data is given in Appendix A.



Scheme 3.3 Synthesis of phy-7NH-m (m=12, 16, and 18). i. Boc_2O , DMAP, CNCH_3 , 2 h; ii. product 3 from scheme 3.1, CH_3CN , 50°C , 3 days; iii. RBr , CNCH_3 , reflux, 24 h; iv. HCl , CH_2Cl_2 , reflux, 2 h.

3.2.5 Characterization of the phytanyl substituted gemini surfactants

The characterization of the phytanyl substituted gemini surfactants was carried out using Krafft temperature, surface tension, specific conductance, particle size, and transmission electron microscopy methods.

3.2.5.1 Krafft Temperature

For ionic surfactants, the solubility undergoes a sharp increase at some temperature, commonly referred to as the Krafft temperature (T_K).¹⁴⁶ In this study, T_K was determined using the specific conductivity method as previously reported.²⁰¹ To determine T_K , clear and saturated aqueous solutions of phy-3-m compounds were prepared and placed in a refrigerator overnight, where the precipitation of the surfactants occurred. The precipitated system was introduced into a temperature-controlled vessel. Temperature was controlled to ± 0.05 °C with a Lauda model RE304 (Lauda, Germany) circulating water bath. The initial temperature was set to ≤ 10 °C and then was incrementally increased. The conductivity of the solution was measured as a function of temperature using the conductivity meter (Fisher Scientific). The cell constant of the conductivity meter is 0.475 cm^{-1} . The Krafft temperature was taken the temperature where the curve of conductance vs. temperature shows a sharp break in slopes, as indicated by the arrows in the plot presented in Figure 3.1. This break coincides with the temperature of full clarification of the surfactant system.

3.2.5.2 Surface tension

Surface tension was measured using a Lauda model TE3 automated tensiometer (Lauda, Germany) by the du Nuoy ring method; all surface tension values (γ) were corrected by the method of Harkins and Jordan. The surface tension was measured after each titration of concentrated surfactant to 50 mL of milli-Q water at 25 °C or at a temperature indicated in the text.

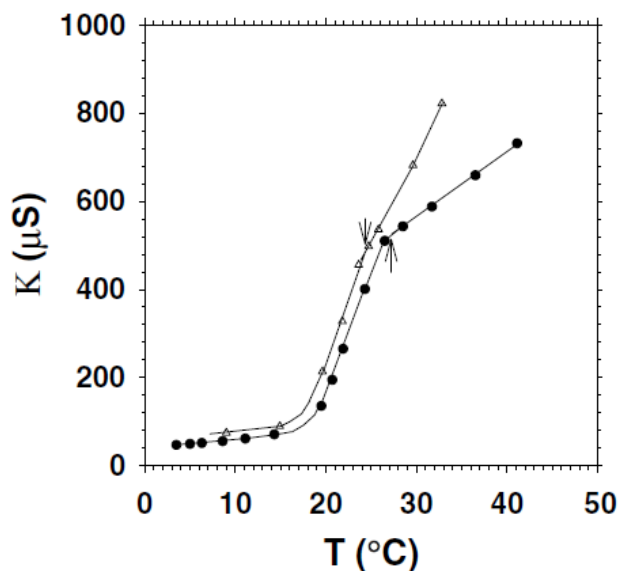


Figure 3.1 Conductance vs. temperature behavior of surfactant solutions: 16-8-16 (●) and 12-16-12 (Δ). The Krafft temperatures (T_K) were indicated by the arrows.²⁰¹

3.2.5.3 Specific conductivity

Specific conductivities were determined using a conductivity meter (Fisher Scientific) with a cell constant of 0.475 cm^{-1} . Experimental temperatures were maintained at 25°C , unless otherwise indicated, by means of a Lauda model RE304 (Lauda, Germany) circulating water bath. The specific conductivity was measured after each addition of an aqueous solution of concentrated surfactant to 15 mL of milli-Q water under stirring. The specific conductivity as a function of concentration was obtained for each surfactant.

3.2.5.4 Particle sizes

Particle size of each surfactant was measured at 25°C and/or a temperature indicated in the text by using a Malvern Zetasizer Nano ZS instrument (Malvern instruments, UK). The particle size distribution in water was obtained from the

light scattered by particles which was illuminated with a laser beam ($\theta = 173^\circ$). The measured sizes are reported using a % volume distribution. Each data point was automatically repeated multiple times, and the average is reported.

3.2.5.5 Transmission Electron Microscopy (TEM)

The morphology of the phy-3-m compounds was observed by TEM. A 20 μ L aliquot of each sample was dropped on a 300 mesh carbon coated copper grid for 30 to 60 seconds. The excess sample was drained off with filter paper and the deposited particles were stained with 1% (w/v) phosphotungstic acid (pH adjusted to 7 with 0.1N NaOH) for 20 seconds, and blotted with filter paper. The dried sample was examined with a JEOL 2010F TEM at the Canadian Centre for Electron Microscopy at McMaster University (Ontario, Canada). Measurements of bilayer thickness were made using a basic graphic drawing program and calibrating the resolution bar on each image to a known number of pixel elements. Measurements were made on three separate images at a minimum of three independent sites on each image for both the phy-3-12 and 12-3-12 systems ($n = 9$, average standard deviation = 0.2 nm).

3.2.6 *In vitro* transfection

The transfection complexes are composed of the plasmid, gemini surfactant, DOPE, in OPTI-MEM medium (GIBCO[®], Fisher Scientific, Canada). The plasmid, pVGteIRL, coding enhanced green fluorescent protein (EGFP) gene,²⁰² a gift from Dr. Roderick Slavcev (School of Pharmacy, University of Waterloo), was used at amount of 0.4 μ g/well (0.4 μ g DNA = 0.6 nmol/bp) for the transfection. All phytanyl substituted

gemini surfactants, 16-3-16, and 12-7NH-12, were prepared at a concentration of 1.5 mM, filtered through a 0.2 μm sterile filter (Catalogue number 09719A, Fisher Scientific, Canada), and used at 4 μL /well (6 nmol/well) to obtain a surfactant to plasmid charge ratio of 10:1. DOPE vesicles were prepared according to the method of Wettig et al,¹⁹³ at a concentration of 1 mM in PBS (pH9) and filtered using a 0.45 μm filter (Catalogue number 09719D, Fisher Scientific, Canada), and used at 15 μL /well for the transfection. The transfection complexes were prepared as follows. 0.4 μg of pVGteIRL was mixed with 4 μL of gemini surfactants solutions and incubated at room temperature for 15min; 15 μL of DOPE vesicles were added to the mixture and incubated at room temperature for 30 min.

Transfection assays were carried out as reported in a previous study.¹⁹³ Briefly, one day prior to the transfection, OVCAR-3 cells were seeded in 24-well plate at a density of 1×10^5 cells/mL. The cells were incubated at 37 °C with 5% CO₂ for approximately 24 h to reach 75% confluence on the day of the transfection. On the second day, the following steps were carried out, once the cell confluence reached approximately 75%. One hour prior to transfection, cells were washed with fresh phosphate buffered saline (PBS), and the old RPMI-1640 medium was replaced by the fresh RPMI-1640 medium without fetal bovine serum (FBS) and antibiotics. Then the transfection complexes were prepared as mentioned above and added to the cells dropwise. The cells were incubated at 37 °C with 5% CO₂ for 5 h. Cells were also transfected using 16-3-16 and 12-7NH-12, LipofectamineTM 2000 (Invitrogen,

used according to the manufacturer's protocol), plasmid only, and plasmid complexed with DOPE as controls. After 5 h incubation, the supernatant medium was replaced by fresh RPMI-1640 with 20% FBS and the cells were incubated at 37 °C with 5% CO₂ overnight for EGFP expression. On the third day, cells were collected and washed using PBS, and resuspended in PBS. The samples were analyzed with fluorescence activated cell sorting (FACS) instrument (BD FACSVantage SE). 10,000 cells were analyzed for each sample. The data was analyzed using WinMDI 2.9 software. Data are expressed as Mean ± SD (standard deviation), and statistical analysis was performed by One-Way ANOVA with a Tukey's post hoc test using Origin software.

3.3 Results and Discussion

3.3.1 Krafft temperature (T_k)

For phy-3-12, no precipitation of the surfactant occurred after overnight incubation in the refrigerator. It had to be frozen and then be melted slowly at room temperature to obtain a precipitation. Under the experimental measuring conditions, the phy-3-12 solution did not show any precipitate. For this system, T_k was considered below room temperature. Different from the phy-3-12, precipitates occurred for phy-3-16 and phy-3-18 systems. The conductance of these two surfactant systems was measured with the increased temperature. The T_k values for phy-3-16 and phy-3-18 were obtained from the plots presented in Figure 3.2. The Krafft temperature is

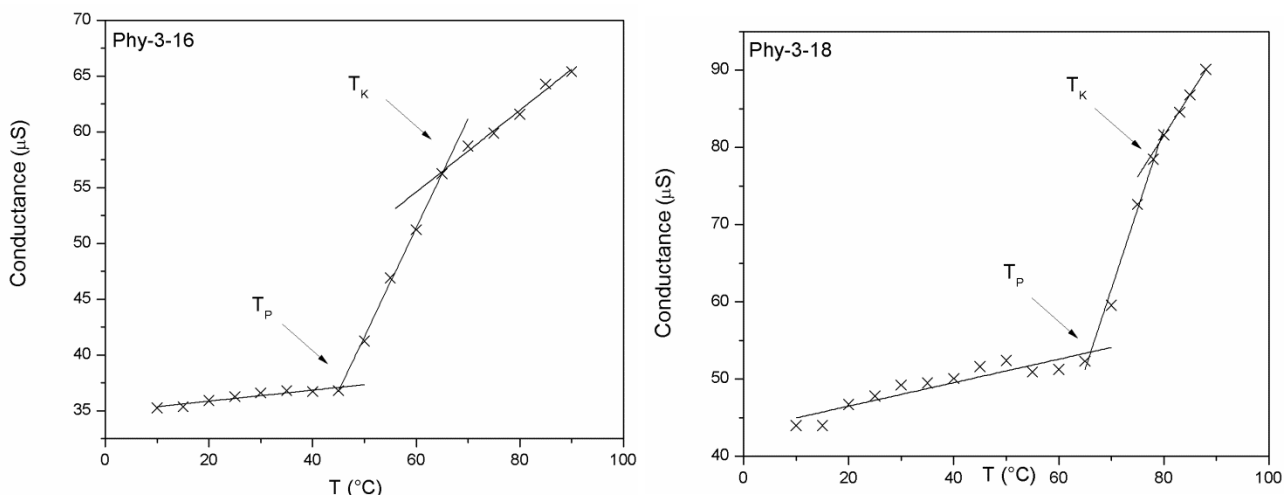


Figure 3.2 Determination of the Krafft temperature of the phy-3-m ($m = 16$ and 18). The Krafft temperature was taken as the temperature where the plot showed a break. The arrows indicate the T_K and T_P of the surfactant systems. The plotted data are seen in Table B-1 in Appendix B. The plotted data is referred to Wang and Wettig.²⁰³

indicated in the plots of phy-3-16 and phy-3-18 by arrows and listed in Table 3.1. As we observed, T_K values of phy-3-m ($m = 12, 16,$ and 18) increased with the increased alkyl tail length. This trend is in agreement with the observation in the m-3-m ($m=12, 16,$ and 18) listed in Table 3.1. Zana and Xia summarized general trends of T_K values for ionic surfactants. One is that T_K increases with the alkyl tail carbon atoms,¹⁴⁶ our results from phy-3-m fits this general trend. This is ascribed to the increased hydrophobicity of a surfactant system with a longer alkyl tail length, which can allow increase of Krafft temperatures. Increase of T_K with the hydrophobicity of alkyl tails can also be observed from the comparison of phy-3-m with m-3-m ($m = 12, 16,$ and 18). The bulky nature of phytanyl tail in the phy-3-m compounds results in a higher T_K values compared to the m-3-m surfactants.

Compared to the conductance vs. temperature behavior of phy-3-m (m = 16 and 18), phy-3-16 showed a gradual rise below the Krafft temperature, while a steep rise in conductance was observed for phy-3-18. This may be caused by a greater solubility for the phy-3-16 at temperatures below the Krafft temperature compared to phy-3-18. Additionally, the curve for phy-3-18 showed a high similarity to 12-16-12 surfactant, which is reported to form vesicles above T_K .²⁰¹

Table 3.1 The Krafft temperature (T_K) and Krafft point (T_P) of the gemini surfactants

Gemini surfactant	T_K (°C)	T_P (°C)
Phy-3-12	< room temperature	< room temperature
Phy-3-16	67.4	45
Phy-3-18	79.5	64.2
12-3-12	12.7 ²⁰¹	-
16-3-16	42.0 ²⁰⁴	-
18-3-18	45.3 ²⁰⁴	-

Note: T_P was misunderstood as T_K in a published article: Wang H., Wettig SD., PCCP, 2011.

It is important to note that Krafft temperature is different from Krafft point (T_P), which is defined as the temperature where the solubility of surfactant monomers becomes equal to the CMC.²⁰⁵ Above the T_P , micelles begin to form, which produces a rapid increase in the solubility of the surfactant. Thus, conductance of the surfactant system increases sharply with increased temperature beginning at T_P until T_K is reached.²⁰⁶ Thus, the Krafft temperature of an ionic surfactant is usually higher

than its Krafft point. The Krafft point is as important as the Krafft temperature for a surfactant system since T_P describes the temperature at which micelle starts to form and T_K indicates the temperature of full clarification of a surfactant system. Thus, researchers can decide experimental temperature depending on a study objective. Based on the conductivity measurements, the T_P values of phy-3-m were obtained and are given in Table 3.1. To obtain CMC values of phy-3-m using surface tension or specific conductivity, experimental temperature was selected based on their T_P values.

3.3.2 Surface tension and head group area

The surface tension as a function of the logarithm of surfactant concentration for the phy-3-m ($m = 12, 16, \text{ and } 18$) at different temperature is plotted in Figure 3.3. Critical micelle concentration (CMC) can be determined by the measurement of surface tension. In a plot of surface tension as a function of the logarithm of surfactant concentration, the CMC is found as the point where two lines intersect: the baseline of minimal surface tension and the slope where surface tension shows a linear decline. Operationally, CMC is determined from regression analysis of the region where surface tension linearly decreased and the post-micellar region. The CMC values of phy-3-m ($m = 12, 16, \text{ and } 18$) are listed in Table 3.2. The CMC for the phy-3-12 at 25 °C is 0.07 mM, much lower than the value for the 12-3-12 (0.98 mM). The value of CMC for the phy-3-16 at 50 °C is 0.0057 mM, which is around 5 times lower than that of the 16-3-16. The same trend was observed for the phy-3-18.

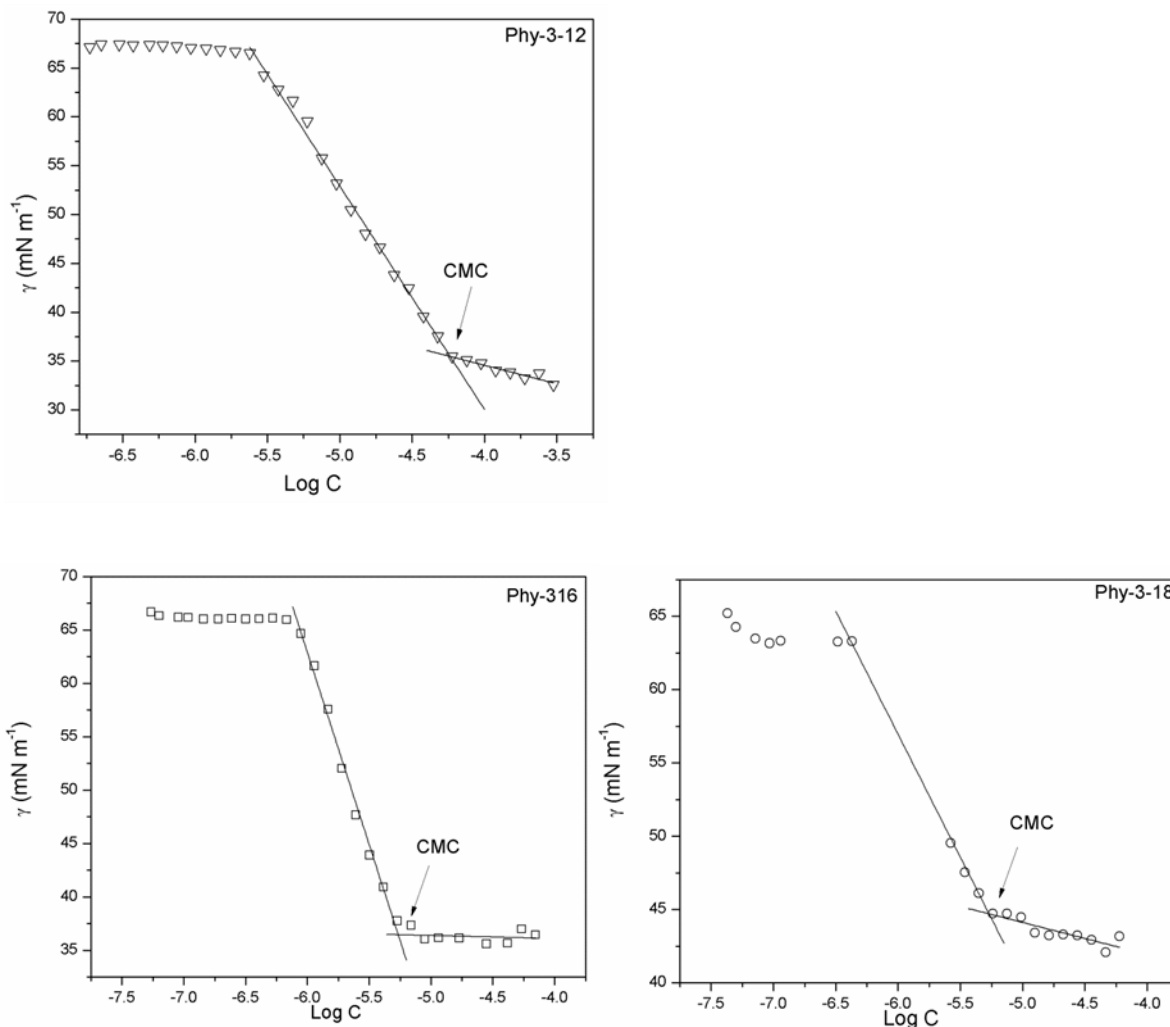


Figure 3.3 Surface tension vs. Log concentration for the phy-3-12 at 25 °C , phy-3-16 at 50 °C, and phy-3-18 at 65 °C. The lines are linear fits. Values of CMC, indicated by arrows, are determined from the intersection of two lines. The plotted data is seen in Table B-2 in Appendix B. The plot is referred to Wang and Wettig.²⁰³

A plot of the logarithm of the CMC as a function of hydrocarbon tail length for the phytanyl compounds is seen in Figure 3.4. As expected, approximately linear line with some minor variation for long tail lengths ($m = 18$) is observed, which is also reported in other studies.²⁰⁷ This observation is attributed to premicellar aggregate

formation.²⁰⁷ The Klevens constant, B, defined as the slopes of the log cmc vs. m plots, for the majority of gemini surfactants are 0.43 ± 0.03 ,¹⁴⁶ which is larger than the values of 0.27 – 0.3 for conventional quaternary ammonium surfactants.¹⁴⁹ The larger value of B reflects the increased hydrophobicity of the gemini surfactants, where the length of both tail groups are usually varied to maintain the overall symmetry of the molecule. When one varies the length of only a single tail group in the gemini surfactant (i.e. *m*-6-6 and phy-3-*m*), the Klevens constants (0.23 for *m*-6-6²⁰⁸ and 0.27 for phy-3-*m*) are again observed to fall below 0.3 similar to that observed for traditional quaternary ammonium surfactants.

The head group area (a_0) for the phytanyl compounds are calculated from the surface excess concentration according to the following equation:

$$a_0 = (N_A \Gamma)^{-1} \quad \text{(Equation 3.1)}$$

where N_A is Avogadro's number, 6.022×10^{23} , and Γ is the surface excess concentration obtained from the Gibb's adsorption equation:

$$\Gamma = - \frac{1}{2.303nRT} \left(\frac{d\gamma}{d \log C} \right)_T \quad \text{(Equation 3.2)}$$

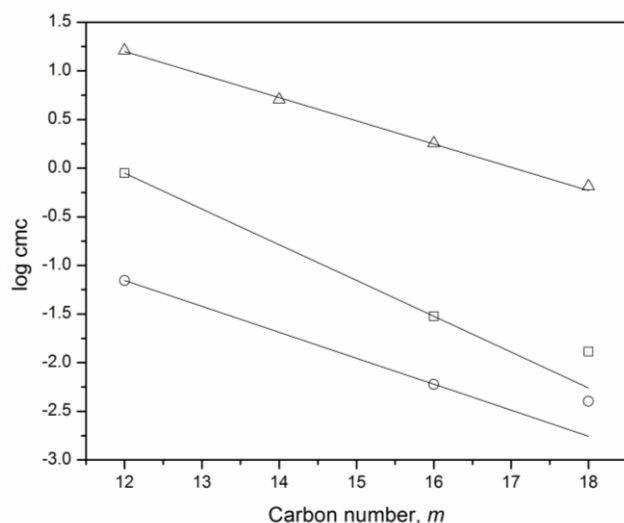


Figure 3.4 Variation of the logarithm cmc as a function of alkyl tail length for the gemini surfactants: m -3- m (\square , data from reference⁴⁴) phy-3- m (\circ ,); m -6-6 (\triangle , data from reference²⁰⁸). The plot is referred to Wang and Wettig.²⁰³

In Equation 3.2 R and T have their usual meaning, n is a constant accounting for the dissociation of ionic surfactants, and for the gemini surfactants $n=3$.¹⁶³ The head group area for the phytanyl substituted gemini surfactants are listed in Table 3.2. The head group area decreased with the decreased alkyl length of phy-3- m ($m = 12, 16, \text{ and } 18$). In another word, the head group area decreased with increased dissymmetry ($C_{16}:C_{12} > C_{16}:C_{16} > C_{16}:C_{18}$), indicating that the packing of surfactant molecules with a higher dissymmetry is more dense at the air-water interface. This trend is also observed in 16-2-8 ($C_{16}:C_8$) and 14-2-12 ($C_{14}:C_{12}$) surfactants, which have a head group area of $0.68 \text{ nm}^2/\text{molecule}$ and $0.81 \text{ nm}^2/\text{molecule}$, respectively.²⁰⁹ For these types of asymmetric gemini surfactants with short spacer groups ($s = 2$ or 3), the dominant factor in determining the variation in head group area is the interaction between the

hydrophobic tails since they do have the same length of spacer groups. With the increased dissymmetry, the attractive interaction between two tails becomes stronger, which results in a reduction of head group area.

However, a different trend was observed from the comparison of phy-3-m with their symmetric surfactants (m-3-m). The head group areas for the phy-3-12 and phy-3-16 surfactants are noticeably smaller than those for the 12-3-12 and 16-3-16 surfactants ($1.11 \text{ nm}^2/\text{molecule}$ and $1.21 \text{ nm}^2/\text{molecule}$, respectively⁴⁴) while that for phy-3-18 is approximately 1.5 times that reported for 18-3-18 ($1.28 \text{ nm}^2/\text{molecule}$ ²¹⁰). Such a discrepancy has also been reported by others. For example, 12-2-12 had a head group area of $1.02 \text{ nm}^2/\text{molecule}$ ²⁰⁹, higher than those for 16-2-8 and 14-2-12; the head group area of 12-6-12 ($1.40 \text{ nm}^2/\text{molecule}$ ^{44, 156}) is bigger than that of 12-6-14 ($1.28 \text{ nm}^2/\text{molecule}$ ²¹¹); while compared to 12-10-12 ($2.20 \text{ nm}^2/\text{molecule}$ ¹⁵⁶), 12-10-14 ($2.48 \text{ nm}^2/\text{molecule}$ ²¹¹) exhibited a higher head group area.

Table 3.2 Critical micelle concentration (CMC) and head group area (a_0) obtained by surface tension measurements.

Surfactant	CMC (mM)	$a_0 (\text{nm}^2 \text{ molecule}^{-1})$
Phy-3-12	0.07 ± 0.0001	0.78 ± 0.09
Phy-3-16	0.0057 ± 0.0005	0.91 ± 0.05
Phy-3-18	0.0054 ± 0.0004	1.92 ± 0.06
12-3-12 ⁴⁴	0.98 ± 0.04	1.11
16-3-16 ⁴⁴	0.026 ± 0.001	1.21
18-3-18 ²¹⁰	0.013 ± 0.001	1.28

Note: the table is referred to Wang and Wettig.²⁰³

3.3.3 Conductivity measurement

The graphs of specific conductivity versus concentration of the phytanyl compounds are plotted in Figure 3.5. Critical micelle concentration is usually estimated from the abrupt change of specific conductivity vs. concentration curve. However, a frequent problem arises when the conductivity-concentration plot exhibits a weak curvature. In this case, it is very difficult to determine the break in the conductivity-concentration plots and then the CMC values are affected by a great uncertainty. To solve this problem, an alternative procedure was proposed and has been used to obtain CMC and other application, for example, a study on the effect of ethylene glycol addition on the micellization of tetradecyltrimethylammonium bromide.²¹² In this method, the CMC values were determined from a fit of the conductivity-concentration plots (κ vs. c) according to the method of Carpena et al.²¹³, using the relation (Equation 3.4):

$$\kappa = \kappa_0 + A_1c + dx(A_2 - A_1) \ln \left(\frac{1 + e^{(c-cmc)/dx}}{1 - e^{-c/dx}} \right) \quad (\text{Equation 3.3})$$

where κ_0 represents the conductivity at $c = 0$, A_1 and A_2 are the asymptotic values for small and large values of c , respectively, and dx is a constant, which accounts for the width of the CMC transition region.

The CMC values obtained from the specific conductivity measurements are listed in Table 3.3. The CMC of phy-3-12 obtained from specific conductance was 0.063 mM, which is very consistent with the value obtained from surface tension

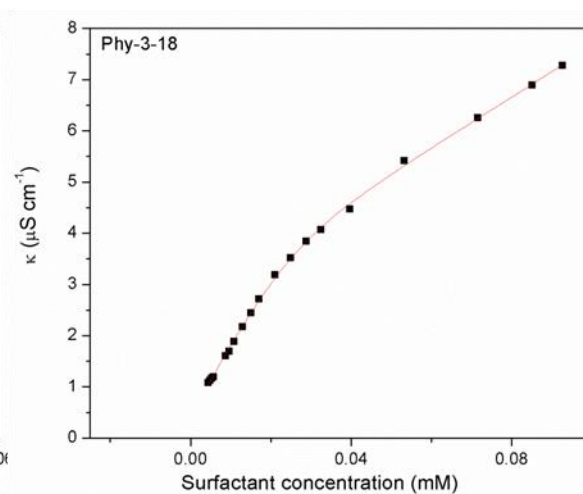
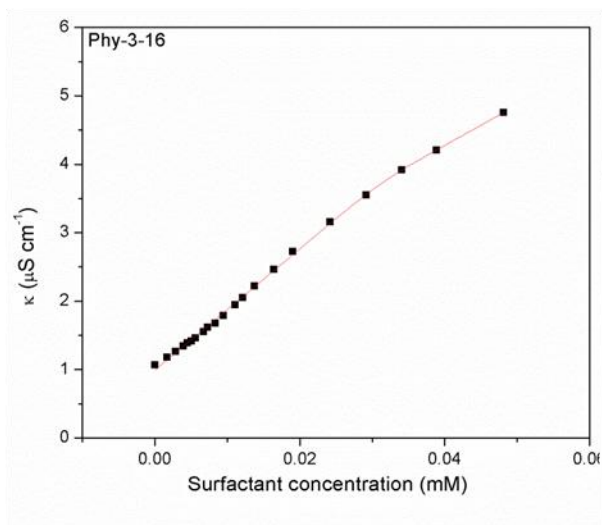
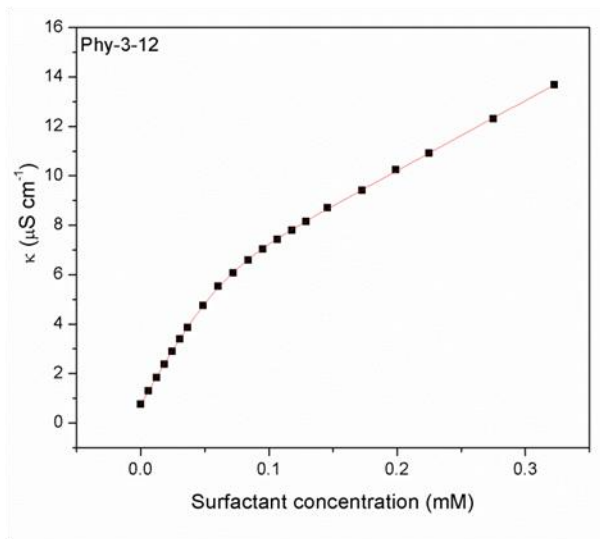


Figure 3.5 Specific conductivity vs. concentration for phy-3-12 at 25 °C, phy-3-16 at 50 °C, and phy-3-18 at 65 °C. The lines are the best fits of data to the equation 3.4. The experimental data is listed in Table B-3 in Appendix B. The data is referred to Wang and Wettig.²⁰³

measurements (Table 3.2). Poorer agreement is obtained for the phy-3-16 and phy-3-18 surfactants, which may be as a result of the different properties measured by these techniques and potentially due to the accuracy of the different methods.¹⁴⁹ Regardless, the same trend of decreasing CMC with increasing m is observed with both methods.

In addition, based on Equation 3.3, the degree of micelle ionization (α) can be obtained from the ratio of A_2/A_1 . This parameter, α , is defined as a fraction of an ionic surfactant's counterions that are dissociated from micelles, leaving the micelles charged.²¹⁴ Generally, counterion binding increases with increasing alkyl tail length for an ionic surfactant,^{215, 216} which means α decreases with the increased tail length for ionic surfactants. The trend of decrease of α on increasing alkyl tail length has been ascribed to the increased micelle surface charge density on increasing tail length.²¹⁶ For example, For $C_mH_{2m+1}(CH_3)_3N^+Br^-$, α values decreased from 0.35 to 0.16 in going from $m = 8$ to 16²¹⁶ (data presented in Figure 3.6). As the results shown in this study, α values of phy-3- m varied with the tail length. It seems inconsistent with the general trend mentioned above. This is caused by the different measuring temperature of α (phy-3-12 at 25 °C, phy-3-16 at 50 °C and phy-3-18 at 65°C). An increase of α with temperature has been reported by others.²¹⁶⁻²¹⁸ The reaction that a bromide ion dissociates from a micelle is believed to be endothermic.²¹⁶ Hence, increasing temperature facilitates the dissociation of

counterions from the micelles, resulting in an increased α . This is also the reason why α values of 16-3-16 and 18-3-18 are higher than that of 12-3-13 (Table 3.3).

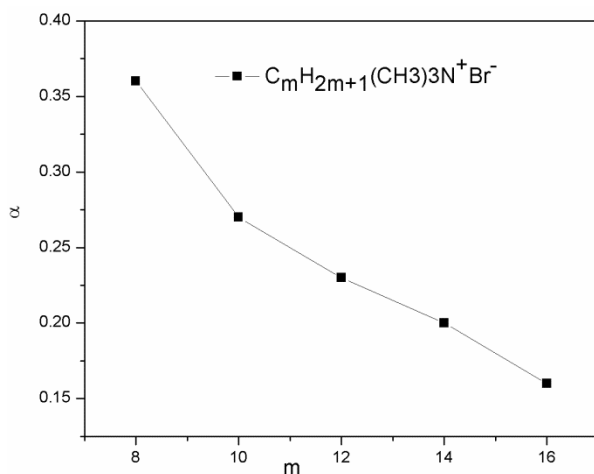


Figure 3.6 Variations of degree of micelle ionization (α) with alkyl tail length of $C_mH_{2m+1}(CH_3)_3N^+Br^-$ at 25°C (data from reference²¹⁶).

The charge of a micelle is very important in such applications that employing the micelle as a charged interface, such as for transgene delivery. The higher α , the easier the counterions can be replaced by other anionic ions. For example, the higher degree of ionization for the phy-3-16 indicates that the counter ions (Br^-) would be more readily replaced when mixed with DNA, as compared to 16-3-16. Compared to the symmetric corresponding ones, the phy-3-m showed a higher α (Table 3.3), which is an advantage of the phy-3-m applied to gene therapy as non-viral vectors.

Table 3.3 Critical micelle concentration (CMC) and degree of micelle ionization (α) obtained from conductivity measurements.

Surfactant	CMC (mM)	α
Phy-3-12	0.063 \pm 0.003	0.46 \pm 0.01
Phy-3-16 ^a	0.031 \pm 0.001	0.67 \pm 0.02
Phy-3-18 ^b	0.027 \pm 0.002	0.44 \pm 0.03
12-3-12 ⁴⁴	0.98 \pm 0.04	0.23 \pm 0.02
16-3-16 ²¹⁹	0.026 \pm 0.001	0.35 \pm 0.02
18-3-18 ²⁰⁴	0.028 \pm 0.002	0.32 \pm 0.05

^ameasured at 50°C, ^bmeasured at 65°C. The table is referred to Wang and Wetig.²⁰³

3.3.4 Aggregate shape and particle size of the phytanyl substituted surfactants

Due to the increased hydrophobicity and bulky nature of the phytanyl group relative to a hexadecyl tail, phytanyl substitution dramatically impacts the molecular packing. The shape of aggregates formed by the phytanyl compounds was predicted from calculation of the packing parameter. As introduced in the section 1.3.1, the packing parameter (P) can be calculated based on the volume and length of the hydrocarbon tail, and the head group area. The volume of the hydrocarbon tail can be estimated from known values for the volume of methylene and methyl groups according to:

$$v = n \times (V_{\text{methylene}}) + m (V_{\text{methyl}}) \quad (\text{Equation 3.4})$$

Where $V_{\text{methylene}} \approx 27 \text{ \AA}^3$ and $V_{\text{methyl}} \approx 54 \text{ \AA}^3$; n and m are the number of carbons in the methylene and methyl groups, respectively²²⁰. The length of hydrocarbon tails can be calculated from the following equation¹⁴⁹:

$$l = 1.5 + 1.265 \times n_c \quad (\text{Equation 3.5})$$

Where n_c is the number of carbons in the alkyl tail.

The calculated values of the volume, length, and the packing parameter for the phy-3-m and their corresponding ones are reported in Table 3.4 where the total volume of the hydrophobic tails is given by ($v_1 + v_2$) and the length of the hydrophobic group will be equal to the length of the longest tail. As seen in Table 3.4, as well as in the literature (both from prior calculations of P and experimental measurements), aggregates formed by m-3-m gemini surfactants tend to form cylindrical micelles with a P value of approximately 0.35 depending upon the alkyl tail length. The replacement of one of the tail groups by a phytanyl chain significantly increases the hydrophobic volume (due to the bulkiness of the additional methyl group branches) without impacting the overall length of the hydrophobic group (except for the phy-3-12 surfactant). This restricts the geometry of the system such that vesicles are now the predicted favorable geometry, as seen experimentally by the larger particle diameters, 13 nm for phy-3-12, 46 nm for phy-3-16, and 30 nm for phy-3-18, that are consistent with vesicle formation (Table 3.4).

Table 3.4 Calculated packing parameter (P) and measured particle sizes (diameter, d) for the phy-3-m and m-3-m (m=12, 16, and 18).

Surfactant	a_0 (Å ²) ^a	v_1 (Å ³) ^b	v_2 (Å ³) ^b	l (Å) ^c	P	d (nm)
Phy-3-12	78	595	351	21.74	0.59	13 ± 5
Phy-3-16	91	595	459	21.74	0.53	46 ± 1
Phy-3-18	192	595	513	24.27	0.24	30 ± 4
12-3-12	111 ^d	351	351	16.68	0.38	2.2±0.2 ^e
16-3-16	121 ^d	459	459	21.74	0.35	3.3±0.2 ^e
18-3-18	128 ^f	513	513	24.27	0.33	4.4±0.05 ^e

Note: ^a from Table 3.2; ^b from equation 3.5; ^c from equation 3.6; ^d from reference ²⁰⁸; ^e from reference ²⁰⁴; ^f from reference ²¹⁰. The table is referred to Wang and Wetig. ²⁰³

To investigate the nature of micellar aggregates, the phy-3-m was imaged by TEM and the images of the phy-3-12 and 12-3-12 were illustrated in Figure 3.7. The TEM images support the finding that the phy-3-m compounds prefer to form a stacked bilayer-type of aggregate rather than spherical or the rod-like micelles which are typically observed in gemini surfactants with shorter spacer groups.

As can be seen in Figure 3.7, micelles observed for the 12-3-12 are smaller and less organized than those for the phy-3-12. Furthermore, analysis of the spacing between layers in Figure 3.7 for phy-3-12 gives an average spacing of 4.6 ± 0.2 nm ($n=9$), or approximately 2.3 nm as the thickness of a monolayer. This corresponds well with the calculated length of the phytanyl chain (2.174 nm or 21.74 Å from Table 3.4). The corresponding thickness of rod-shaped structures observed for the 12-3-12 micelles is around 3.2 ± 0.2 nm ($n=10$), giving a monolayer thickness of 1.6 nm, again in good agreement with the calculated length of a dodecyl chain (16.68 Å from Table 3.4).

The exception to the above is the phy-3-18 surfactant, which has a head group area of 192 \AA^2 per molecule and results in a P value of 0.24 which would predict the formation of spherical micelles. It should be noted however, that the equilibrium surface tension method may not give truly representative values for the head group area, and suggests that these calculations may need to be repeated with molecular areas derived from Langmuir – Blodgett film studies. Nevertheless, given our interest in designing novel surfactants for gene therapy applications, the constraint on molecular geometries resulting from phytanyl substitution may ultimately prove

useful in the formation of lipoplexes with higher orders of bilayer structure, known to favorably increase transfection efficiencies.¹⁶⁸

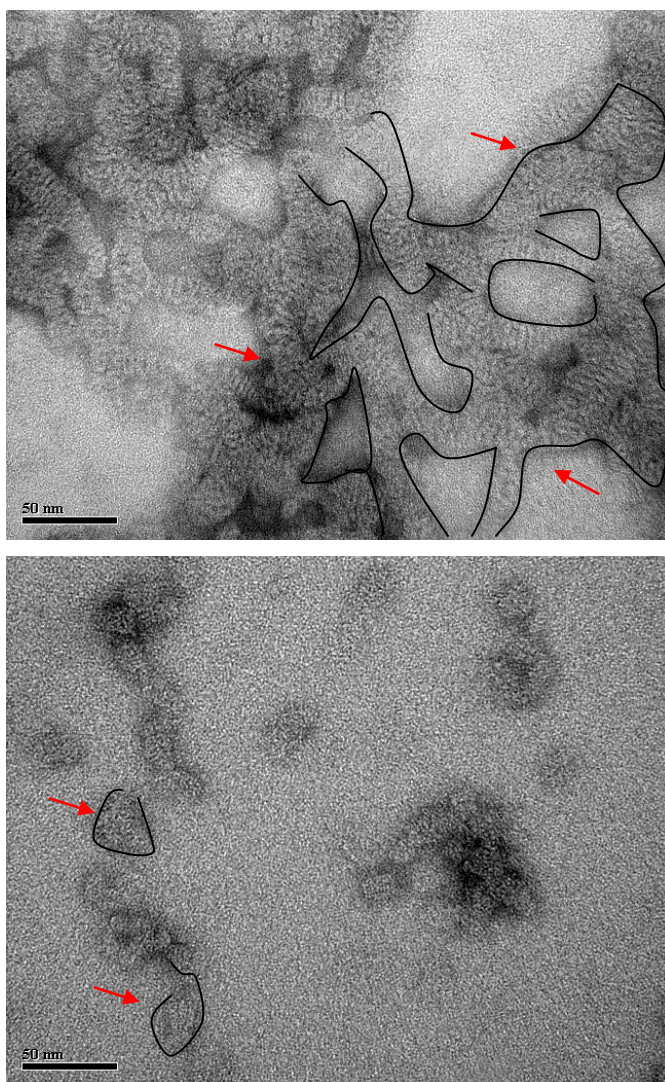


Figure 3.7 Transmission electronic micrographs of phy-3-12 (upper) and 12-3-12 (lower), bar represents 50 nm. Red arrows represent stacked bilayers in the upper graph, and rod-shaped micelles in the lower graph. Concentrations of 12-3-12 and phy-3-12 were 4.9 and 0.35 mM, respectively. The plot is referred to Wang and Wettig.²⁰³

3.3.5 Preliminary investigation on transfection activity of the phytanyl substituted gemini surfactants

The capacity of phytanyl substituted compounds for gene delivery was investigated in OVCAR-3 cells, and EGFP expressed in the cells is shown in Figure 3.8. The phy-3-m series of compounds exhibited significantly higher EGFP expression as compared to the 16-3-16 surfactant ($p < 0.1$), previously demonstrated to be efficient in not only *in vitro* transfection, but also as an *in vivo* topical treatment using a mouse model.¹⁵² Such promising results could be interpreted as following. The higher degree of micelle ionization of phy-3-m could produce the favorable formation of gemini surfactant-DNA complex. Additionally, the bulky nature of phytanyl substitution that results in vesicle formation without DNA could give rise to the formation of higher order structures upon complexation with DNA, which is similar to what is observed with DOPE and 12-3-12 surfactant as previously reported.¹⁸⁸

The other series of phytanyl compounds, phy-7NH-m, were not able to deliver EGFP in OVCAR-3 cells, shown in Figure 3.8. Additionally, 12-7NH-12 showed poor transfection ability in OVCAR-3 cells. The lack of transfection ability for the phy-7NH-m and 12-7NH-12 is in disagreement with the expected results reported by Wettig et al..¹⁹³ The amino-substituted 12-7NH-12 showed great Luciferase expression in COS7 cells, significantly higher than 12-3-12 did. Different cell lines have an effect(s) on transgene efficiency. Cell surface receptors and possible roles related to the cellular binding may depend on cell lines. For example, heparan sulfate proteoglycans (HSPGs), located in cellular membrane and functioning as specific

growth factors, has been reported to vary in cell lines,¹⁰⁷ which then influences HSPGs mediated binding in gene transfection. In addition, transfection efficiency may not truly describe transfection ability of a delivery vector. It only gives how much proteins expressed in the cells, but no information about efficiency of the delivery vector internalized in the cells, escaped from endosomes, and DNA release from the complexes. Thus, the above limitations of using transfection efficiency to measure transfection ability of a delivery vector should be considered when evaluating transfection ability of the delivery vector. Meanwhile, other techniques, such as confocal, may be employed to track a delivery vector inside cells.

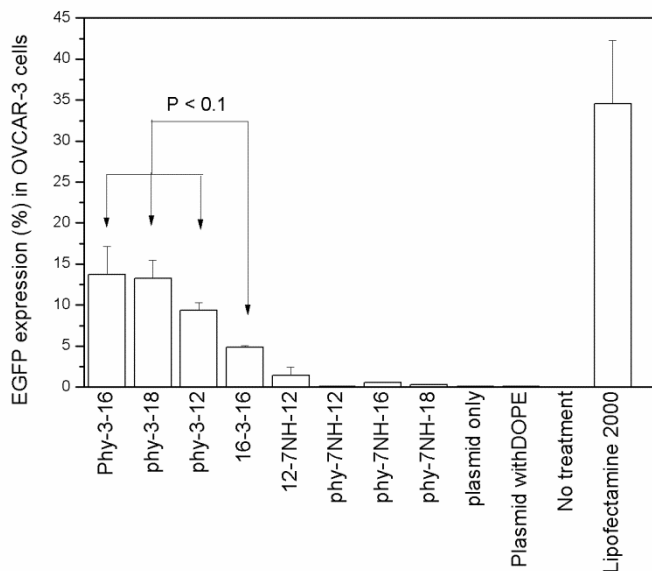


Figure 3.8 *In vitro* transfection of OVCAR-3 cells with plasmid-gemini surfactant-DOPE complexes. Data are also presented for cells without any treatment, treated by plasmid with and without DOPE, and LipofectamineTM 2000. Significant differences between phy-3-m (m = 12, 16, and 18) and 16-3-16 were observed ($p < 0.1$) ($n = 3$ except for complexes formed by phy-7NH-m, error bar = standard deviation). The plotting data are given in Appendix E. The data of phy-3-m and 16-3-16 is referred to Wang and Wettig.²⁰³

3.4 Conclusions

The phytanyl substituted gemini surfactants, phy-3-m and phy-7NH-m (m = 12, 16, and 18) were synthesized. The aggregation properties of phy-3-m were characterized. The Krafft temperature of phy-3-m increased with the tail length, consistent with general observations for other gemini surfactants. Compared to their symmetric m-3-m compounds, phy-3-m showed much lower CMC values due to the higher hydrophobicity caused by the phytanyl substitution. The higher degree of micelle ionization (α) of phy-3-m indicates that phy-3-m compounds more readily form DNA-surfactant complexes compared to their symmetric m-3-m. Head group areas for phy-3-m compounds are smaller than those for the m-3-m surfactants (with the exception of phy-3-18) and likely point to the increased affinity of the alkyl tail group of the phytanyl compounds for the more hydrophobic air side of the air-water interface.

Packing parameters calculated for the phy-3-m compounds are indicative of the formation of vesicles, which is in agreement with experimental determination of particle diameters and the morphologies imaged by TEM. Such structures are advantageous in forcing the preferential formation of higher order bilayer structures (i.e. inverted hexagonal and/or cubic) upon complexing with DNA. Preliminary transfection assays *in vitro* demonstrated that the phytanyl substitution does result in increased transfection efficiencies, compared to the symmetric 16-3-16 surfactant.

Chapter 4 Transfection and structural properties of phytanyl substituted gemini surfactant-based vectors for gene delivery

4.1 Introduction

As introduced in Chapter 1, application of cationic gemini surfactants as transgene delivery vectors for gene therapy has been attracting more and more researchers. To evaluate the ability of a non-viral vector to deliver transgenes, transfection assays are a must. Transfection efficiency depends on many factors, such as chemical structure of cationic surfactants, formulation of transfection complexes (i.e. ratio of cationic vector to DNA, corporation with or without a helper lipid), the type of cell line, duration of post-transfection (time for transgene expression), transfection complex surface charge, and structures of the complexes, etc. General observations based on studies about m-s-m type of gemini surfactants as transgene delivery vectors have been listed in Chapter 1.

A group of phytanyl substituted asymmetric gemini surfactants, phy-3-m ($m = 12, 16, \text{ and } 18$) was rationally designed, synthesized, and characterized. One of the primary goals of our study is to develop suitable gemini surfactant-based vectors for ovarian cancer gene therapy. Thus, the ability of phy-3-m to transfect ovarian cancer cells is the first step. The preliminary results showed that phy-3-m can be able to deliver transgene in an ovarian cancer cell line, as described in the previous chapter. In this chapter, transfection ability of phy-3-m was investigated by varying the ratio of surfactant to DNA; transfection complexes were characterized by measuring particle size and zeta potential; and complex structures were studied with small angle X-ray

scattering. All of these measurements provide valuable information that can aid in the optimization of phytanyl gemini surfactants-based gene delivery system for ovarian cancer gene therapy; moreover, study on structural activity of phy-3-m will assist in the rational design of more surfactants that are efficient in transgene delivery.

4.2 Methods and Materials

Phy-3-m (m =12, 16, and 18) and 16-3-16 were synthesized as described in the previous chapter. The plasmid used in the study was pVGtelRL coding enhanced green fluorescent protein (EGFP) gene,²⁰² a gift from Dr. Roderick Slavcev (School of Pharmacy, University of Waterloo). The amplification of the plasmid was done in our laboratory. DOPE was prepared at 1 mM in PBS (pH9) according to the method introduced in section 3.2.6. Lipofectamine™ 2000 was purchased from Invitrogen and used according to the manufacturer's protocol.

4.2.1 The preparation of the plasmid

To obtain enough plasmid for *in vitro* transfection experiments, the plasmid pVGtelRL was prepared from *E.coli* grown in Luria Bertani (LB) medium with 0.1% (v/v) kanamycin. After overnight growth, the plasmids were extracted and purified using a PureYield™ Plasmid Midiprep System kit (Promega, USA). Briefly, the culture was centrifuged at 5,000 x g for 10 min; cell pellets were resuspended; cell lysis solution was added and incubated for 3 min at room temperature; cell lysate was obtained after adding neutralization solution and centrifuging at 15,000 x g at

room temperature. DNA was purified from cell lysate using the Clearing Column and Binding Columns offered in the kit. The Binding Column was washed with the provided Endotoxin Removal and Column Wash solutions, and dried by applying a vacuum for 30-60 seconds. 600 μ L of Nuclease-free water was added to the DNA binding membrane and the Binding Column was centrifuged at 2,000 x g for 5 min using a swinging bucket rotor. The purified DNA was quantified by Nanodrop 2000 spectrophotometer (Thermo Scientific, Canada).

4.2.2 OVCAR-3 Cell preparation

Transfection study was performed using OVCAR-3. OVCAR-3 cells were grown on 75 cm² tissue culture flasks in 15-20 mL RPMI-1640 medium (HyClone®, Fisher Scientific, Canada) supplemented with 20% of fetal bovine serum (FBS) (Fisher Scientific, Canada) and 1% of Penicillin-Streptomycin (antibiotics) (Fisher Scientific, Canada). The cells were incubated at 37 °C with 5% CO₂ in tissue culture incubator.

4.2.3 Transfection assay

All gemini surfactants were prepared at 1.5 mM, filtered through a 0.2 μ m of a sterile filter (Catalogue number 09719A, Fisher Scientific, Canada). The molar ratio of gemini surfactant to DOPE was kept at 1:2.5 since the complexes at this ratio are able to transfect cells efficiently as showed in the previous chapter. The transfection complexes were prepared as follows: 0.4 μ g of pVGteIRL was mixed with aliquots of sterile gemini surfactant solutions to obtain a gemini surfactant/DNA charge ratio of 2:1, 5:1, 10:1, or 20:1, and incubated at room temperature for 15 min. To this

mixture, an aliquot of DOPE vesicles were added to keep the molar ratio of surfactant to DOPE at 1:2.5, and incubated at room temperature for 30 min to allow the transfection complexes to form, followed by addition of the complexes to cells according to the transfection protocol mentioned in section 3.2.6. After 5 h incubation, the supernatant medium on the cells were replaced by the fresh RPMI-1640 with 20% of FBS. The resulting EGFP expression was determined in approximately 18 h.

4.2.4 Fluorescence microscopy

Before harvesting the cells, Images of EGFP expressed in OVCAR-3 cells were obtained using a PTI (Photon Technology International, Canada) image system equipped with a Nikon fluorescence microscopy (Nikon Eclipse Ti, Japan). Samples were excited at a wavelength of 470 nm and emission was monitored at 510 nm.

4.2.5 Fluorescence activated cell sorting (FACS)

The EGFP expression and cell viability was quantified using FACS technique. Briefly, cells were detached using 0.25% trypsin-EDTA (Fisher Scientific, Canada), pooled for each treatment condition, then centrifuged at 4 °C and 1800 rpm for 7 min. The cell pellet was washed with PBS twice and resuspended in 350 µL of PBS. To determine the cytotoxicities of the treatments, 10 µL of propidium iodide (PI, 50 mg/mL) was added to each sample and incubated in an ice bath for at least 30 min before the FACS analysis. 10,000 cells for each sample were counted using a BD FACSVantage SE instrument (Biology, University of Waterloo). The data was

analyzed using WinMDI 2.9 software. Data are expressed as Mean \pm SE (standard error).

4.2.6 Characterization of the transfection complexes

The transfection complexes were prepared as described earlier for the transfection assay, with the exception that, the complexes were prepared in milli-Q water instead of OPTI-MEM medium (GIBCO[®], Fisher Scientific, Canada) in larger volumes (1 mL). Fresh transfection complexes were prepared at charge ratios (+/-) of 2:1, 5:1, and 10:1. Initial characterization of the complexes was carried out by measuring particle size and zeta potential of the nanoparticles. The measurement of the particle size and zeta potential was carried out using a Malvern Zetasizer Nano ZS instrument (Malvern instrument, UK).

The method to determine the particle size was described earlier. The measurement of zeta potential of the complexes was performed by using electrophoretic light scattering. Zeta potentials were measured using disposable Malvern zeta potential cells, illustrated in Figure 4.1. When an electric field is applied across a sample, charged particles suspended in the sample attract toward the electrode of opposite charge. Their velocity is measured using Laser Doppler Velocimetry (LDV) technique. The zeta potential of the particle is obtained in terms of the Henry equation:²²¹ $U_E = \frac{2\varepsilon\zeta f(\kappa a)}{3\eta}$, where U_E is electrophoretic mobility, ε is dielectric constant, ζ is zeta potential, η is viscosity, and $f(\kappa a)$ is Henry's function. The velocity of a particle in an electric field is referred to its electrophoretic mobility.

Thus, calculation of zeta potential from the electrophoretic mobility is straightforward. Operationally, the laser beam passes through the center of the sample cell and scattering light at an angle of 17° is detected. The samples were prepared by the same method as the one used for measuring particle size. All measurements were made at 25°C . Size measurements of transfection complexes are expressed as a % intensity basis. All measurements were repeated multiple times and results are reported as the mean \pm standard deviation.

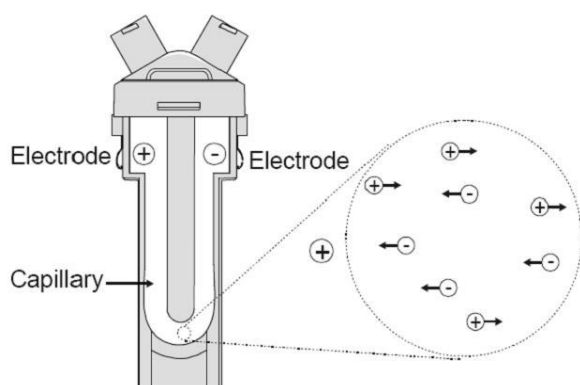


Figure 4.1 A classical cell for measuring zeta potential.²²¹

4.2.7 Small angle X-ray scattering (SAXS)

The samples for SAXS were prepared as following. DOPE and a gemini surfactant were mixed in chloroform (Fisher Scientific, Canada). The solvent was evaporated under reduced pressure. The dry mixture was hydrated using milli-Q water to make lipid mixture. The final concentration of DOPE and the gemini surfactant in the lipid mixture was 100 mM and 40 mM, respectively, which gives the mole ratio of gemini surfactant to DOPE at 1:2.5. The salmon sperm DNA (Sigma) was prepared at 20 mM in milli-Q water as a stock. A portion of 150 μL of the DNA was added into 150,

375, and 750 μL of the above lipid mixture to make complexes at the charge ratios of 2:1, 5:1, and 10:1, respectively. The samples were then vortexed for 30 seconds, and placed at 4 $^{\circ}\text{C}$ prior to SAXS investigation.

SAXS experiments were performed using a SAXSess mc² instrument (Anton Paar, Austria), located in Dr. Eric Prouzet's group in the Department of Chemistry at the University of Waterloo. The wavelength of X-ray generated is 0.154 nm. SAXSess mc² has a sample-to-detector distance of 0.267 m. The scattering pattern is recorded by an imaging plate reader at a size of 15 x 5 cm (L x W) (Anton Paar, Austria), and 2D scattering pattern is integrated into a one-dimensional scattering plot using SAXSquantTM software (Anton Paar, Austria); the one-dimensional scattering plot is the scattering intensity as a function of q, where q is the scattering vector. The scattering wave vector (q) is given by²²² $q = \frac{4\pi \sin \theta}{\lambda}$, where 2θ is the scattering angle and λ is the wavelength of X-ray. In this study, the data was collected in a q-range from 0 to 3 nm^{-1} .

The sample was loaded into the capillary sample holder (Anton Paar, Austria) at room temperature and equilibrated for at least 10 min. The scattering was scanned for 30 min and the scattering pattern was recorded on the image plate. All spectra were subtracted from the background which is the scattering profile obtained for a capillary containing water only. The data acquisition and analysis was performed using the SAXSquantTM software (Anton Paar, Austria). The scattering peaks were fitted according to a Gaussian function using the fityk software.¹⁹³

4.2.8 Statistical analysis

Statistical analysis was performed by One-Way ANOVA with a Tukey's post hoc test using Origin software.

4.3 Results and Discussion

The ratio of gemini surfactant to DNA influences many properties, such as surface charge of the complexes, particle size, the phase structure(s) the complexes form, all of which are known to impact transfection efficiency and cytotoxicity. To investigate the influence of the amount of gemini surfactants on DNA delivery, a series of transfection complexes formulated at different charge ratios of the gemini surfactants to DNA was tested in OVCAR-3 cells. The charge ratios of the gemini surfactant to DNA were 2:1, 5:1, 10:1, and 20:1.

4.3.1 Evaluation of transfection efficiency *in vitro*

4.3.1.1 EGFP expression imaged using fluorescence microscopy

Firstly, the transfected OVCAR-3 cells were observed using fluorescence microscopy. Representative images are displayed in Figure 4.2. The black background without any bright spots indicates that the protein EGFP has not been expressed in the cells, while the cells expressing EGFP showed bright spots. The images (Figure 4.2 a, b, and g) obtained from non-treated OVCAR-3 cells, the cells transfected by plasmid only, and the cells treated with the complexes formed by the phy-3-16 compound at 20:1, did not show any bright spots, indicating there is no EGFP expressed in the cells. This is in agreement with the results obtained with

FACS analysis, shown in the next paragraph. Bright spots were found in the images (Figure 4.2 c, d, e, and f) obtained from the cells transfected by Lipofectamine™ 2000, and the complexes formed by the phy-3-16 compound at the charge ratios of 2:1, 5:1, and 10:1, indicating that Lipofectamine™ 2000, and the gemini surfactants at charge ratios of 2:1, 5:1, and 10:1, can deliver EGFP into the OVCAR-3 cells. Fluorescence microscopic images for transfection complexes formed by other gemini surfactants are seen in Appendix D.

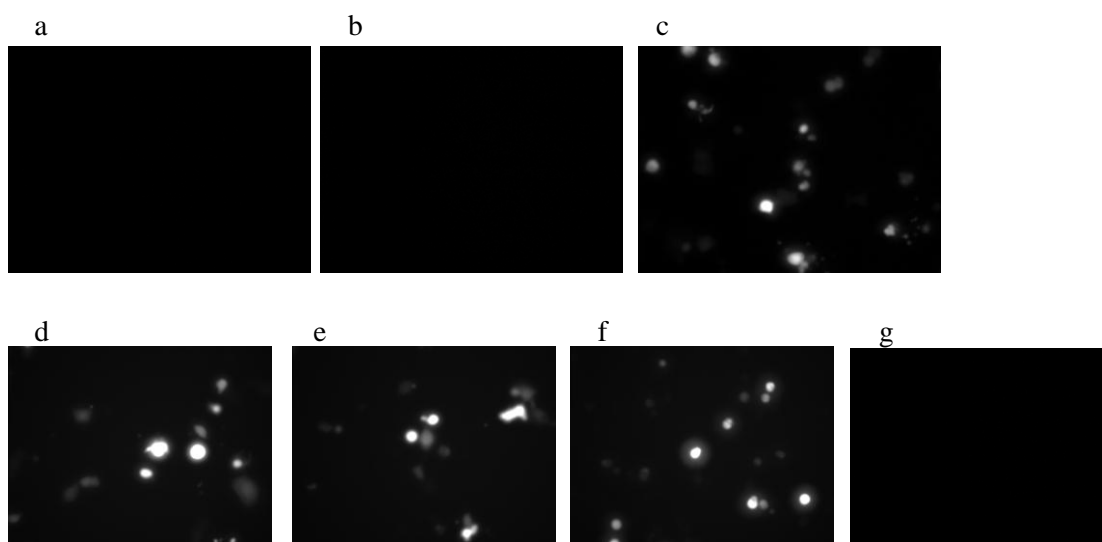


Figure 4.2 EGFP images for non-treated cells (a), cells treated with plasmid only (b), cells treated with Lipofectamine™ 2000 (c), and cells treated with complexes comprised of phy3-16, plasmid, and DOPE at charge ratios of 2:1 (d), 5:1 (e), 10:1 (f), and 20:1 (g). The bright spots represent live cells expressing EGFP.

4.3.1.2 EGFP expression quantification using FACS

To quantitatively evaluate EGFP expression in the OVCAR-3 cells and to measure cell toxicities, the transfected cells were analyzed using FACS. The dot plots obtained for the controls and treatments are shown in Figure 4.3. Live cells positive for EGFP are counted along the X-axis and are differentiated from the dying or dead cells positive for propidium iodide (PI) counted along the Y-axis. The upper right quadrant of the plots indicates the dying or dead cells expressing EGFP. According to our results, no EGFP-positive cells were found in the samples of non-treated cells (Figure 4.3a), or for cells treated with the plasmid only (Figure 4.3b). Live cells expressing EGFP were observed for the positive control (treatment with Lipofectamine™ 2000, Figure 4.3c) and in cells treated with the gemini surfactants at charge ratios of 2:1, 5:1, 10:1, and 20:1 (Taking phy-3-16 as an example, seen in Figure 4.3 d to g). PI-positive cells along the Y-axis were found in all samples, indicating that some techniques involved in the transfection assays are toxic to cells. These techniques include the detachment reagent (trypsin) and detaching time, and resuspension medium (PBS) for FACS measurement.

EGFP-positive cells were quantified and plotted in Figure 4.4A. As a positive control, the commercial vector Lipofectamine™ 2000 showed 32.2% of EGFP expression in OVCAR-3 cells while untreated cells did not show any EGFP expression. No EGFP expression was found for cells treated by plasmid with and without DOPE, but without gemini surfactant. For complexes containing the phytanyl

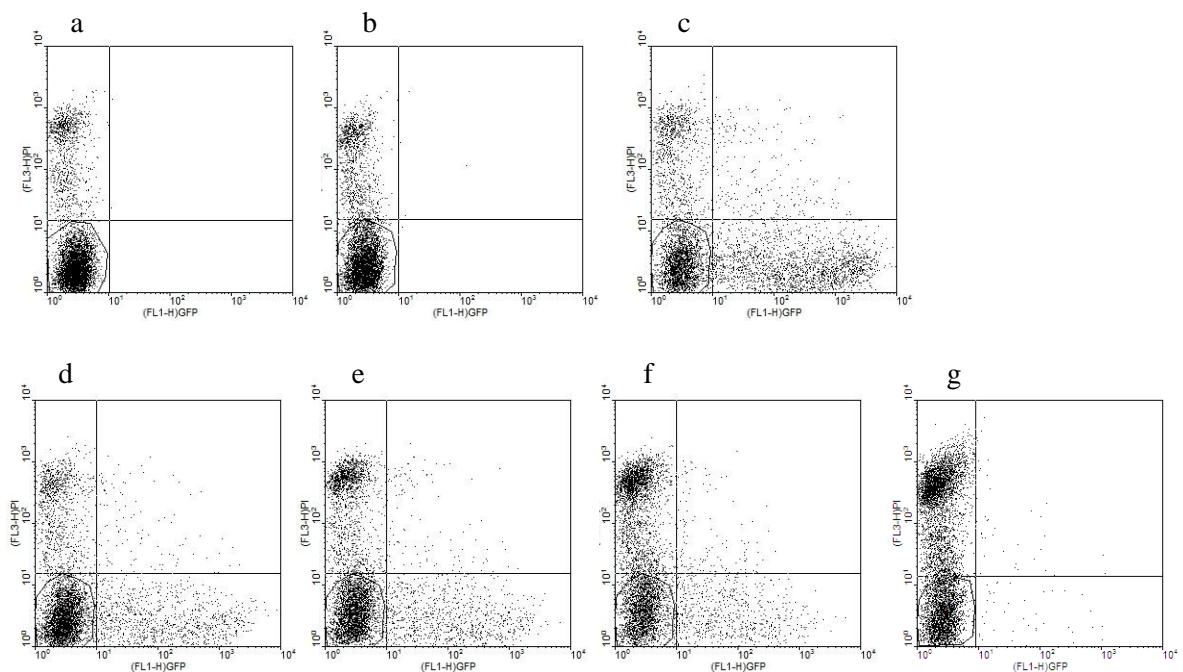


Figure 4.3 FACS dot plots for OVCAR-3 cells: untreated (a), cells treated with plasmid only (b), Lipofectamine™ 2000 (c), and phy-3-16 at charge ratios of 2:1 (d), 5:1 (e), 10:1 (f), and 20:1 (g). The points in the plot correspond to the cells. The cells positive for EGFP distribute along the X-axis, the cells positive for PI distribute along the Y-axis, and the upper right quadrant of the plot indicates cells positive for both EGFP and PI.

substituted gemini surfactants at charge ratios between 2:1 to 10:1, significant EGFP-positive cells were observed compared to non-treated cells ($p < 0.001$), indicating that the plasmid coding EGFP was successfully delivered by the gemini surfactant based system. At 2:1, phy-3-16 compound achieved 16.4% of EGFP, significantly higher than those obtained with phy-3-12 and phy-3-18 ($p < 0.2$); while both phy-3-12 and phy-3-18 showed a high level of EGFP expression though the difference between them was not significant. At 10:1, EGFP expression slightly dropped for all gemini surfactants compared to transfection efficiencies observed at 5:1, but not significantly changed. At 20:1, less than 1% of EGFP expression was

observed for the complexes containing the phytanyl compounds, a dramatic decrease of transfection efficiency probably caused by increased cytotoxicity at higher charge ratios (+/-). Due to poor transfection efficiency at 20:1, further experiments did not contain this treatment. As expected, the positive control 16-3-16 also demonstrated the ability to deliver genes in OVCAR-3 cells, but at substantially lower levels. For example, at 5:1, approximately 15.5% of EGFP was observed from both phy-3-16 and phy-3-18, significantly higher than from 16-3-16 ($p < 0.1$).

To improve transfection ability of gemini surfactant-based non-viral vectors, variations in alkyl tail length or the nature and length of spacer group have been investigated. Recent studies have shown that transfection efficiency increases with the alkyl tail length.^{194, 223} Three groups of surfactants: m-3-m, m-7-m, and m-7NH-m (m = 12, 16, and 18), were reported to be able to deliver Luciferase gene in PAM 212 cells.¹⁹⁴ The transfection efficiency of Luciferase expression increased with the alkyl tail length, as an order of $m = 12 < m = 16 < m = 18$, although the difference between any two of them was not statistically significant in most cases. This is in agreement with our results that phy-3-12 showed the lowest level of EGFP expression in OVCAR-3 cells compared to the other two compounds. The increased tail length of surfactants results in increased hydrophobicity, which can enhance compaction with DNA molecules. The resulting transfection efficiency, however, is not enhanced as strongly as the enhancement observed from the variations in spacer group of gemini surfactants. For example, IFN γ expression in PAM 212 cells decreased with the increased spacer length of 12-s-12 (s = 4, 6, 8, 10, 12, and 16),

the lowest observed from 12-8-12, then increased with the spacer length.¹⁸⁷

Compared to m-7-m group, m-3-m (m = 12, 16, and 18) showed higher Luciferase expression in PAM 212 cells, though the difference between these two groups are not statistically significant.¹⁹⁴

Although the enhancement correlated with variations in tail length of phy-3-m was not statistically significant, the improvement of transfection efficiency due to the introduction of phytanyl group was significant in most cases. It was found that the phytanyl substituted compounds showed higher transfection efficiency than the positive control, 16-3-16. The enhancement is significant for most cases (i.e. at charge ratios of 10:1 and 5:1). This is consistent with the results obtained from the previous chapter.

Another observation based on this study is that no clear trend for transfection efficiency was observed with varied charge ratios, though the charge ratio of the gemini surfactant to DNA is clearly observed to influence the transfection efficiency. The effect of charge ratio on EGFP expression is illustrated in Figure 4.4B. For each gemini surfactant complex, the transfection efficiency goes through a more or less well-evidenced maximum, occurring at different values of the charge ratio. The maximum value of transfection is observed at a charge ratio of 5:1 for the complexes containing phy-3-12 and phy-3-18, and also observed at 2:1 for the complexes formed by phy-3-16. Charge ratio effect on transfection efficiency has been reported

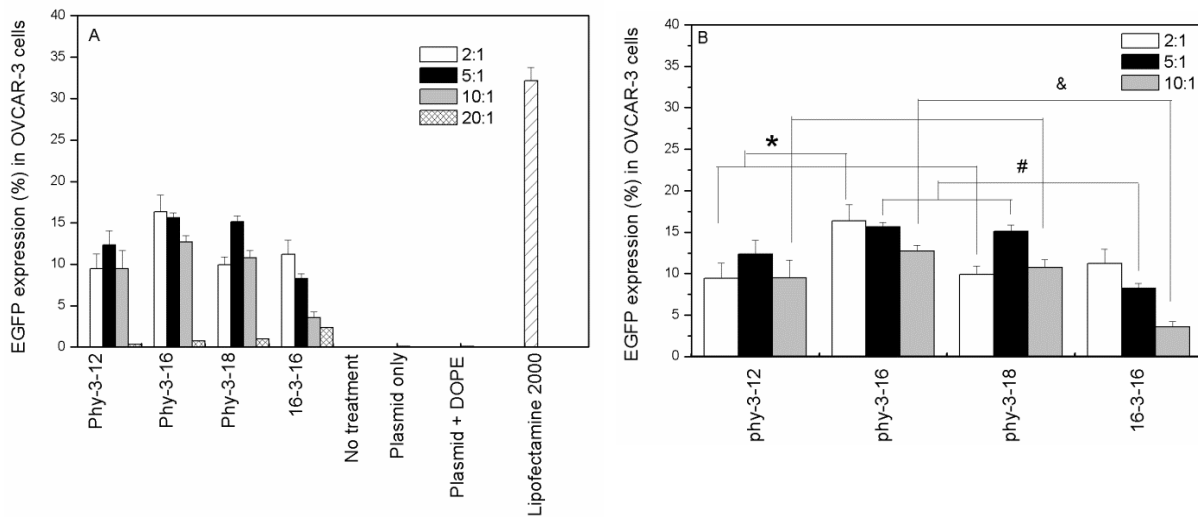


Figure 4.4 EGFP expression in OVCAR-3 cells was quantified by FACS. (A) The cells were transfected by the complexes composed of the gemini surfactant, pVGtelRL, and DOPE at charge ratio of 2:1, 5:1, 10:1, and 20:1, respectively. The cells were treated by the plasmid with and without DOPE, and also treated by Lipofectamine™ 2000 as a positive control; cells growing in the medium without any treatment were taken as a negative control. The data (except 20:1) is the mean of EGFP expression in the cells (n = 5, error bar = standard error). (B) Comparison of transfection efficiency at charge ratios of 2:1, 5:1, and 10:1. Data are the same as those for plotting graph A. * represents that at p < 0.2, EGFP expression observed from phy-3-16 is significantly higher than those obtained with phy-3-12 and phy-3-18, at the ratio of 2:1; # indicates that at p < 0.1, transfection efficiencies obtained both from phy-3-16 and phy-3-18 are significantly higher than that from 16-3-16 at charge ratio of 5:1; & describes that a significant difference was observed between phy-3-m and 16-3-16 at p < 0.1.

by other investigators. Badea et al. showed that GFP expression in PAM 212 cells varied with the charge ratio (+/-) of 16-3-16 to pGTmCMV.IFN-GFP plasmid, the highest GFP expression observed at 40:1, then at 10:1, 5:1, and lowest at 20:1.¹⁸⁷

Donkuru found that the highest Luciferase expression in PAM 212 was achieved at charge ratio (+/-) of 10:1 for m-3-m, m-7-m, and m-7NH-m (m = 12, 16, and 18) surfactants to pMASIA. Luc plasmid.¹⁹⁴ Such a discrepancy could be resulted from

cell line type and plasmid size used in these studies. Additionally, it should be noted that plasmid conformation (e.g. supercoiled vs. linear) may affect the effective charge ratio (+/-). Due to a compact form, some negatively charged phosphate groups may be wrapped in the supercoiled plasmid, which reduces the number of free negative charges (phosphate groups) on the surface of the plasmid.

4.3.1.3 Cytotoxicity of transfection complexes

Our final goal is to find better gemini surfactant-based gene delivery system. Thus, cytotoxicity is one of major concerns to evaluate the feasibility of gemini surfactant as gene delivery vectors. Cytotoxicity of transfection complexes as a function of surfactant/DNA charge ratio for all the system in this study is shown in Figure 4.5. For each sample, the DNA amount was maintained constant and the gemini surfactant amount was varied in order to obtain the desired charge ratios. As assessed by FACS, the results were expressed as the percentage of viable cells. As observed, the higher surfactant/DNA charge ratio, the higher was the observed toxicity. As a general trend, for all transfection complexes, a more or less significant increase of cytotoxicity as a function of the charge ratio increase is evidenced. The increased toxicity can be attributed to the free gemini surfactants whose quaternary ammonium head groups and counterions have been reported to be toxic.²²⁴ In addition, phy-3-m showed lower toxic effect on the cells than 16-3-16 did. This may be related to the different interactions of the surfactants with cell membrane.

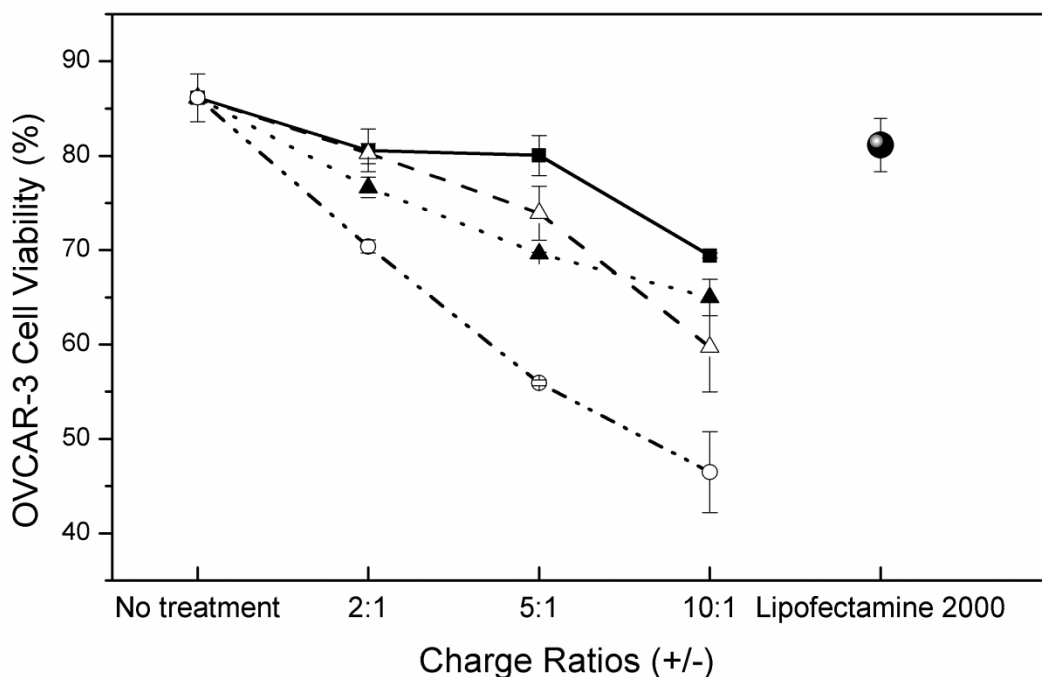


Figure 4.5 Cell viability for OVCAR-3 cells (expressed as percentage of viable cells) varied with charge ratios for the transfection complexes containing phy-3-12 (■), phy-3-16 (Δ), phy-3-18 (▲), or 16-3-16 (○). At all charge ratios, cell viability is significantly higher for the complexes containing phy-3-m than that for the 16-3-16 delivery complex ($p < 0.05$). Data are also presented for non-treated cells and cells treated with Lipofectamine™ 2000 (indicated by ●). All data is the mean of viable cells ($n = 5$, error bar = standard error).

Although it has been found that cationic surfactants with higher CMC are more toxic to bacteria, the toxicity towards mammalian cells varies differently; for example, the toxicity of the surfactants to *E.coli* was shown as an order: $C_{10}TAB > C_{12}TAB > C_{14}TAB$, while to an epithelium cell model, the order was: $C_{12}TAB > C_{10}TAB > C_{14}TAB$.²²⁴ Such a difference may be attributed to the different physico-chemical properties of cell membranes and the interactions of surfactants with cells.

Given cellular cytotoxicity, it is desirable for cancer gene therapy since cancer cells are killed by a delivery vector due to its toxicity. As long as delivery vectors are

targeted to cancer cells, their cellular toxicity may not be a consideration for their application to cancer gene therapy. But for other gene therapies, cellular cytotoxicity is still a major factor.

4.3.2 Characterization of transfection complexes (size and zeta potential)

Transfection complexes were characterized by measuring their particle size and zeta potential. The importance of particle size for gene transfection has been reported.

Although the optimal lipoplex size for efficient gene delivery is still under debate,^{225,}
²²⁶ there is a general agreement that lipoplex size plays a significant role in determining the nature of the entry pathway of the lipoplexes into the cells.^{127, 227-229}

On one hand, the larger complexes result in more cell membrane contact and active phagocytosis. On the other hand, particles with larger versus smaller size may enter cells through different internalization mechanisms. As introduced in chapter 1, endocytosis has been widely accepted as the major pathway of lipoplex internalization into the cells.¹¹⁹ Two distinct endocytic pathways: clathrin-mediated and caveolin-mediated endocytosis, have been investigated (see in Figure 4.6). A size-dependent mechanism has been proposed.¹²⁷ With the clathrin-mediated pathway inhibited, B16F10 (murine melanoma cell line) cells showed a significant inhibition of internalization of nanoparticles with sizes between 200 and 50 nm, while the uptake of those with a size of 500 nm was unaltered or even slightly higher, which means large particles are internalized through a different pathway. Moreover, the uptake of the 500 nm particles was reduced by more than 50% due to the blockage of caveolin-mediated pathway. Further experiments revealed that the

internalization of the 500 nm particles occurred through caveolin-mediated pathway. It has been hypothesized that larger particles are even more efficient in transgene delivery because they are internalized through caveolin-mediated pathway, therefore avoiding lysosomal targeting as occurs along the clathrin-mediated mechanism.²³⁰

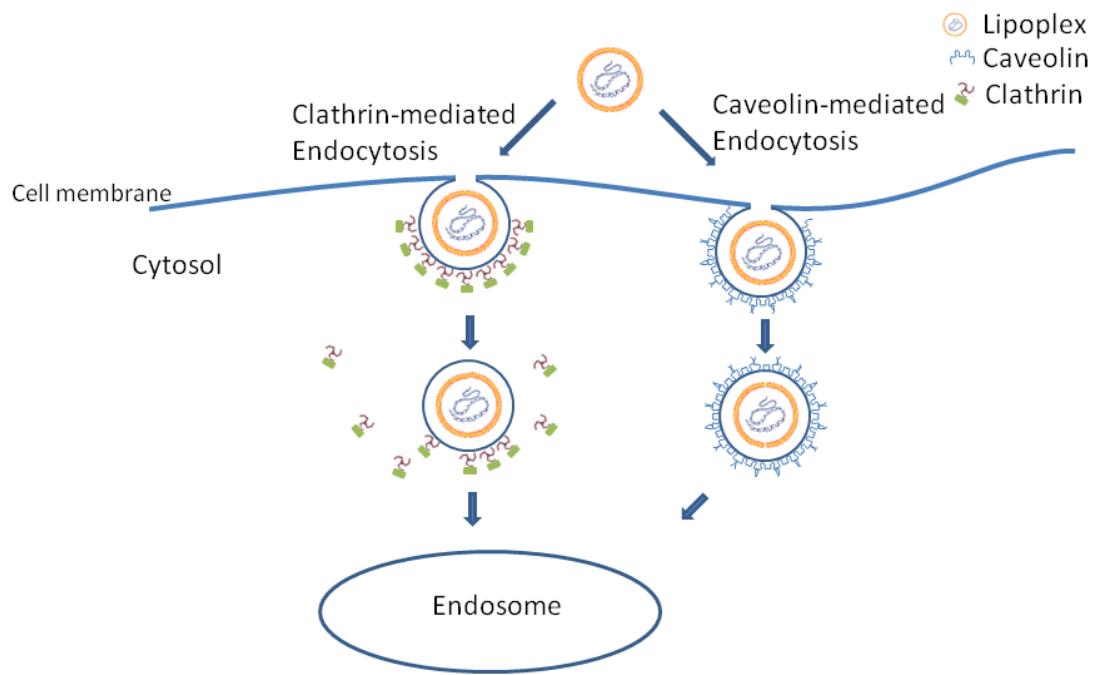


Figure 4.6 Two main endocytotic pathways for lipoplexes: clathrin-mediated and caveolin-mediated endocytosis.¹¹⁹

The size and zeta potential of the transfection complexes was measured and tabulated in Table 4.1. Without compaction, the plasmid was 360 nm. With varied charge ratios, the particle size dramatically changed, indicating the effect of charge ratio on DNA conformation. DNA structure change induced by the gemini surfactant has been investigated using circular dichroism (CD) measurement. It has been

reported that the dramatic change of signal intensity and band shift of CD spectrum caused by the increase in the charge ratio indicates the conformational change in DNA molecules upon binding with the gemini surfactant.^{175, 231}

Table 4.1 Size and zeta potential measurements of the transfection complexes at different charge ratios of gemini surfactants to DNA.

Size (nm) ^a				ζ-potential (mV) ^a		
DOPE	114 ± 12			-32 ± 5		
Plasmid	360 ± 90			-65 ± 3		
DOPE+ Plasmid	172 ± 5			-10 ± 4		
Surfactant	2:1	5:1	10:1	2:1	5:1	10:1
Phy-3-12	1220 ± 73	343 ± 77	188 ± 9	13 ± 1	31 ± 4	37 ± 5
Phy-3-16	1619 ± 125	899 ± 27	169 ± 8	12 ± 1	27 ± 4	44 ± 8
Phy-3-18	1361 ± 124	404 ± 64	151 ± 10	12 ± 1	38 ± 3	41 ± 7
16-3-16	709 ± 95	460 ± 40	130 ± 6	14 ± 1	28 ± 2	32 ± 7

^a Mean ± standard deviation. DOPE and DNA inclusive in all surfactants.

The transfection complexes at the lower charge ratios of 2:1 and 5:1 were observed to be large. It has been reported that particle size for 14-2-14:Chol:DOPE lipoplexes was 1634 nm at charge ratio (+/-) of 2:1, but dropped to 173 nm at 8:1.²³² This is consistent with our results. At the lower charge ratios, the plasmid may not be completely compacted by the gemini surfactant, which results in the formation of larger particles. At the charge ratio of 10:1, all complexes had sizes less than 200 nm, indicating the plasmid was more completely compacted by the gemini surfactants. At higher charge ratios, transfection complexes with smaller size have been reported. For example, at charge ratio (+/-) of 10:1, particle size for complexes composed of 12-s-12, plasmid, and DOPE, were below 200 nm and approximately 200 nm for the complexes containing 16-3-16.¹⁸⁸

As can be seen from particle size and transfection data (Figure 4.4), for the phy-3-16, the results displayed a marked increase of the transfection with the complex size increase. This is also observed from other m-s-m surfactants. For example, 16-3-16 showed higher transfection ability than 12-3-12.^{187, 188} Larger particles giving rise to higher transfection efficiency has been evidenced.^{120, 225} This may be attributed to their efficiency in delivering transgenes through phagocytosis or caveolin-mediated cellular pathway. However, for the phy-3-12 and phy-3-18, there is no clear trend observed with the increase in the complex size. Thus, no specific correlation can be concluded between particle size and transfection efficiency. Transfection complexes with larger size may enter cells through a different pathway compared to those smaller particles.

The surface charge represented by the zeta potential has been reported as a factor for lipoplex stability and interaction with cell membrane.^{119, 233} For the complexes containing phy-3-m (m = 12, 16, and 18), the zeta potential were above +30 mV at the charge ratio greater than 5:1, indicating that the complexes are normally stable. Compared with transfection results, no correlation was observed between the zeta potential and transfection efficiency. This is in agreement with the observation from 12-s-12 (s = 2, 3, 4, 6, 8, 10, 12, and 16) and 16-3-16 compounds.¹⁸⁸ Nevertheless, transfection complexes with positive charges are needed not only for effective transfection but also for complexes stability.

4.3.3 Structures investigation using SAXS

One of the applications of the SAXS technique is to provide structural information on polymorphic systems, such as highly ordered lipoplexes composed of cationic lipid and DNA, or partially ordered membranes or lipid mesophases. Lipoplexes resulting in a self-assembled complex with ordered structures were extensively investigated by synchrotron SAXS and shown to influence transfection efficiencies.^{94, 96, 103, 136, 234, 235} Using SAXS diffraction method, an ordered mesophase appears as one or more sharp peaks, named Bragg peaks, in the diffraction pattern. The long-range ordering of the lipid/water aggregates (i.e. bilayers, cylinders, micelles) onto 1-, 2-, or 3-dimensional lattices produces Bragg peaks whose reciprocal spacings ($s_{hkl} = 1/d_{hkl}$) are characteristic of special ratios.²³⁶ For lamellar lipid-water mesophases: $s_l = l/d$,²³⁶ d is the lamellar repeat distance, which is the thickness of the lipid bilayer (δ_m) plus that of the adjacent water layer (δ_w) (seen in Figure 1.3). The ratio of distances

between neighbouring bilayers follows a pattern of 1:2:3:....; the Bragg peaks occur at the scattering vector $q = 2\pi/d$. For hexagonally arranged mesophases: $s_{hk} = 2(h^2+k^2+hk)^{1/2}/\sqrt{3}a$,²³⁶ where a is the distance between the centers of two neighbouring rods (seen in Figure 1.3). The hexagonal phases are characteristic of the peaks at the ratios of 1: $\sqrt{3}$:2:....; the Bragg peaks occur at $q = \frac{4\pi}{\sqrt{3}a}\sqrt{h^2 + k^2 + hk}$.⁹³ For cubic phase: $s_{hkl} = (h^2+k^2+l^2)^{1/2}/a$,²³⁶ it is characteristic of 1: $\sqrt{2}$: $\sqrt{3}$:....; the Bragg peaks occur at $q = \frac{2\pi}{a}\sqrt{h^2 + k^2 + l^2}$.⁹³ The letters, h , k , and l in the above equations are Miller indices, a notation system in crystallography for planes in crystal lattices, and the detailed description is referred to Hopcroft et al..²³⁷

In this study, the internal structure of the complexes composed of gemini surfactant, plasmid, and DOPE, at different charge ratios (+/-) was investigated using SAXS. The mixture of DOPE and gemini surfactant was made at a molar ratio of 1:2.5 (surfactant to lipid) and maintained constant for all complexes at the different charge ratios of gemini surfactant to DNA. The SAXS profile for the mixture of the gemini surfactant and DOPE consists of a single broad peak and no long-range ordering was observed (Figure 4.7A). This feature has been reported to be characteristic of interparticle interactions between the nanoparticles.¹⁵² The addition of plasmid DNA to the mixture of the surfactant and neutral lipid resulted in significant changes in the scattering profiles (see Figure 4.7B-E). Interlayer spacing for lamellar phases and unit cell spacing for hexagonal phases are calculated and tabulated in Table 4.2.

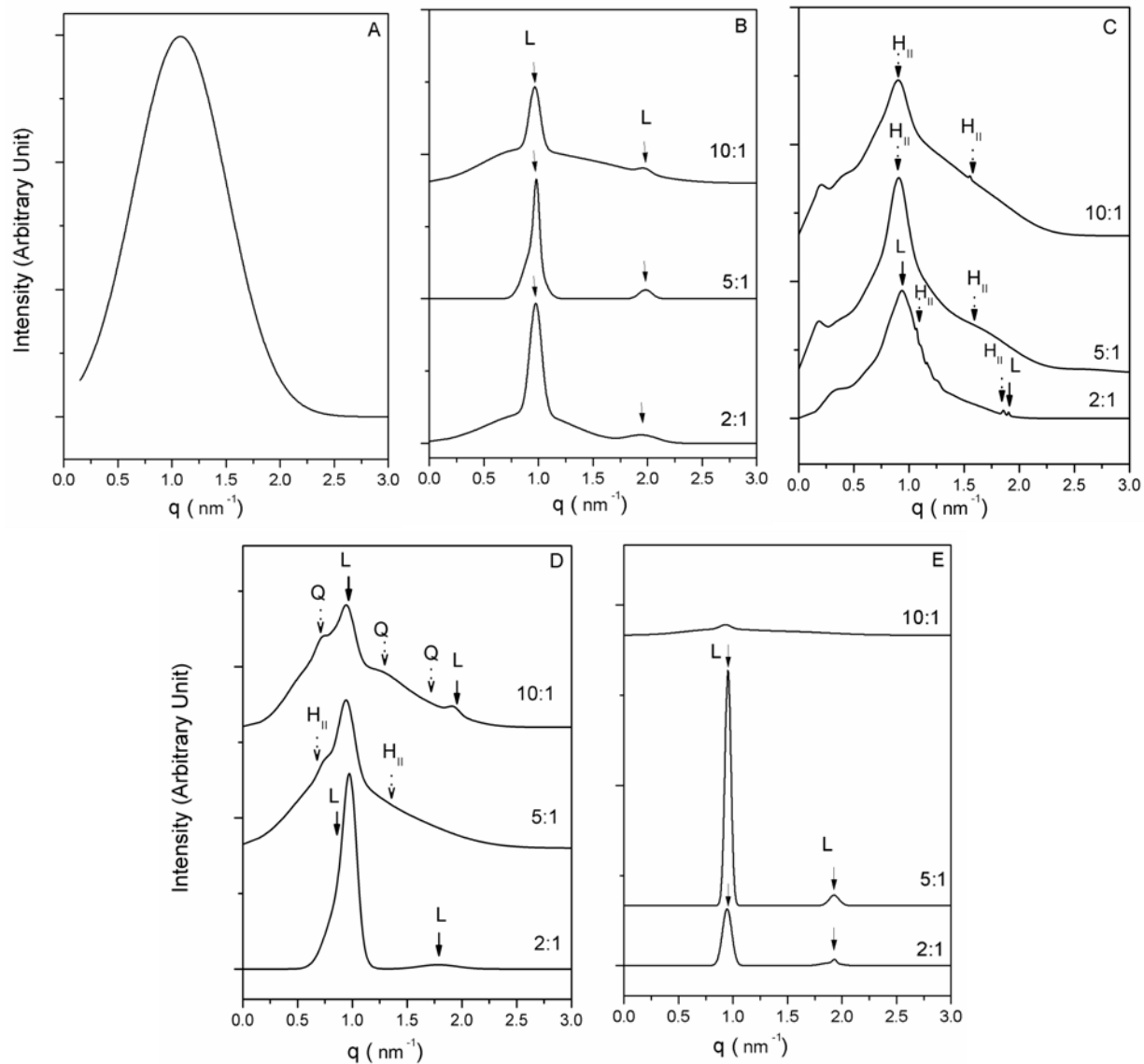


Figure 4.7 SAXS profiles of the lipid mixture of DOPE and 16-3-16 (A), and the complexes formed phy-3-12 (B), phy-3-16 (C), phy-3-18 (D), or 16-3-16 (E), plasmid, and DOPE, at the charge ratios of 2:1, 5:1, and 10:1. Black solid arrows represent the lamellar phase peaks. Dotted arrows indicate the peaks identified as the inverted hexagonal or cubic phases. All spectra were subtracting from the blank (water as a blank).

The most notable change is the appearance of narrow peaks instead of a single broad peak. For the complexes containing phy-3-12 at different charge ratios, two scattering peaks, one sharp and the other weak, were present in the profiles. These two scattering peaks are characteristic of a lamellar phase which is identified by the peaks position in the ratio of 1:2. The peaks of the periodic lamellar structures display an interlayer distance approximately 6.4 nm which is independent of the charge ratio of phy-3-12 to DNA. The spacing between layers for pure phy-3-12 is 4.6 ± 0.2 nm, the result obtained from TEM imaging given in Figure 3.7. The diameter for DNA is around 2.0 nm, thus, the distance of a lamellar structure containing phy-3-12 bilayers with intercalated monolayers of DNA is approximately 6.6 nm ($4.6+2.0$), which matches very well the distances calculated from the scattering vector q .

For complexes containing phy-3-16, different SAXS profiles were observed at different charge ratios. At 2:1, two scattering peaks appeared at 0.946 nm^{-1} and 1.905 nm^{-1} , identifying as a lamellar structure (L) with an interlayer spacing of 6.64 nm ($d = 2\pi/q = 6.64 \text{ nm}$). It was observed that peak splitting occurred at 1.072 nm^{-1} and 1.857 nm^{-1} , respectively, characteristic of an inverted hexagonal phase structure with a unit cell spacing of $a = 4\pi/\sqrt{3}q_{10} = 6.77 \text{ nm}$. Additionally, two peaks corresponding to another phase were observed at 0.753 nm^{-1} and 1.521 nm^{-1} , respectively. In addition, there are a few weak peaks that do not correspond to a lamellar or hexagonal phase. Due to the finite information extracted from SAXS

spectra, it is difficult to assign these peaks. However, they are indicative of the presence of an unidentified phase(s).

Table 4.2 Structural parameters and possible phase structures of the complexes composed of gemini surfactant, plasmid, and DOPE, at different charge ratios.

Surfactant	Charge ratio (+/-)	q (nm ⁻¹)	d (nm)	a (nm)	Phase
Phy-3-12	2:1	0.975,1.953 0.919	6.45		L Others
	5:1	0.982,1.982 0.946	6.39		L Others
	10:1	0.966,1.974 1.368,0.759	6.50		L Others
Phy-3-16	2:1	0.946,1.905 0.753,1.521 <i>1.072,1.857</i> 0.317,0.856,1.038,1.18,1.255	6.64	6.77	L <i>H_{II}</i> Others
	5:1	<i>0.908,1.563</i> 0.161,0.313,0.856,2.616		7.99	<i>H_{II}</i> Others
	10:1	<i>0.91,1.554</i> 0.182,0.359,0.785,1.223,1.7		7.97	<i>H_{II}</i> Others
Phy-3-18	2:1	0.884,1.79 0.987	7.10		L
	5:1	<i>0.755,1.304</i> 0.773,0.946		9.62	<i>H_{II}</i> Other
	10:1	0.973, 1.927 0.828, 1.17, 1.694 0.626,0.738	6.52		L Q Others
16-3-16	2:1	0.945, 1.895 1.932	6.65		L
	5:1	0.954,1.928	6.59		L
	10:1	0.932,1.511,0.846			Others

By contrast, the scattering peaks for complexes formed by phy-3-16 at 5:1 and 10:1 are less in quantity. At both ratios, the first and second-order peaks corresponding to an inverted hexagonal phase occur at $q = 0.91 \text{ nm}^{-1}$ and $q = 1.55 \text{ nm}^{-1}$. The inverted hexagonal phase at both ratios has a unit cell spacing of approximately 8 nm, indicating that the distance between two neighbouring rods from the inverted hexagonal lattice may reach to a maximum in the complexes at 5:1. With the increase in the charge ratio, the spacing of one unit cell kept constant. Additionally, SAXS profiles show two peaks at $q < 0.5 \text{ nm}^{-1}$. However, it is difficult to assign these peaks due to the finite information.

Figure 4.8D shows SAXS profiles for the complexes containing phy-3-18 at different charge ratios. At 2:1, the position of the main peak corresponds to a lamellar phase, consistent with the observation presented for the complexes containing 12-s-12 ($s = 3, 8, \text{ and } 16$).¹⁷⁹ The interlayer spacing for the lamellar phase is 7.10 nm, which is larger than those observed from the complexes formed by phy-3-16 or phy-3-12 at 2:1. This may be caused by the larger bilayer spacing of pure phy-3-18 due to its longer C_{18} tail. At 5:1, a sharp peak appeared at $q = 0.946 \text{ nm}^{-1}$, and peak splitting occurred at $q_{10} = 0.755$ and $q_{11} = 1.304 \text{ nm}^{-1}$ respectively, corresponding to an inverted hexagonal phase with a unit cell spacing of 9.62 nm. At 10:1, coexistence of lamellar and cubic phase structures is observed. The peaks of a lamellar phase occur at $q = 0.973 \text{ nm}^{-1}$ and 1.927 nm^{-1} . Peak splitting is an evidence that was observed at $q = 0.828 \text{ nm}^{-1}$, 1.17 nm^{-1} , and 1.694 nm^{-1} , corresponding to a cubic phase.

As a positive control, the SAXS profiles for complexes containing 16-3-16 display a lamellar phase structure at both ratios of 2:1 and 5:1, and weakly scattering peaks which do not correspond to a lamellar or inverted hexagonal phase at 10:1. Compared to the phy-3-m system described above, it is evidenced that the 16-3-16 system clearly lacks complexity on polymorphic characteristics. This noticeable difference is attributed to the use of the phy-3-m compounds. As expected, the introduction of phytanyl branch into gemini surfactants as one of tails increases the number of polymorphic phases formed with plasmid and DOPE.

SAXS study is particularly important since it can provide information to predict the correlation of morphologies of transfection complexes with transfection efficiency. Tenchov et al. demonstrate that highly efficient cationic lipids promote the formation of an inverted cubic phase.²³⁸ This correlation may be ascribed to enhanced fusogenicity of the lipoplexes. Zuhorn et al. indicate that the formation of inverted hexagonal structure is crucial for efficient cellular internalization and endosomal escape of transgene.¹³² Lamellar lipoplexes may achieve higher transfection efficiency because they remain stable when in contact with membranes.⁹⁶ Polymorphic structures have been reported to be an important factor for efficient transfection.¹⁸⁸ Wettig et al. found the presence of multiple phase formed by the amino-substituted gemini surfactant 12-7NH-12, which was highly efficient.¹⁹³ In this study, SAXS results indicate that the complexes formed by plasmid, DOPE, and phy-3-m, are also able to adopt multiple phases, such as lamellar, inverted

hexagonal, cubic, and other indentified structures. This may be considered a reason why phy-3-m compounds are efficient in gene delivery in OVCAR-3 cells.

4.4 Conclusions

Transfection ability of the phytanyl substituted gemini surfactants with a shorter spacer, phy-3-m ($m = 12, 16, \text{ and } 18$), at different charge ratios (+/-) of surfactant to DNA, was investigated in OVCAR-3 cells. At charge ratios of 2:1, 5:1, and 10:1, EGFP expression can be observed in OVCAR-3 cells using fluorescence microscopy and FACS. Charge ratio of surfactant to DNA showed an effect on EGFP expression; transfection efficiency displayed highest values for phy-3-12 and phy-3-18 at 5:1, and also for phy-3-16 at 2:1. As a general observation, cytotoxicity increased with increased charge ratios. Thus, considering both transfection efficiency and cell viability, the optimal charge ratio for phy-3-m as transgene delivery vectors in OVCAR-3 cells is 5:1. This result will be helpful in the application of phy-3-m to the primary cells or *in vivo* study for ovarian cancer gene therapy.

The characterization of the transfection complexes was carried out by measuring particle size and zeta potential. At lower charge ratios, transfection complexes showed larger particles. This is the evidence that size below 200 nm is not a requirement for higher transfection efficiency. Larger particles were efficient in transgene delivery, which may be ascribed to their different endocytosis mechanism. Although no correlation was observed between the surface charge and transfection efficiency, transfection complexes with positive zeta potential is needed not only for effective cellular interaction but also for enhanced stability.

The complex structure was investigated using SAXS. The phy-3-m system showed very notable polymorphic properties, while the 16-3-16 system lacked complexity on polymorphism. The ability of phy-3-m to adopt multiple phases may play an important role in enhancing transfection efficiency. In fact, combined with transfection results, it may provide evidence that transfection efficiency increased by increasing the number of polymorphic phases. At this point, our goal to improve transfection efficiency by introducing phytanyl group is achieved.

Chapter 5 Conclusions and future perspectives

To improve transfection efficiency for gene therapy, one of the strategies is to design efficient vectors for transgene delivery. In this study, a series of phytanyl substituted gemini surfactants were rationally designed, synthesized, and characterized. Their transfection ability was evaluated in an ovarian cancer cell line to determine its application *in vivo*. It is the first time that the m-s-n type of asymmetric gemini surfactants having a bulky alkyl tail is synthesized and characterized; and transfection ability and phase structure investigation of the asymmetric gemini surfactants based gene delivery complexes is being reported firstly.

Chapter 3 focuses on the synthesis and characterization of the phytanyl compounds, phy-3-m and phy-7NH-m ($m = 12, 16, \text{ and } 18$). The results show that phy-3-m compounds have different aggregate properties, such as much lower CMC values, higher degree of micelle ionization, and the preference to form vesicle-like aggregates, compared to their symmetric ones (m-3-m). This project could be expanded using TEM or atomic force microscopy (AFM) imaging on phy-3-16, phy-3-18, and their symmetric ones, to obtain all information about aggregate morphology of phy-3-m. As novel asymmetric gemini surfactants, it is interesting to know how many monomers aggregate to form vesicle-like micelles that were observed from phy-3-m. This study could be expanded by estimating aggregation number of phytanyl compounds using fluorescence quenching technique. The other group of phytanyl compounds, phy-7NH-m, was synthesized and they did not transfect OVCAR-3 cells effectively. However, no further studies on characterization

with phy-7NH- m were done in this project. From the perspective of a chemist, the future studies on phy-7NH- m characterization could be carried out to help understand why this group of compounds was not as efficient as phy-3-m.

In this project, the comparison regarding surfactant aggregate properties was done between phy-3-m and m-3-m compounds. It would be interesting to look into the difference of phy-3-m with other asymmetric gemini surfactants (i.e. m'-3-n') with three methylene units in the spacer, such as 12-3-16, 14-3-16, and 18-3-16, having the same alkyl tail length as phy-3-m. Further comparison with the m'-3-n' could help us not only understand the effect of branched phytanyl group on the aggregate properties of the gemini surfactants, but also provide valuable information on rational design of gemini surfactants for practical applications. This is underway in our lab.

The interaction between the gemini surfactants and DNA is another interesting study. Since the gemini surfactants were designed for gene delivery, it would be questioned that how the properties of gemini surfactants are influenced by the addition of DNA, or how the cationic gemini surfactants bind to anionic DNA molecules. This project could be expanded by the determination of critical aggregate concentration (CAC) using surface tensiometer, and thermodynamic investigation of the binding of the phytanyl compounds to DNA. Due to a strong intercalation of the pyrene group between DNA base pairs, the binding interaction between asymmetric pyrenyl-gemini surfactants and DNA has been reported to be distinctly different from the interaction observed from 12-s-12 and DNA.¹⁷⁵ An intercalated binding for the phy-3-m compounds would not be found since there is no similarity between

phytanyl chain and pyrene structure. However, the branched phytanyl gemini surfactants would show different binding interactions compared to the 12-s-12 or other symmetric gemini surfactants. Such studies would help us understand the influence of gemini surfactant structures on the interaction with DNA and/or a possible mechanism(s) of DNA release from the gemini surfactant-DNA complexes during gene transfection. Moreover, it would provide valuable information for rational design of more efficient gemini surfactants in the future.

The transfection ability of the phytanyl compounds was examined in OVCAR-3 cells, as reported in Chapter 4. The results indicate that phy-3-m is able to deliver plasmid DNA to OVCAR-3 cells, and showed higher transfection efficiency than 16-3-16. Considering both transfection efficiency and cytotoxicity, the optimal charge ratio of surfactant to DNA for effective transfection was found to be 5:1. Initial characterization of the transfection complexes indicates that particles are larger at lower charge ratios and smaller than 200 nm at 10:1. These results provide evidence that small particles (i.e. less than 200 nm) are not a requirement for efficient transfection *in vitro*. This finding is consistent with results reported recently.¹⁸⁸ However, it would cause a problem for *in vivo* study because larger particles may be rapidly degraded by phagocytic cells and the reticuloendothelial system. Further studies using animal models should explore both charge ratios (+/-) of 5:1 and 10:1 to investigate their resulting influence on gene delivery.

Additionally, stability of transfection complexes may be increased by modifying transfection complexes with the attachment of polyethylene glycol (PEG) to the

nanoparticles. It would be interesting since no studies involving PEGylation of gemini surfactants-based DNA delivery vectors have been carried out. PEG conjugation approach, the length and conformation of PEG chain, the linkage to gemini surfactants-based nanoparticles, will be considered if the modification of transfection complexes with PEG is studied.

The hypothesis of this project was that the asymmetric phytanyl chained gemini surfactants will improve transgene delivery efficiency because introducing phytanyl chain to the gemini surfactants may force the formation of transfection complexes with higher level morphologies. SAXS profiles displayed multiple phases observed from the complexes containing phy-3-m, while 16-3-16 system lacks the complexity of polymorphic properties. Thus, the structural investigation is the evidence that the phy-3-m compounds are able to form the flexible phase structures. Compared to the transfection results, the higher transfection efficiency achieved with phy-3-m system relative to 16-3-16 system appears correlated with their ability to adopt higher level bilayer structures.

As evidenced, phy-3-m compounds showed high transfection efficiency in an established ovarian cancer cell line, OVCAR-3. Our primary goal is the development of efficient gemini surfactants as transgene delivery vectors for cancer gene therapy. Therefore, primary cells and/or animal models will be employed to investigate transgene delivery efficiency of phytanyl compounds *in vivo* studies. In cancer therapy, cell-specific targeting is one of considerations. Gemini surfactants can be flexibly attached with a targeting group (i.e. folate) that allow both increased cell

uptake and cell specificity. Transfection formulations formed by modified gemini surfactants with the conjugation of a target ligand and the resulting transfection ability should be investigated both at *in vitro* and *in vivo* levels.

References

1. R. M. Blaese, K. W. Culver, A. Miller, C. S. Carter, T. Fleisher, M. Clerici, G. Shearer, L. Chang, Y. Chiang and P. Tolstoshev, *Science*, 1995, **270**, 475.
2. G. J. Nabel, E. G. Nabel, Z. Y. Yang, B. A. Fox, G. E. Plautz, X. Gao, L. Huang, S. Shu, D. Gordon and A. E. Chang, *Proceedings of the National Academy of Sciences*, 1993, **90**, 11307.
3. M. Asanuma, I. Miyazaki and N. Ogawa, *Neurotoxicity Research*, 2003, **5**, 165-176.
4. K. Garber, *Journal of the National Cancer Institute*, 2006, **98**, 298.
5. M. L. Edelstein, M. R. Abedi and J. Wixon, *The Journal of Gene Medicine*, 2007, **9**, 833-842.
6. J. Raty, J. Pikkarainen, T. Wirth and S. Yla-Herttuala, *Current Molecular Pharmacology*, 2008, **1**, 13-23.
7. N. Miller, *Nature Reviews Drug Discovery*, 2012, **11**, 419-419.
8. J. A. Wolff, R. W. Malone, P. Williams, W. Chong, G. Acsadi, A. Jani and P. L. Felgner, *Science*, 1990, **247**, 1465.
9. V. Budker, G. Zhang, S. Knechtle and J. Wolff, *Gene Therapy*, 1996, **3**, 593.
10. H. Maruyama, N. Higuchi, Y. Nishikawa, S. Kameda, N. Iino, J. Kazama, N. Takahashi, M. Sugawa, H. Hanawa and N. Tada, *The Journal of Gene Medicine*, 2002, **4**, 333-341.
11. K. A. Choate and P. A. Khavari, *Human Gene Therapy*, 1997, **8**, 1659-1665.
12. K. Meyer, M. Thompson, M. Levy, L. Barron and F. Szoka Jr, *Gene Therapy*, 1995, **2**, 450.
13. P. Dash, M. Read, L. Barrett, M. Wolfert and L. Seymour, *Gene Therapy*, 1999, **6**, 643.
14. X. Gao, K. Kim and D. Liu, *AAPS J.*, 2007, **9**, 92-104.
15. H. Maruyama, K. Ataka, N. Higuchi, F. Sakamoto, F. Gejyo and J. Miyazaki, *Gene Therapy*, 2001, **8**, 1808-1812.
16. H. Maruyama, K. Ataka, F. Gejyo, N. Higuchi, Y. Ito, H. Hirahara, I. Imazeki, M. Hirata, F. Ichikawa and T. Neichi, *Gene Therapy*, 2001, **8**, 461-468.
17. D. Dean, D. Machado-Aranda, K. Blair-Parks, A. Yeldandi and J. Young, *Gene Therapy*, 2003, **10**, 1608-1615.
18. C. Magin Lachmann, G. Kotzamanis, L. D'Aiuto, H. Cooke, C. Huxley and E. Wagner, *The Journal of Gene Medicine*, 2004, **6**, 195-209.

19. A. C. Durieux, R. Bonnefoy, T. Busso and D. Freyssenet, *The Journal of Gene Medicine*, 2004, **6**, 809-816.
20. S. Patil, D. Rhodes and D. Burgess, *The AAPS Journal*, 2005, **7**, 61-77.
21. H. Kamiya, H. Tsuchiya, J. Yamazaki and H. Harashima, *Advanced Drug Delivery Reviews*, 2001, **52**, 153-164.
22. T. E. Shenk, D. Knipe and P. Howley, *Adenoviridae: the viruses and their replication*, Lippincott Williams & Wilkins, 2001.
23. D. M. Shayakhmetov, T. Papayannopoulou, G. Stamatoyannopoulos and A. Lieber, *Journal of Virology*, 2000, **74**, 2567-2583.
24. M. Havenga, A. Lemckert, O. Ophorst, M. Van Meijer, W. Germeraad, J. Grimbergen, M. van Den Doel, R. Vogels, J. Van Deutekom and A. Janson, *Journal of Virology*, 2002, **76**, 4612-4620.
25. C. S. Manno, G. F. Pierce, V. R. Arruda, B. Glader, M. Ragni, J. J. E. Rasko, M. C. Ozelo, K. Hoots, P. Blatt and B. Konkle, *Nature Medicine*, 2006, **12**, 342-347.
26. B. K. Kaspar, D. Erickson, D. Schaffer, L. Hinh, F. H. Gage and D. A. Peterson, *Molecular Therapy*, 2002, **5**, 50-56.
27. D. Schaffer, J. Koerber and K. Lim, *Annual Review of Biomedical Engineering*, 2008, **10**, 169.
28. K. J. Garton, N. Ferri and E. W. Raines, *Biotechniques*, 2002, **32**, 830-843.
29. L. Naldini, *Nature Medicine*, 2001, **7**, 33.
30. D. Favre, N. Provost, V. Blouin, G. Blancho, Y. Chérel, A. Salvetti and P. Moullier, *Molecular Therapy*, 2001, **4**, 559-566.
31. T. L. Timme, S. J. Hall, R. Barrios, S. Woo, E. Aguilar-Cordova and T. C. Thompson, *Cancer Gene Therapy*, 1998, **5**, 74.
32. S. G. Stolberg, *New York Times Magazine*, 1999, **28**, 716-720.
33. S. Hacein-Bey-Abina, A. Garrigue, G. P. Wang, J. Soulier, A. Lim, E. Morillon, E. Clappier, L. Caccavelli, E. Delabesse and K. Beldjord, *The Journal of Clinical Investigation*, 2008, **118**, 3132.
34. J. Kaiser, *Science (New York, NY)*, 2003, **299**, 495.
35. X. Danthinne and M. Imperiale, *Gene Therapy*, 2000, **7**, 1707.
36. S. McTaggart and M. Al-Rubeai, *Biotechnology Advances*, 2002, **20**, 1-31.
37. B. Martin, M. Sainlos, A. Aissaoui, N. Oudrhiri, M. Hauchecorne, J. P. Vigneron, J. M. Lehn and P. Lehn, *Current Pharmaceutical Design*, 2005, **11**, 375-394.

38. A. D. Miller, *Chemical Society Reviews*, 2005, **34**, 970-994.
39. N. D. Sonawane, F. C. Szoka and A. Verkman, *Journal of Biological Chemistry*, 2003, **278**, 44826.
40. J. P. Behr, *CHIMIA International Journal for Chemistry*, 1997, **1**, 34-36.
41. D. Pack, A. Hoffman, S. Pun and P. Stayton, *Nature Reviews Drug Discovery*, 2005, **4**, 581-593.
42. A. Akinc, M. Thomas, A. M. Klibanov and R. Langer, *The Journal of Gene Medicine*, 2005, **7**, 657-663.
43. D. Fischer, T. Bieber, Y. Li, H. P. Elsässer and T. Kissel, *Pharmaceutical Research*, 1999, **16**, 1273-1279.
44. S. Wettig and R. Verrall, *Journal of Colloid and Interface Science*, 2001, **235**, 310-316.
45. M. Mintzer and E. Simanek, *Chemical Reviews*, 2008, **109**, 259-302.
46. F. C. MacLaughlin, R. J. Mumper, J. Wang, J. M. Tagliaferri, I. Gill, M. Hinchcliffe and A. P. Rolland, *Journal of Controlled Release*, 1998, **56**, 259-272.
47. D. Kivotides, S. L. Wilkin and T. G. Theofanous, *Physical Review-Section E-Statistical Nonlinear and Soft Matter Physics*, 2009, **80**, 41808.
48. M. Huang, C. W. Fong, E. Khor and L. Y. Lim, *Journal of Controlled Release*, 2005, **106**, 391-406.
49. A. U. Bielinska, C. Chen, J. Johnson and J. R. Baker Jr, *Bioconjugate Chemistry*, 1999, **10**, 843-850.
50. M. F. Ottaviani, F. Furini, A. Casini, N. J. Turro, S. Jockusch, D. A. Tomalia and L. Messori, *Macromolecules*, 2000, **33**, 7842-7851.
51. W. Chen, N. J. Turro and D. A. Tomalia, *Langmuir*, 2000, **16**, 15-19.
52. C. Brus, H. Petersen, A. Aigner, F. Czubayko and T. Kissel, *Bioconjugate Chemistry*, 2004, **15**, 677-684.
53. H. Petersen, P. M. Fechner, A. L. Martin, K. Kunath, S. Stolnik, C. J. Roberts, D. Fischer, M. C. Davies and T. Kissel, *Bioconjugate Chemistry*, 2002, **13**, 845-854.
54. T. Kim, H. J. Seo, J. S. Choi, H. S. Jang, J. Baek, K. Kim and J. S. Park, *Biomacromolecules*, 2004, **5**, 2487-2492.
55. W. Godbey, K. K. Wu and A. G. Mikos, *Proceedings of the National Academy of Sciences*, 1999, **96**, 5177.
56. H. Yu, X. Chen, T. Lu, J. Sun, H. Tian, J. Hu, Y. Wang, P. Zhang and X. Jing, *Biomacromolecules*, 2007, **8**, 1425-1435.

57. A. Harada, M. Kawamura, T. Matsuo, T. Takahashi and K. Kono, *Bioconjugate Chemistry*, 2006, **17**, 3-5.
58. M. Thanou, B. Florea, M. Geldof, H. Junginger and G. Borchard, *Biomaterials*, 2002, **23**, 153-159.
59. T. Kean, S. Roth and M. Thanou, *Journal of Controlled Release*, 2005, **103**, 643-653.
60. D. Wang, A. S. Narang, M. Kotb, A. O. Gaber, D. D. Miller, S. W. Kim and R. I. Mahato, *Biomacromolecules*, 2002, **3**, 1197-1207.
61. T. Merdan, J. Kopecek and T. Kissel, *Advanced Drug Delivery Reviews*, 2002, **54**, 715-758.
62. P. L. Felgner, T. R. Gadek, M. Holm, R. Roman, H. W. Chan, M. Wenz, J. P. Northrop, G. M. Ringold and M. Danielsen, *Proceedings of the National Academy of Sciences*, 1987, **84**, 7413.
63. J. S. Remy, C. Sirlin, P. Vierling and J. P. Behr, *Bioconjugate Chemistry*, 1994, **5**, 647-654.
64. W. Braunlin, T. Strick and M. Record Jr, *Biopolymers*, 1982, **21**, 1301-1314.
65. S. H. KANG, E. L. ZIRBES and R. KOLE, *Antisense and Nucleic Acid Drug Development*, 1999, **9**, 497-505.
66. A. J. Geall, M. A. W. Eaton, T. Baker, C. Catterall and I. S. Blagbrough, *FEBS letters*, 1999, **459**, 337-342.
67. J. Gaucheron, T. Wong, K. F. Wong, N. Maurer and P. R. Cullis, *Bioconjugate Chemistry*, 2002, **13**, 671-675.
68. V. Floch, S. Loisel, E. Guenin, A. C. Hervé, J. C. Clément, J. J. Yaouanc, H. des Abbayes and C. Férec, *Journal of Medicinal Chemistry*, 2000, **43**, 4617-4628.
69. I. Van Der Woude, A. Wagenaar, A. A. P. Meekel, M. Ter Beest, M. H. J. Ruiters, J. B. F. N. Engberts and D. Hoekstra, *Proceedings of the National Academy of Sciences*, 1997, **94**, 1160.
70. J. H. Felgner, R. Kumar, C. Sridhar, C. J. Wheeler, Y. J. Tsai, R. Border, P. Ramsey, M. Martin and P. L. Felgner, *Journal of Biological Chemistry*, 1994, **269**, 2550.
71. J. A. Heyes, D. Niculescu-Duvaz, R. G. Cooper and J. Caroline, *Journal of Medicinal Chemistry*, 2002, **45**, 99-114.
72. G. Byk, C. Dubertret, V. Escriou, M. Frederic, G. Jaslin, R. Rangara, B. Pitard, J. Crouzet, P. Wils and B. Schwartz, *Journal of Medicinal Chemistry*, 1998, **41**, 224-235.

73. C. McGregor, C. Perrin, M. Monck, P. Camilleri and A. Kirby, *Journal of the American Chemical Society*, 2001, **123**, 6215-6220.
74. J. K. Guy-Caffey, V. Bodepudi, J. S. Bishop, K. Jayaraman and N. Chaudhary, *Journal of Biological Chemistry*, 1995, **270**, 31391.
75. X. Gao and L. Huang, *Biochemical and Biophysical Research Communications*, 1991, **179**, 280-285.
76. C. L. Densmore, T. H. Giddings, J. C. Waldrep, B. M. Kinsey and V. Knight, *The Journal of Gene Medicine*, 1999, **1**, 251-264.
77. P. Belmont, A. Aissaoui, M. Hauchecorne, N. Oudrhiri, L. Petit, J. P. Vigneron, J. M. Lehn and P. Lehn, *The Journal of Gene Medicine*, 2002, **4**, 517-526.
78. O. Le Bihan, R. Chèvre, S. Mornet, B. Garnier, B. Pitard and O. Lambert, *Nucleic Acids Research*, 2011, **39**, 1595-1609.
79. J. Heyes, L. Palmer, K. Bremner and I. MacLachlan, *Journal of Controlled Release*, 2005, **107**, 276-287.
80. R. Balasubramaniam, M. Bennett, A. Aberle, J. Malone, M. Nantz and R. Malone, *Gene Therapy*, 1996, **3**, 163.
81. A. Elouahabi and J. M. Ruyschaert, *Molecular Therapy*, 2005, **11**, 336-347.
82. F. Sakurai, R. Inoue, Y. Nishino, A. Okuda, O. Matsumoto, T. Taga, F. Yamashita, Y. Takakura and M. Hashida, *Journal of Controlled Release*, 2000, **66**, 255-269.
83. P. Pires, S. Simões, S. Nir, R. Gaspar, N. D'Almeida and M. Pedroso de Lima, *Biochimica et Biophysica Acta (BBA)-Biomembranes*, 1999, **1418**, 71-84.
84. S. Eastman, C. Siegel, J. Tousignant, A. Smith, S. Cheng and R. Scheule, *Biochimica et Biophysica Acta (BBA)-Biomembranes*, 1997, **1325**, 41-62.
85. D. D. Lasic, H. Strey, M. C. A. Stuart, R. Podgornik and P. M. Frederik, *Journal of the American Chemical Society*, 1997, **119**, 832-833.
86. M. Ruponen, S. Ylä-Herttuala and A. Urtti, *Biochimica et Biophysica Acta (BBA)-Biomembranes*, 1999, **1415**, 331-341.
87. D. Hirsch-Lerner and Y. Barenholz, *Biochimica et Biophysica Acta (BBA)-Biomembranes*, 1999, **1461**, 47-57.
88. B. A. Lobo, S. A. Rogers, C. M. Wiethoff, S. Choosakoonkriang, S. Bogdanowich-Knipp and C. R. Middaugh, *Methods in Molecular Medicine*, 2001, **65**, 319-348.
89. R. Koynova and R. C. MacDonald, *Biophysical Journal*, 2003, **85**, 2449-2465.

90. E. Pozharski and R. C. MacDonald, *Biophysical Journal*, 2002, **83**, 556-565.
91. Y. Xu, S. Hui, P. Frederik and F. Szoka Jr, *Biophysical Journal*, 1999, **77**, 341-353.
92. A. E. Ouahabi, M. Thiry, S. Schiffmann, R. Fuks, H. Nguyen-Tran, J. M. Ruyschaert and M. Vandenbranden, *Journal of Histochemistry & Cytochemistry*, 1999, **47**, 1159.
93. R. Winter and R. Köhling, *Journal of Physics: Condensed Matter*, 2004, **16**, S327.
94. I. Koltover, T. Salditt and C. Safinya, *Biophysical Journal*, 1999, **77**, 915-924.
95. B. Ma, S. Zhang, H. Jiang, B. Zhao and H. Lv, *Journal of Controlled Release*, 2007, **123**, 184-194.
96. I. Koltover, T. Salditt, J. R dler and C. Safinya, *Science*, 1998, **281**, 78.
97. C. P. S. Tilcock, *Chemistry and Physics of Lipids*, 1986, **40**, 109-125.
98. V. A. Rakhmanova, T. J. McIntosh and R. C. MacDonald, *Cellular and Molecular Biology Letters*, 2000, **5**, 51-66.
99. R. Koynova, *Methods in Molecular Biology*, 2010, **606**, 399-423.
100. D. Siegel and R. Epand, *Biophysical Journal*, 1997, **73**, 3089-3111.
101. K. Mok and P. R. Cullis, *Biophysical Journal*, 1997, **73**, 2534-2545.
102. D. Simberg, D. Danino, Y. Talmon, A. Minsky, M. Ferrari, C. Wheeler and Y. Barenholz, *Journal of Biological Chemistry*, 2001, **276**, 47453.
103. C. Safinya, *Current Opinion in Structural Biology*, 2001, **11**, 440-448.
104. S. May and A. Ben-Shaul, *Biophysical Journal*, 1997, **73**, 2427-2440.
105. O. Boussif, F. Lezoualc'h, M. A. Zanta, M. D. Mergny, D. Scherman, B. Demeneix and J. P. Behr, *Proceedings of the National Academy of Sciences of the United States of America*, 1995, **92**, 7297.
106. F. Labat-Moleur, A. Steffan, C. Brisson, H. Perron, O. Feugeas, P. Furstenberger, F. Oberling, E. Brambilla and J. Behr, *Gene Therapy*, 1996, **3**, 1010.
107. I. Kopatz, J. S. Remy and J. P. Behr, *The Journal of Gene Medicine*, 2004, **6**, 769-776.
108. B. B. Finlay and P. Cossart, *Science*, 1997, **276**, 718.
109. C. Dehio, E. Freissler, C. Lanz, O. G. Gómez-Duarte, G. David and T. F. Meyer, *Experimental Cell Research*, 1998, **242**, 528-539.
110. K. A. Mislick and J. D. Baldeschwieler, *Proceedings of the National Academy of Sciences of the United States of America*, 1996, **93**, 12349.

111. M. Ogris, G. Walker, T. Blessing, R. Kircheis, M. Wolschek and E. Wagner, *Journal of Controlled Release*, 2003, **91**, 173-181.
112. P. S. Low and A. C. Antony, *Advanced Drug Delivery Reviews*, 2004, **56**, 1055.
113. P. S. Low, W. A. Henne and D. D. Doorneweerd, *Accounts of chemical research*, 2007, **41**, 120-129.
114. A. Gabizon, A. T. Horowitz, D. Goren, D. Tzemach, H. Shmeeda and S. Zalipsky, *Clinical Cancer Research*, 2003, **9**, 6551-6559.
115. X. Q. Pan, H. Wang and R. J. Lee, *Pharmaceutical Research*, 2003, **20**, 417-422.
116. X. Q. Pan, X. Zheng, G. Shi, H. Wang, M. Ratnam and R. J. Lee, *Blood*, 2002, **100**, 594-602.
117. P. J. Stevens and R. J. Lee, *Anticancer Research*, 2003, **23**, 4927.
118. T. Shiokawa, Y. Hattori, K. Kawano, Y. Ohguchi, H. Kawakami, K. Toma and Y. Maitani, *Clinical Cancer Research*, 2005, **11**, 2018.
119. I. S. Zuhorn and D. Hoekstra, *Journal of Controlled Release*, 2012.
120. I. S. Zuhorn, R. Kalicharan and D. Hoekstra, *Journal of Biological Chemistry*, 2002, **277**, 18021.
121. S. Simões, V. Slepushkin, P. Pires, R. Gaspar, M. C. Pedroso de Lima and N. Düzgüne, *Biochimica et Biophysica Acta (BBA)-Biomembranes*, 2000, **1463**, 459-469.
122. H. Matsui, L. G. Johnson, S. H. Randell and R. C. Boucher, *Journal of Biological Chemistry*, 1997, **272**, 1117.
123. A. Fasbender, J. Zabner, B. Zeiher and M. Welsh, *Gene Therapy*, 1997, **4**, 1173.
124. Q. Chu, J. Tousignant, S. Fang, C. Jiang, S. Eastman, L. Chen, S. Cheng and R. Scheule, *Human Gene Therapy*, 1999, **10**, 25-36.
125. T. Bieber, W. Meissner, S. Kostin, A. Niemann and H. P. Elsasser, *Journal of Controlled Release*, 2002, **82**, 441-454.
126. A. El Ouahabi, M. Thiry, V. Pector, R. Fuks, J. Ruysschaert and M. Vandenbranden, *FEBS letters*, 1997, **414**, 187-192.
127. J. Rejman, V. Oberle, I. S. Zuhorn and D. Hoekstra, *Biochemical Journal*, 2004, **377**, 159.
128. S. Grosse, Y. Aron, G. Thévenot, D. François, M. Monsigny and I. Fajac, *The Journal of Gene Medicine*, 2005, **7**, 1275-1286.

129. H. Farhood, N. Serbina and L. Huang, *Biochimica et Biophysica Acta (BBA)-Biomembranes*, 1995, **1235**, 289-295.
130. I. Hafez and P. Cullis, *Advanced Drug Delivery Reviews*, 2001, **47**, 139-148.
131. J. Smisterová, A. Wagenaar, M. C. A. Stuart, E. Polushkin, G. ten Brinke, R. Hulst, J. B. F. N. Engberts and D. Hoekstra, *Journal of Biological Chemistry*, 2001, **276**, 47615.
132. I. Zuhorn, U. Bakowsky, E. Polushkin, W. Visser, M. Stuart, J. Engberts and D. Hoekstra, *Molecular Therapy*, 2005, **11**, 801-810.
133. I. S. Zuhorn, W. H. Visser, U. Bakowsky, J. B. F. N. Engberts and D. Hoekstra, *Biochimica et Biophysica Acta (BBA)-Biomembranes*, 2002, **1560**, 25-36.
134. M. Hope and P. Cullis, *Biochemical and Biophysical Research Communications*, 1980, **92**, 846-852.
135. A. Ahmad, H. Evans, K. Ewert, C. George, C. Samuel and C. Safinya, *The Journal of Gene Medicine*, 2005, **7**, 739-748.
136. A. Lin, N. Slack, A. Ahmad, C. George, C. Samuel and C. Safinya, *Biophysical Journal*, 2003, **84**, 3307-3316.
137. G. Caracciolo, D. Pozzi, R. Caminiti, C. Marchini, M. Montani, A. Amici and H. Amenitsch, *The Journal of Physical Chemistry B*, 2008, **112**, 11298-11304.
138. A. Miller and D. Dean, *Advanced drug delivery reviews*, 2009, **61**, 603-613.
139. C. M. Feldherr, D. Akin and R. J. Cohen, *Journal of Cell Science*, 2001, **114**, 4621.
140. S. Brunner, T. Sauer, S. Carotta, M. Cotten, M. Saltik and E. Wagner, *Gene Therapy*, 2000, **7**, 401.
141. S. Brunner, E. Furtbauer, T. Sauer, M. Kursa and E. Wagner, *Molecular Therapy*, 2002, **5**, 80-86.
142. D. Kalderon, B. L. Roberts, W. D. Richardson and A. E. Smith, *Cell*, 1984, **39**, 499-509.
143. D. A. Dean, *Experimental Cell Research*, 1997, **230**, 293-302.
144. M. A. Ilies, W. A. Seitz, B. H. Johnson, E. L. Ezell, A. L. Miller, E. B. Thompson and A. T. Balaban, *Journal of Medicinal Chemistry*, 2006, **49**, 3872-3887.
145. M. In and R. Zana, *Journal of Dispersion Science and Technology*, 2007, **28**, 143-154.
146. J. Xia and R. Zana, *Gemini surfactants: Synthesis, interfacial and solution-phase behavior and applications*, CRC Press, 2003.

147. M. Johnsson and J. B. F. N. Engberts, *Journal of Physical Organic Chemistry*, 2004, **17**, 934-944.
148. J. N. Israelachvili, D. J. Mitchell and B. W. Ninham, *Journal of the Chemical Society, Faraday Transactions 2*, 1976, **72**, 1525-1568.
149. D. Myers, *Surfactant science and technology*, Wiley Online Library, 1992.
150. W. M. Gelbart, A. Ben-Shaul and D. Roux, *Micelles, membranes, microemulsions, and monolayers*, Springer-Verlag New York, 1995.
151. D. J. Mitchell, G. J. T. Tiddy, L. Waring, T. Bostock and M. P. McDonald, *Journal of the Chemical Society, Faraday Transactions 1*, 1983, **79**, 975-1000.
152. I. Badea, S. Wettig, R. Verrall and M. Foldvari, *European Journal of Pharmaceutics and Biopharmaceutics*, 2007, **65**, 414-422.
153. N. Hattori, M. Hara, H. Okabayashi and C. O'Connor, *Colloid & Polymer Science*, 1999, **277**, 306-317.
154. D. Danino, Y. Talmon and R. Zana, *Langmuir*, 1995, **11**, 1448-1456.
155. S. De, V. K. Aswal, P. S. Goyal and S. Bhattacharya, *The Journal of Physical Chemistry*, 1996, **100**, 11664-11671.
156. E. Alami, G. Beinert, P. Marie and R. Zana, *Langmuir*, 1993, **9**, 1465-1467.
157. R. Zana, M. Benraou and R. Rueff, *Langmuir*, 1991, **7**, 1072-1075.
158. Y. Han and Y. Wang, *Physical Chemistry Chemical Physics*, 2011.
159. G. Bai, Y. Wang, H. Yan, R. K. Thomas and J. C. T. Kwak, *The Journal of Physical Chemistry B*, 2002, **106**, 2153-2159.
160. R. Zana, *Current Opinion in Colloid & Interface Science*, 1996, **1**, 566-571.
161. S. Wettig, X. Li and R. Verrall, *Langmuir*, 2003, **19**, 3666-3670.
162. M. Dreja, W. Pyckhout-Hintzen, H. Mays and B. Tieke, *Langmuir*, 1999, **15**, 391-399.
163. S. Wettig, P. Nowak and R. Verrall, *Langmuir*, 2002, **18**, 5354-5359.
164. M. J. Rosen and L. D. Song, *Journal of Colloid and Interface Science*, 1996, **179**, 261-268.
165. M. J. Rosen and L. Liu, *Journal of the American Oil Chemists' Society*, 1996, **73**, 885-890.
166. S. D. Wettig, C. Wang, R. E. Verrall and M. Foldvari, *Physical Chemistry Chemical Physics*, 2007, **9**, 871-877.
167. X. Wang, J. Wang, Y. Wang, H. Yan, P. Li and R. K. Thomas, *Langmuir*, 2004, **20**, 53-56.

168. S. Wettig, R. Verrall and M. Foldvari, *Current Gene Therapy*, 2008, **8**, 9-23.
169. A. Kirby, P. Camilleri, J. Engberts, M. Feiters, R. Nolte, O. S derman, M. Bergsma, P. Bell, M. Fielden and C. Garcia, *Angewandte Chemie International Edition*, 2003, **42**, 1448-1457.
170. R. Dias, M. Rosa, A. C. Pais, M. Miguel and B. Lindman, *Journal of the Chinese Chemical Society*, 2004, **51**, 447-469.
171. R. Dias, S. Mel'nikov, B. Lindman and M. G. Miguel, *Langmuir*, 2000, **16**, 9577-9583.
172. D. Uhrikova, I. Zajac, M. Dubnickova, M. Pisarcik, S. S. Funari, G. Rapp and P. Balgavy, *Colloids and Surfaces B: Biointerfaces*, 2005, **42**, 59-68.
173. N. Jiang, J. Wang, Y. Wang, H. Yan and R. Thomas, *Journal of Colloid and Interface Science*, 2005, **284**, 759-764.
174. C. Wang, S. D. Wettig, M. Foldvari and R. E. Verrall, *Langmuir*, 2007, **23**, 8995-9001.
175. S. D. Wettig, R. Deubry, J. Akbar, T. Kaur, H. Wang, T. Sheinin, J. W. Joseph and R. A. Slavcev, *Physical Chemistry Chemical Physics*, 2010, **12**, 4821-4826.
176. L. Karlsson, M. C. P. van Eijk and O. Söderman, *Journal of Colloid and Interface Science*, 2002, **252**, 290-296.
177. N. Zuidam, Y. Barenholz and A. Minsky, *FEBS letters*, 1999, **457**, 419.
178. C. Bombelli, F. Faggioli, P. Luciani, G. Mancini and M. Sacco, *Journal of Medicinal Chemistry*, 2005, **48**, 5378-5382.
179. I. Badea, 2006.
180. Q. Chen, X. Kang, R. Li, X. Du, Y. Shang, H. Liu and Y. Hu, *Langmuir*, 2012, **28**, 3429-3438.
181. X. Chen, J. Wang, N. Shen, Y. Luo, L. Li, M. Liu and R. K. Thomas, *Langmuir*, 2002, **18**, 6222-6228.
182. A. Kirby, P. Camilleri, J. Engberts, M. Feiters, R. Nolte, O. S derman, M. Bergsma, P. Bell, M. Fielden and C. Garcia Rodriguez, *Angewandte Chemie International Edition*, 2003, **42**, 1448-1457.
183. M. L. Fielden, C. Perrin, A. Kremer, M. Bergsma, M. C. Stuart, P. Camilleri and J. B. F. N. Engberts, *European Journal of Biochemistry*, 2001, **268**, 1269-1279.
184. P. C. Bell, M. Bergsma, I. P. Dolbnya, W. Bras, M. C. A. Stuart, A. E. Rowan, M. C. Feiters and J. B. F. N. Engberts, *Journal of the American Chemical Society*, 2003, **125**, 1551-1558.

185. L. Wasungu, M. Scarzello, G. van Dam, G. Molema, A. Wagenaar, J. Engberts and D. Hoekstra, *Journal of Molecular Medicine*, 2006, **84**, 774-784.
186. H. S. Rosenzweig, V. A. Rakhmanova and R. C. MacDonald, *Bioconjugate Chemistry*, 2001, **12**, 258-263.
187. I. Badea, R. Verrall, M. Baca Estrada, S. Tikoo, A. Rosenberg, P. Kumar and M. Foldvari, *The Journal of Gene Medicine*, 2005, **7**, 1200-1214.
188. M. Foldvari, I. Badea, S. Wettig, R. Verrall and M. Bagonluri, *Journal of Experimental Nanoscience*, 2006, **1**.
189. E. Dauty, J. S. Remy, T. Blessing and J. P. Behr, *Journal of the American Chemical Society*, 2001, **123**, 9227-9234.
190. I. Badea, R. Verrall, M. Baca Estrada, S. Tikoo, A. Rosenberg, P. Kumar and M. Foldvari, *The Journal of Gene Medicine*, 2005, **7**, 1200-1214.
191. A. L. Dunehoo, M. Anderson, S. Majumdar, N. Kobayashi, C. Berkland and T. J. Siahaan, *Journal of Pharmaceutical Sciences*, 2006, **95**, 1856-1872.
192. L. Marinelli, A. Meyer, D. Heckmann, A. Lavecchia, E. Novellino and H. Kessler, *Journal of Medicinal Chemistry*, 2005, **48**, 4204-4207.
193. S. D. Wettig, I. Badea, M. Donkuru, R. E. Verrall and M. Foldvari, *The Journal of Gene Medicine*, 2007, **9**, 649-658.
194. M. D. Donkuru, S. D. Wettig, R. E. Verrall, I. Badea and M. Foldvari, *Journal of Materials Chemistry*, 2012, **22**, 6232-6244.
195. M. Johnsson, A. Wagenaar, M. C. A. Stuart and J. B. F. N. Engberts, *Langmuir*, 2003, **19**, 4609-4618.
196. C. Fong, D. Wells, I. Krodkiewska, J. Booth and P. Hartley, *Journal of Physical Chemistry B*, 2007, **111**, 1384-1392.
197. H. Minamikawa and M. Hato, *Langmuir*, 1997, **13**, 2564-2571.
198. A. Bendavid, C. Burns, L. Field, K. Hashimoto, D. Ridley, K. Sandanayake and L. Wieczorek, *Journal of Organic Chemistry*, 2001, **66**, 3709-3716.
199. K. Hioki, M. Kinugasa, M. Kishimoto, M. Fujiwara, S. Tani and M. Kunishima, *Synthesis*, 2006, **2006**, 1931-1933.
200. O. Hara, K. Sugimoto, K. Makino and Y. Hamada, *Synlett*, 2004, **15**, 2646.
201. R. Zana, *Journal of Colloid and Interface Science*, 2002, **252**, 259-261.
202. J. Heinrich, J. Schultz, M. Bosse, G. Ziegelin, E. Lanka and K. Moelling, *Journal of Molecular Medicine*, 2002, **80**, 648-654.
203. H. Wang and S. D. Wettig, *Physical Chemistry Chemical Physics*, 2011, **13**, 637-642. Reproduced by permission of the PCCP owner societies.

204. M. D. Donkuru, College of Graduate Studies and Research in Partial Fulfillment of the Requirements for the Degree of Master of Science in the College of Pharmacy and Nutrition, University of Saskatchewan, 2008.
205. Y. Moroi, T. Oyama and R. Matuura, *Journal of Colloid and Interface Science*, 1977, **60**, 103-111.
206. C. Vautier-Giongo and B. L. Bales, *The Journal of Physical Chemistry B*, 2003, **107**, 5398-5403.
207. R. Zana, *Journal of Colloid and Interface Science*, 2002, **246**, 182-190.
208. Y. Fan, Y. Li, M. Cao, J. Wang, Y. Wang and R. K. Thomas, *Langmuir*, 2007, **23**, 11458-11464.
209. X. Wang, Q. Li, X. Chen and Z. Li, *Langmuir*, 2012, **28**, 16547-16554.
210. Q. Chen, D. Zhang, R. Li, H. Liu and Y. Hu, *Thin Solid Films*, 2008, **516**, 8782-8787.
211. M. Sikirić, I. Primožič, Y. Talmon and N. Filipović-Vinceković, *Journal of Colloid and Interface Science*, 2005, **281**, 473-481.
212. C. Carnero Ruiz, *Colloid & Polymer Science*, 1999, **277**, 701-707.
213. P. Carpena, J. Aguiar, P. Bernaola-Galvan and C. C. Ruiz, *Langmuir*, 2002, **18**, 6054-6058.
214. B. L. Bales, *The Journal of Physical Chemistry B*, 2001, **105**, 6798-6804.
215. Y. Moroi, *Micelles: theoretical and applied aspects*, Springer, 1992.
216. R. Zana, *Journal of Colloid and Interface Science*, 1980, **78**, 330-337.
217. A. Gonzalez-Perez, J. Del Castillo, J. Czapkiewicz and J. Rodríguez, *Colloids and Surfaces A: Physicochemical and Engineering Aspects*, 2004, **232**, 183-189.
218. S. Mehta, K. Bhasin, R. Chauhan and S. Dham, *Colloids and Surfaces A: Physicochemical and Engineering Aspects*, 2005, **255**, 153-157.
219. K. Jenkins, University of Saskatchewan, 2000.
220. B. W. Koenig and K. Gawrisch, *Biochimica et Biophysica Acta (BBA)-Biomembranes*, 2005, **1715**, 65-70.
221. M. Instruments, *Malvern Instruments Ltd., Worcestershire WR14 1XZ, UK*, 2007.
222. D. Svergun and M. Koch, *Reports on Progress in Physics*, 2003, **66**, 1735.
223. M. Castro, D. Griffiths, A. Patel, N. Patrick, C. Kitson and M. Ladlow, *Organic & Biomolecular Chemistry*, 2004, **2**, 2814-2820.

224. O. V. Vieira, D. O. Hartmann, C. M. P. Cardoso, D. Oberdoerfer, M. Baptista, M. A. S. Santos, L. Almeida, J. Ramalho-Santos and W. L. C. Vaz, *PLoS One*, 2008, **3**, e2913.
225. P. Ross and S. Hui, *Gene Therapy*, 1999, **6**, 651.
226. J. S. Zhang, S. Li and L. Huang, *Methods in Enzymology*, 2003, **373**, 332-342.
227. D. Hoekstra, J. Rejman, L. Wasungu, F. Shi and I. Zuhorn, *Biochemical Society Transactions*, 2007, **35**, 68-71.
228. D. Lechardeur, A. Verkman and G. L. Lukacs, *Advanced Drug Delivery Reviews*, 2005, **57**, 755-767.
229. T. K. Prasad, N. Rangaraj and N. M. Rao, *FEBS letters*, 2005, **579**, 2635-2642.
230. J. Rejman, M. Conese and D. Hoekstra, *Journal of Liposome Research*, 2006, **16**, 237-247.
231. T. Zhou, G. Xu, M. Ao, Y. Yang and C. Wang, *Colloids and Surfaces A: Physicochemical and Engineering Aspects*, 2012.
232. A. Cardoso, H. Faneca, J. Almeida, A. Pais, E. Marques, M. de Lima and A. Jurado, *Biochimica et Biophysica Acta (BBA)-Biomembranes*, 2010.
233. M. C. Pedroso de Lima, S. Simões, P. Pires, H. Faneca and N. Düzgüneş, *Advanced Drug Delivery Reviews*, 2001, **47**, 277-294.
234. J. O. Radler, I. Koltover, T. Salditt and C. R. Safinya, *Science*, 1997, **275**, 810.
235. J. Yan, N. V. Bereznoy, N. Korolev, C. J. Su and L. Nordenskiöld, *Biochimica et Biophysica Acta (BBA)-Biomembranes*, 2012.
236. J. Seddon and R. Templer, *Polymorphism of lipid-water systems*, 1995.
237. M. A. Hopcroft, W. D. Nix and T. W. Kenny, *Journal of Microelectromechanical Systems* 2010, **19**, 229-238.
238. B. G. Tenchov, L. Wang, R. Koynova and R. C. MacDonald, *Biochimica et Biophysica Acta (BBA)-Biomembranes*, 2008, **1778**, 2405-2412.

Appendices

Appendix A ¹H-NMR data for the synthesized compound

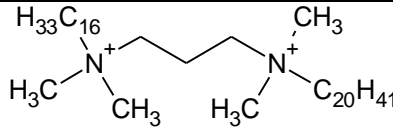
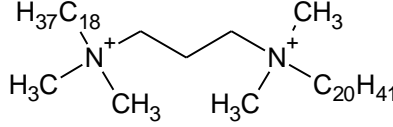
Compound	δ (ppm)	Number of protons	Group
Phytanyl Bromide	0.80-0.94	15	CH₃'s
	0.94-1.69	24	CH₂'s and CH's
	3.34-3.49	2	CH₂Br
Boc-protected	1.43	4	N(CH ₃) ₂ -CH ₂ CH₂CH₂
3,3'-iminobis(N,N-dimethylpropylamine)	1.86	4	N(CH ₃) ₂ - CH₂CH₂CH₂
	2.19	4	N(CH ₃) ₂ -CH ₂ CH ₂ CH₂
	6.45-6.47	12	N(CH₃)₂
	8.19-8.21	9	C (CH₃)₃
Phy-3-12	0.81-0.85	18	CH₃ (Phytanyl and C ₁₂ chains)
	0.94-1.33	38	CH₂ (Phytanyl and C ₁₂ chains)
	1.46-1.77	4	CH (Phytanyl chain)
	1.92	2	CH₂ (Phytanyl chain)
	2.74	2	CH₂ (spacer)
	3.45-3.48	16	N- CH₃ , N- CH₂ (chains)
	3.87	4	N- CH₂ (spacer)
Phy-3-16	0.81-0.85	18	CH₃ (Phytanyl and C ₁₆ chains)
	0.94-1.33	46	CH₂ (Phytanyl and C ₁₆ chains)
	1.46-1.77	4	CH (Phytanyl chain)
	1.92	2	CH₂ (Phytanyl chain)

	2.74	2	CH ₂ (spacer)
	3.45-3.48	16	N-CH ₃ , N-CH ₂ (chains)
	3.87	4	N-CH ₂ (spacer)
Phy-3-18	0.81-0.85	18	CH ₃ (Phytanyl and C ₁₈ chains)
	0.94-1.33	50	CH ₂ (Phytanyl and C ₁₈ chains)
	1.46-1.77	4	CH (Phytanyl chain)
	1.92	2	CH ₂ (Phytanyl chain)
	2.74	2	CH ₂ (spacer)
	3.45-3.48	16	N-CH ₃ , N-CH ₂ (chains)
	3.87	4	N-CH ₂ (spacer)
Phy-7NH-12	0.80-0.87	18	CH ₃ (Phytanyl and C ₁₂ chains)
	0.94-1.29	38	CH ₂ (Phytanyl and C ₁₂ chains)
	1.40-1.55	4	CH (Phytanyl chain)
	1.84	2	CH ₂ (Phytanyl chain)
	2.62-2.70	4	NH-CH ₂ (spacer)
	2.95	1	NH (spacer)
	3.24	16	N-CH ₃ , N-CH ₂ (chains)
	4.02-4.06	8	(CH ₃) ₂ N-CH ₂ -CH ₂ (spacer)
Phy-7NH-16	0.80-0.87	18	CH ₃ (Phytanyl and C ₁₆ chains)
	0.94-1.29	46	CH ₂ (Phytanyl and C ₁₆ chains)
	1.40-1.55	4	CH (Phytanyl chain)
	1.84	2	CH ₂ (Phytanyl chain)

	2.62-2.70	4	NH-CH ₂ (spacer)
	2.95	1	NH (spacer)
	3.24	16	N-CH ₃ , N-CH ₂ (chains)
	4.02-4.06	8	(CH ₃) ₂ N-CH ₂ - CH ₂ (spacer)
Phy-7NH-18	0.80-0.87	18	CH ₃ (Phytanyl and C ₁₈ chains)
	0.94-1.29	50	CH ₂ (Phytanyl and C ₁₈ chains)
	1.40-1.55	4	CH (Phytanyl chain)
	1.84	2	CH ₂ (Phytanyl chain)
	2.62-2.70	4	NH-CH ₂ (spacer)
	2.95	1	NH (spacer)
	3.24	16	N-CH ₃ , N-CH ₂ (chains)
	4.02-4.06	8	(CH ₃) ₂ N-CH ₂ - CH ₂ (spacer)

Appendix B Low resolution electrospray ionization mass spectroscopic data for the phytanyl substituted compounds

Surfactant	Gemini surfactant ion	Results of analysis	
		m/z	%BPI
Phy-3-12		131.16	3.73
		150.19	7.30
		290.36	30.41
		299.38	100.00
		300.38	23.33
		411.51	22.43
		412.52	7.48

Phy-3-16		182.99	4.81
		290.33	3.61
		318.36	100.00
		346.40	10.84
		355.42	6.63
		411.48	3.01
Phy-3-18		149.02	3.61
		257.25	6.02
		318.37	6.63
		332.39	100.00
		346.40	16.27
		522.61	7.23
	550.64	33.73	

Appendix C Characterization of the gemini surfactants

Table C 1 Specific conductivity vs. temperature

Phy-3-16

Temperature (°C)	Conductivity ($\mu\text{S}/\text{cm}$)			Average \pm SD	Conductance (μS)
10	16.73	16.71	16.83	16.76 \pm 0.06	35.28
15	16.76	16.71	16.92	16.80 \pm 0.11	35.36
20	17.04	17.12	17.04	17.07 \pm 0.05	35.93
25	17.34	17.1	17.26	17.23 \pm 0.12	36.28
30	17.34	17.47	17.36	17.39 \pm 0.07	36.61
35	17.57	17.5	17.4	17.49 \pm 0.08	36.82
40	17.4	17.5	17.45	17.45 \pm 0.05	36.74
45	17.57	17.46	17.44	17.49 \pm 0.07	36.82
50	19.65	19.43	19.7	19.60 \pm 0.14	41.25

55	22.13	22.28	22.45	22.29 ± 0.16	46.92
60	24.02	24.57	24.41	24.33 ± 0.28	51.23
65	26.67	26.78	26.69	26.71 ± 0.06	56.24
70	27.71	27.89	28.1	27.90 ± 0.19	58.74
75	28.51	28.41	28.43	28.45 ± 0.05	59.90
80	29.16	29.40	29.21	29.26 ± 0.13	61.59
85	30.60	30.70	30.30	30.53 ± 0.21	64.28
90	31.30	31.40	30.50	31.07 ± 0.49	65.41

Phy-3-18

Temperature (°C)	Conductivity (μS/cm)			Average ±SD	Conductance (μS)
10	20.86	20.53	21.29	20.90 ± 0.38	43.99
15	21.10	20.68	20.90	20.90 ± 0.21	43.99
20	22.24	22.19	22.16	22.20 ± 0.04	46.73
25	22.80	22.72	22.62	22.71 ± 0.09	47.82
30	23.82	23.36	22.99	23.39 ± 0.42	49.24
35	23.78	23.45	23.33	23.52 ± 0.23	49.52
40	24.31	23.53	23.52	23.78 ± 0.45	50.08
45	25.57	24.22	23.78	24.52 ± 0.93	51.63
50	26.44	24.1	24.14	24.89 ± 1.33	52.41
55	24.2	24.23	24.14	24.19 ± 0.04	50.93
60	24.28	24.42	24.38	24.36 ± 0.07	51.28
65	24.48	25.01	25.09	24.86 ± 0.33	52.34
70	28.22	28.31	28.35	28.29 ± 0.06	59.56
75	34.70	34.40	34.40	34.5 ± 0.17	72.63
78	37.20	37.30	37.30	37.27 ± 0.06	78.46
80	38.60	38.90	38.80	38.77 ± 0.15	81.61
83	40.00	40.30	40.20	40.17 ± 0.15	84.56

85	41.10	41.30	41.30	41.23 ± 0.12	86.81
88	42.60	42.90	42.90	42.80 ± 0.17	90.11

Table C 2 Surface tension (γ) vs. surfactant concentration

Phy-3-12

Concentration (M)	Log C	γ (mN/m)	St.dev. (mN/m)	Dosing ml	Total dos. ml	Temperature °C
0.00E+00		67.05	0.039	0	0	25
1.87E-07	-6.73E+00	67.12	0.2	0.005	0.005	25
2.24E-07	-6.65E+00	67.41	0.016	0.001	0.006	25
2.98E-07	-6.53E+00	67.39	0.005	0.002	0.008	25
3.73E-07	-6.43E+00	67.3	0.14	0.002	0.01	25
4.85E-07	-6.31E+00	67.36	0.018	0.003	0.013	25
5.97E-07	-6.22E+00	67.3	0.021	0.003	0.016	25
7.46E-07	-6.13E+00	67.22	0.027	0.004	0.02	25
9.32E-07	-6.03E+00	67.05	0.0068	0.005	0.025	25
1.19E-06	-5.92E+00	66.99	0.023	0.007	0.032	25
1.49E-06	-5.83E+00	66.84	0.021	0.008	0.04	25
1.90E-06	-5.72E+00	66.67	0.031	0.011	0.051	25
2.39E-06	-5.62E+00	66.5	0.021	0.013	0.064	25
2.98E-06	-5.53E+00	64.24	0.13	0.016	0.08	25
3.76E-06	-5.42E+00	62.79	0.055	0.021	0.101	25
4.73E-06	-5.33E+00	61.63	0.026	0.026	0.127	25
5.95E-06	-5.23E+00	59.54	0.41	0.033	0.16	25
7.51E-06	-5.12E+00	55.74	0.12	0.042	0.202	25
9.47E-06	-5.02E+00	53.15	0.067	0.053	0.255	25
1.19E-05	-4.92E+00	50.46	0.12	0.066	0.321	25
1.50E-05	-4.82E+00	48.02	0.038	0.084	0.405	25
1.89E-05	-4.72E+00	46.63	0.53	0.106	0.511	25
2.38E-05	-4.62E+00	43.81	0.051	0.134	0.645	25
2.99E-05	-4.52E+00	42.46	0.35	0.17	0.815	25
3.77E-05	-4.42E+00	39.56	0.084	0.216	1.031	25
4.75E-05	-4.32E+00	37.53	0.051	0.274	1.305	25
5.98E-05	-4.22E+00	35.47	0.084	0.35	1.655	25
7.53E-05	-4.12E+00	35.07	0.81	0.447	2.102	25
9.48E-05	-4.02E+00	34.79	1.00	0.574	2.676	25

1.19E-04	-3.92E+00	34.03	0.41	0.741	3.417	25
1.50E-04	-3.82E+00	33.81	0.41	0.963	4.38	25
1.89E-04	-3.72E+00	33.23	0.064	1.263	5.643	25
2.38E-04	-3.62E+00	33.75	1.20	1.677	7.32	25
3.00E-04	-3.52E+00	32.55	2.00	2.261	9.581	25

Phy-3-16

Concentration M	log C	γ (mN/m)	St.dev. (mN/m)	Dosing ml	Total dos. ml	Temperature °C
0.00E+00		67.39	0.13	0	0	50
5.44E-08	-7.26E+00	66.67	0.07	0.006	0.006	50
6.35E-08	-7.20E+00	66.31	0.024	0.001	0.007	50
9.07E-08	-7.04E+00	66.18	0.017	0.003	0.01	50
1.09E-07	-6.96E+00	66.15	0.016	0.002	0.012	50
1.45E-07	-6.84E+00	66.01	0.052	0.004	0.016	50
1.91E-07	-6.72E+00	66.01	0.059	0.005	0.021	50
2.45E-07	-6.61E+00	66.06	0.0095	0.006	0.027	50
3.17E-07	-6.50E+00	66.01	0.03	0.008	0.035	50
4.08E-07	-6.39E+00	66.03	0.027	0.01	0.045	50
5.26E-07	-6.28E+00	66.09	0.01	0.013	0.058	50
6.79E-07	-6.17E+00	65.95	0.0027	0.017	0.075	50
8.87E-07	-6.05E+00	64.65	0.13	0.023	0.098	50
1.14E-06	-5.94E+00	61.61	0.28	0.028	0.126	50
1.47E-06	-5.83E+00	57.56	0.34	0.037	0.163	50
1.91E-06	-5.72E+00	52.03	0.38	0.048	0.211	50
2.47E-06	-5.61E+00	47.66	0.28	0.063	0.274	50
3.20E-06	-5.50E+00	43.9	0.32	0.081	0.355	50
4.13E-06	-5.38E+00	40.91	0.29	0.105	0.46	50
5.34E-06	-5.27E+00	37.74	0.21	0.136	0.596	50
6.92E-06	-5.16E+00	37.33	0.46	0.178	0.774	50
8.94E-06	-5.05E+00	36.03	0.12	0.231	1.005	50
1.16E-05	-4.94E+00	36.16	0.26	0.303	1.308	50
1.50E-05	-4.83E+00	34.18	0.075	0.397	1.705	50
1.93E-05	-4.71E+00	38.09	1.5	0.522	2.227	50
2.50E-05	-4.60E+00	34.26	0.14	0.692	2.919	50
3.24E-05	-4.49E+00	37.62	0.81	0.922	3.841	50
4.18E-05	-4.38E+00	35.65	2.10	1.241	5.082	50
5.41E-05	-4.27E+00	36.97	1.50	1.693	6.775	50

7.00E-05	-4.15E+00	36.45	1.70	2.35	9.13	50
----------	-----------	-------	------	------	------	----

Phy-3-18

Concentration M	Log C	γ (mN/m)	St.dev. (mN/m)	Dosing ml	Total dos. ml	Temperature °C
0.00E+00		67.63	0.3	0	0	65
4.29E-08	-7.37E+00	65.21	0.16	0.006	0.006	65
5.00E-08	-7.30E+00	64.26	0.087	0.001	0.007	65
7.15E-08	-7.15E+00	63.48	0.15	0.003	0.01	65
9.29E-08	-7.03E+00	63.16	0.092	0.003	0.013	65
1.14E-07	-6.94E+00	63.33	0.027	0.003	0.016	65
3.29E-07	-6.48E+00	63.27	0.084	0.01	0.046	65
4.29E-07	-6.37E+00	63.31	0.062	0.014	0.06	65
2.65E-06	-5.58E+00	49.54	0.048	0.086	0.373	65
3.44E-06	-5.46E+00	47.55	0.23	0.112	0.485	65
4.45E-06	-5.35E+00	46.11	0.19	0.145	0.63	65
5.78E-06	-5.24E+00	44.73	0.59	0.191	0.821	65
7.49E-06	-5.13E+00	44.73	0.52	0.249	1.07	65
9.71E-06	-5.01E+00	44.49	0.55	0.326	1.396	65
1.26E-05	-4.90E+00	43.41	0.56	0.43	1.826	65
1.63E-05	-4.79E+00	43.24	0.35	0.569	2.395	65
2.12E-05	-4.67E+00	43.31	0.35	0.756	3.151	65
2.75E-05	-4.56E+00	43.25	1.50	1.014	4.165	65
3.57E-05	-4.45E+00	42.93	1.30	1.375	5.54	65
4.63E-05	-4.33E+00	42.08	0.97	1.89	7.43	65
6.00E-05	-4.22E+00	43.18	0.71	2.652	10.082	65

Table C 3 Specific conductivity vs. surfactant concentration

Phy-3-12

Concentration (M)	Specific conductivity ($\mu\text{S/cm}$)			Average \pm SD
0	0.79	0.75	0.77	0.77 \pm 0.020
6.17E-06	1.28	1.31	1.31	1.30 \pm 0.017
1.23E-05	1.84	1.84	1.86	1.85 \pm 0.012
1.84E-05	2.36	2.38	2.39	2.38 \pm 0.015
2.45E-05	2.85	2.92	2.91	2.89 \pm 0.038
3.05E-05	3.39	3.40	3.40	3.40 \pm 0.006

3.65E-05	3.86	3.86	3.87	3.86 ± 0.006
4.85E-05	4.73	4.76	4.76	4.75 ± 0.017
6.03E-05	5.49	5.54	5.56	5.53 ± 0.036
7.20E-05	6.06	6.08	6.09	6.08 ± 0.015
8.37E-05	6.58	6.59	6.61	6.59 ± 0.015
9.52E-05	7.00	7.05	7.06	7.04 ± 0.032
1.06E-04	7.41	7.45	7.45	7.44 ± 0.023
1.18E-04	7.78	7.82	7.82	7.81 ± 0.023
1.29E-04	8.14	8.15	8.16	8.15 ± 0.010
1.46E-04	8.73	8.71	8.69	8.71 ± 0.020
1.73E-04	9.42	9.40	9.43	9.42 ± 0.016
1.99E-04	10.25	10.26	10.24	10.25 ± 0.010
2.25E-04	10.75	11.01	11.01	10.92 ± 0.015
2.75E-04	12.32	12.34	12.30	12.32 ± 0.020
3.23E-04	13.65	13.68	13.70	13.68 ± 0.025

Phy-3-16

Concentration (mM)	Specific conductivity (μS/cm)			Average ± SD
0	1.07	1.06	1.07	1.07 ± 0.006
1.13E-04	1.13	1.12	1.13	1.13 ± 0.006
1.69E-03	1.17	1.18	1.19	1.18 ± 0.01
2.82E-03	1.26	1.28	1.25	1.26 ± 0.015
3.93E-03	1.32	1.36	1.35	1.34 ± 0.021
4.49E-03	1.38	1.37	1.41	1.38 ± 0.021
5.05E-03	1.41	1.43	1.41	1.42 ± 0.012
5.60E-03	1.45	1.47	1.47	1.46 ± 0.012
6.70E-03	1.57	1.53	1.55	1.55 ± 0.020
7.25E-03	1.61	1.60	1.64	1.62 ± 0.021
8.35E-03	1.70	1.67	1.67	1.68 ± 0.017
9.44E-03	1.78	1.77	1.81	1.79 ± 0.021
1.11E-02	1.94	1.96	1.94	1.95 ± 0.012
1.21E-02	2.03	2.06	2.06	2.05 ± 0.017
1.37E-02	2.22	2.22	2.23	2.22 ± 0.006
1.64E-02	2.45	2.48	2.47	2.47 ± 0.015
1.90E-02	2.74	2.72	2.72	2.73 ± 0.012
2.42E-02	3.14	3.16	3.17	3.16 ± 0.015
2.92E-02	3.55	3.56	3.54	3.55 ± 0.010

3.41E-02	3.94	3.89	3.93	3.92 ± 0.026
3.89E-02	4.2	4.23	4.19	4.21 ± 0.021
4.81E-02	4.73	4.76	4.78	4.76 ± 0.025

Phy-3-18

Concentration (mM)	Specific conductivity ($\mu\text{S}/\text{cm}$)			Average \pm SD
4.41E-03	1.07	1.09	1.09	1.08 ± 0.012
4.85E-03	1.11	1.14	1.13	1.13 ± 0.015
5.28E-03	1.17	1.17	1.16	1.17 ± 0.006
5.72E-03	1.20	1.18	1.20	1.19 ± 0.012
8.72E-03	1.60	1.62	1.59	1.60 ± 0.015
9.57E-03	1.69	1.68	1.72	1.70 ± 0.021
1.08E-02	1.89	1.86	1.90	1.88 ± 0.021
1.29E-02	2.17	2.16	2.19	2.17 ± 0.015
1.50E-02	2.46	2.45	2.44	2.45 ± 0.010
1.70E-02	2.73	2.71	2.71	2.72 ± 0.015
2.10E-02	3.18	3.22	3.17	3.19 ± 0.026
2.49E-02	3.48	3.56	3.52	3.52 ± 0.040
2.88E-02	3.83	3.85	3.84	3.84 ± 0.010
3.25E-02	4.04	4.09	4.08	4.07 ± 0.026
3.97E-02	4.45	4.5	4.48	4.48 ± 0.025
5.33E-02	5.38	5.41	5.45	5.41 ± 0.035
7.15E-02	6.22	6.26	6.29	6.26 ± 0.035
8.51E-02	6.86	6.88	6.93	6.89 ± 0.036
9.27E-02	7.25	7.28	7.30	7.28 ± 0.025

Appendix D Fluorescence microscopic images

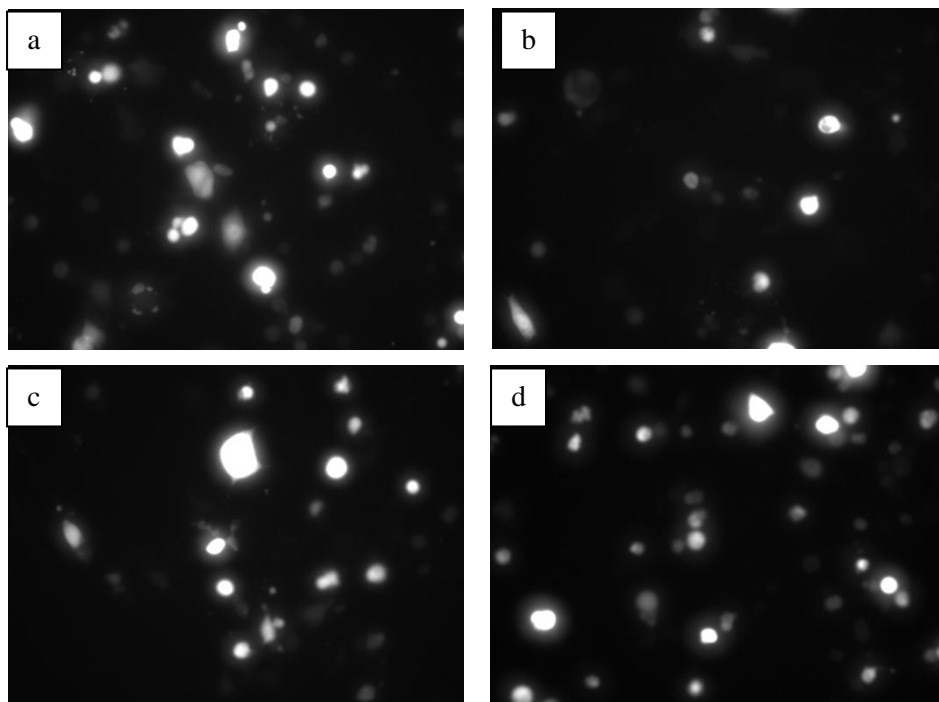


Figure D 1. EGFP images for the cells treated with complexes comprised of phy-3-18 at charge ratio of 2:1 (a), 5:1 (b), and 10:1 (c), and complexes comprised of 16-3-16 at 2:1.

Appendix E Transfection data

Table E 1 Preliminary investigation on transfection of the phytanyl gemini surfactants in OVCAR-3 cells (data for Figure 3.8).

	EGFP expression (%)		EGFP expression (%)
No treatment	0.03 ± 0.01	Phy-3-18	13.28 ± 2.16
Lipofectamine™ 2000	34.56 ± 7.73	16-3-16	4.82 ± 0.22
Plasmid only	0.05 ± 0.05	12-7NH-12	1.43 ± 0.99
Plasmid with DOPE	0.08 ± 0.03	Phy-7NH-12	0.08
Phy-3-12	9.35 ± 0.94	Phy-7NH-16	0.52
Phy-3-16	13.74 ± 3.39	Phy-7NH-18	0.3

Table E 2 EGFP expression in OVCAR-3 (data for Figure 4.4).

EGFP expression (%)				
No treatment	0.01± 0.006			
Lipofectamine™ 2000	32.18 ± 1.56			
Plasmid only	0.09 ± 0.02			
Plamid+DOPE	0.11 ± 0.04			
	2:1	5:1	10:1	20:1
Phy-3-12	9.44 ± 1.81	12.35 ± 1.68	9.48 ± 2.17	0.32
phy-3-16	16.35 ± 1.97	15.63 ± 0.56	12.69 ± 0.77	0.74
phy-3-18	9.92 ± 0.99	15.12 ± 0.76	10.77 ± 0.92	0.96
16-3-16	11.19 ± 1.72	8.26 ± 0.59	3.56 ± 0.68	2.36

Table E 3 Cytotoxicity in OVCAR-3 cells (expressed as cell viability) (data for Figure 4.5)

Cell viability (%)				
No treatment	86.14 ± 2.52			
	2:1	5:1	10:1	
Phy-3-12	80.57 ± 2.26	80.02 ± 2.12	69.41 ± 0.26	
phy-3-16	80.24 ± 1.06	73.91 ± 2.86	59.75 ± 4.76	
phy-3-18	76.65 ± 1.09	69.61 ± 0.16	64.99 ± 1.92	
16-3-16	70.37 ± 0.70	55.93 ± 0.31	46.49 ± 4.28	